

國立交通大學

材料科學與工程學系

博士論文

合成與鑑定具發光基團之主鏈型與側鏈型液晶塊式高
分子

**Synthesis and Characterization of Main-chain and
Side-Chain Liquid Crystalline Block Copolymers
Based on Luminescent Aromatic Cores**

研究生：李冠緯

指導教授：林宏洲 博士

中華民國九十六年五月

合成與鑑定具發光基團之主鏈型與側鏈型液晶塊式高分子

**Synthesis and Characterization of Main-chain and
Side-Chain Liquid Crystalline Block Copolymers Based on
Luminescent Aromatic Cores**

研究生：李冠緯

Student: Kuan-Wei Lee

指導教授：林宏洲 博士

Advisor: Prof. Hong-Cheu Lin



博士論文

A Thesis
Submitted to Department of Materials Science and Engineering
College of Engineering
National Chiao Tung University
In Partial Fulfillment of the Requirement
For the Degree of Doctor of Philosophy of Science
In Materials Science and Engineering
May 2007
Hsinchu, Taiwan

中華民國九十六年五月

合成與鑑定具發光基團之主鏈型與側鏈型液晶塊式高分子

研究生：李冠緯

指導教授：林宏洲 博士

國立交通大學材料科學與工程學系

博士班

摘要

以 Suzuki coupling 反應合成以 fluorene, thiophene, and biphenyl 基團所形成具發光性質之共軛硬段，再以不同分子量的 poly(ethylene oxide)s (PEO, $M_n = 750$ and 2000 , $n = 17$ and 44) 作為軟鏈段來形成具發光性質之主鏈型液晶塊式高分子系統。其自我組織之性質會隨著不同的 PEO 長度而產生不同的液晶相，當軟鏈段長度逐漸加長，其排列方式由較不規則之向列相 (nematic phases) 到層列相 (smectic phases) 最後到規則性高的柱狀相 (columnar phase)。在光學顯微鏡下的光學紋理圖與 X 光繞射圖譜 (XRD) 可以更進一步證明各種不同液晶相。除了液晶性質外，藉由一系列的光學量測以了解不同的軟鏈段 (PEO) 長度對其共軛硬段發光性質之影響。

除了主鏈型液晶塊是高分子，以各種巨起始劑 (macroinitiators,

如 polystyrene, polyethylene oxide, 與 polystyrene-block-polyethylene oxide) 經過原子轉移自由基聚合法 (atom transfer radical polymerization ,ATRP) 聚合出含有不同液晶基 (如 cyanoterphenyl, biphenyl-4-ylthiophene, biphenyl-4-ylfluorene, 與 4,4'-bis(biphenyl)-fluorene units) 的側鏈型液晶塊式高分子。所合成出之側鏈型液晶塊式高分子主要形成之液晶相為向列相 (nematic phases) 與層列 A 相 (smectic A phases)。其液晶相也經過其光學紋理圖與 X 光繞射圖譜 (XRD) 之鑑定。



Synthesis and Characterization of Main-chain and Side-Chain Liquid Crystalline Block Copolymers Based on Luminescent Aromatic Cores

Student: Kuan-Wei Lee

Advisor: Dr. Hong-Cheu Lin

Department of Materials Science and Engineering National Chiao Tung University

The logo of National Chiao Tung University is a circular emblem with a gear-like border. Inside the circle, there is a stylized building and the year '1896' at the bottom. The word 'Abstrate' is overlaid on the logo in a bold, black, sans-serif font.

Abstrate

A novel conjugated aromatic core containing direct-coupled fluorene, thiophene, and biphenyl groups via Suzuki coupling reaction was synthesized. The asymmetrical molecules contain two kinds of poly(ethylene oxide)s (PEO, $M_n = 750$ and 2000 , $n = 17$ and 44) on one side of the rigid cores. Asymmetrical **FOC₈PEO₁₇** and **FOC₁₆PEO₁₇** contain flexible PEO chains ($n = 17$) display the smectic phases. However, **FOC₈PEO₄₄** and **FOC₁₆PEO₄₄** consisting of flexible PEO chains ($n = 44$) exhibit two kinds of columnar phases, Col_h and Col_r. Besides, alkoxy groups with different lengths (-OC₈H₁₇ and -OC₁₆H₃₃) on both sides of the rigid cores were used as another flexible chains to form symmetrical molecules. Symmetrical **FOC₈** and **FOC₁₆** exhibit the nematic and smectic mesophases, respectively. Optical textures (POM) and XRD patterns have confirmed the structure of the mesophases and the molecular arrangements. The photophysical characteristics of all luminescent compounds were studied by photoluminescence and UV-visible absorption. In

addition, A series of double-layered PLED devices with the configuration of PVK:emitters(100:8 by weight)/TPBI/MgAg/Ag were fabricated and investigated.

A series of new mesomorphic block copolymers composed of different macroinitiators, including poly(ethylene oxide), polystyrene, and poly(ethylene oxide)-b-polystyrene, and polymethacrylate with a pendent cyanoterphenyl group, were synthesized through atom transfer radical polymerization (ATRP). The mesomorphic and optical properties of all block copolymers were investigated, and all polymers possess the smectic A phase with mesophasic ranges wider than 100 °C. Moreover, X-ray diffraction (XRD) patterns provided the evidence of the smectic A phase and the corresponding interdigitated packing of all polymers. Besides a pendent cyanoterphenyl group, new liquid crystalline homopolymers and block copolymers composed of methacrylates containing pendent biphenyl-4-ylthiophene and biphenyl-4-ylfluorene units were synthesized. The thermal, mesogenic, and photoluminescence (PL) properties of all polymers were investigated. Polymers containing biphenyl-4-ylthiophene possessed the smectic A phase and polymer composed of biphenyl-4-ylfluorene units exhibited the nematic phase. However, new Luminescent liquid crystalline homopolymers, copolymers, and block copolymers were also polymerized from styrene-macroinitiator and methacrylates with pendent 4,4'-bis(biphenyl)fluorene and biphenyl-4-ylfluorene groups through atom transfer radical polymerization (ATRP). All polymers exhibit the nematic phase. The thermal, mesogenic, and photoluminescent (PL) properties of all polymers were investigated.

3.2 Experimental Section.....	42
3.2.1 Measurements.....	42
3.2.2 Materials.....	42
3.2.3 Synthesis.....	43
3.3 Results and Discussion.....	49
3.3.1 Synthesis and Characterization.....	49
3.3.2 Thermal Properties and X-ray Investigation.....	52
3.3.3 Optical Properties.....	56
3.4 Conclusion.....	58
Chapter 4. Synthesis and Characterization of Side-Chain Liquid Crystalline Homopolymers and Block Copolymers Containing Biphenyl-4- ylthiophene and Biphenyl-4-ylfluorene Pendants.....	59
4.1 Introduction.....	59
4.2 Experimental Section.....	60
4.2.1 Measurements.....	60
4.2.2 Materials.....	60
4.2.3 Synthesis.....	61
4.3 Results and Discussion.....	68
4.3.1 Synthesis and Characterization.....	68
4.3.2 Thermal and mesogenic properties.....	70
4.3.3 X-ray Measurement.....	73
4.3.4 Photophysical Properties.....	75
4.4 Conclusion.....	80
Chapter 5. Synthesis and Characterization of Liquid Crystalline Side-Chain Block Copolymers Containing Luminescent 4,4'-Bis(biphenyl)fluorene Pendants.....	81

5.1 Introduction.....	81
5.2 Experimental Section.....	82
5.2.1 Measurements.....	82
5.2.2 Materials.....	83
5.2.3 Synthesis.....	83
5.3 Results and Discussion.....	91
5.3.1 Synthesis and Characterization.....	91
5.3.2 Thermal and mesogenic properties.....	92
5.3.3 Photophysical Properties.....	94
5.4 Conclusion.....	97
Chapter 6. Conclusions.....	98
References.....	100
Appendix : NMR spectra.....	105



Table Lists

Table 2.1 Phase Behavior of Synthesized Molecules.....	28
Table 2.2 Absorption and Photoluminescence Spectral Data of Synthesized Molecules.....	34
Table 2.3 HOMO and LUMO Energies, and Electrochemical Properties.....	37
Table 2.4 EL Data of PLED Devices.....	38
Table 3.1 Molecular Weights and Thermal Properties of Block Copolymers P1-P4	52
Table 3.2 Phase Behavior of Block Copolymers P1-P4	53
Table 3.3 XRD Diffraction Data of All Polymers P1-P5 at 190 °C.....	56
Table 3.4 Absorption and Photoluminescence Spectral Data of Block Copolymers P1-P4	57
Table 4.1 Molecular weight and thermal properties of polymers P1-P4	70
Table 4.2 Phase behavior of polymers P1-P4	73
Table 4.3 XRD diffraction data of polymers P1 and P3	72
Table 4.4 UV-visible absorption and photoluminescence spectral data of monomers (M1 and M2) and polymers (P1-P4)	76
Table 5.1 Molecular weights and polydispersity indexes of polymers P1-P4	91
Table 5.2 Thermal properties of polymers P1-P4	93
Table 5.3 UV-visible Absorption and Photoluminescence Spectral Data of Monomers M1-M2 and Polymers P1-P4	95

Figure Lists

Figure 1.1 Possible melting sequences for a liquid crystalline material.....	1
Figure 1.2 The important issues when considering lateral substitution.....	3
Figure 1.3 Schematic representations of two types of LC block copolymers (a) main-chain LC diblock copolymers (b) side-chain LC diblock copolymers.....	4
Figure 1.4 The chemical structure of rod-coil LC triblock polymers (Molecule 1)	6
Figure 1.5 GPC traces of rod-coil triblock molecule 1 and macromolecular object	6
Figure 1.6 (A) A TEM micrograph at high magnification of a film that was formed by regularly sized and shaped supramolecular clusters composed of triblock molecules (B) A TEM micrograph at high magnification of a film that was formed by the isolated molecular objects. (C) An optical micrograph between crossed polarizers showing the smectic to isotropic phase transition at 330°C. (D) An optical micrograph between crossed polarizers showing the smectic texture of the macromolecular product at 420°C	7
Figure 1.7 The chemical structure of Molecule 2.....	8
Figure 1.8 Schematic representations of supramolecular structures of rod-coil molecules 2. (a) Smectic A (b) bicontinuous cubic phases (c) hexagonal columnar phases.....	9
Figure 1.9 The chemical structure of side-chain LC polymers (P1 and P2)	10
Figure 1.10 Typical polarized optical micrographs of P1e at (A) 115, (B) 90, and (C) 30 °C.....	10
Figure 1.11 Terphenyl methacrylate monomers and derived side-chain polymers.....	11
Figure 2.1 Phase diagrams of mesophases in all materials upon (a) heating, (b) cooling.....	26

Figure 2.2 The optical textures of the mesophases observed by POM. (a) The nematic phase in **FOC₈ (8)** at 280°C (cooling). (b) The SmA phase in **FOC₈PEO₁₇ (17)** at 200°C (heating). (c) The SmC phase in **FOC₁₆ (10)** at 175°C (cooling). (d) The Col_h phase in **FOC₈PEO₄₄ (19)** at 115°C (cooling). (e) The Col_r phase in **FOC₁₆PEO₄₄ (20)** at 139°C (heating)27

Figure 2.3 X-ray diffraction data (a) SmA (170°C) and SmC (120°C) phases of **FOC₁₆ (10)** (b) SmA (120°C) phase of **FOC₈PEO₁₇ (17)**, Col_h (50°C) phase of **FOC₈PEO₄₄ (19)** and Col_r (30°C) phase of **FOC₁₆PEO₄₄ (20)**.....31

Figure 2.4 (a) Absorption and PL spectra of **FOC₈PEO₄₄ (19)** in solutions (CHCl₃ as solvent) and films. (b) PL spectra of films of materials contain different flexible chains.....35

Figure 2.5 (a) PLE spectra of **FOC₈PEO₁₇ (17)** film monitored at 464 nm and 496 nm respectively (normalized at 412 nm). (b) PL spectra of **FOC₈PEO₄₄ (19)** in solid state and at 50°C (Col_h phase).....36

Figure 2.6 (a) Normalized EL spectra of PLED devices, PVK:emitters(100:8 by weight)/TPBI(30 nm)/MgAg(50 nm)/Ag(100 nm). (b) Current-voltage and luminescence-voltage characteristics of the PLED device, PVK:**FOC₈**(100:8 by weight)/TPBI (30 nm)/MgAg (50 nm)/Ag (100 nm)39

Figure 3.1 ¹H NMR spectra of block copolymers **P1, P3, and P4**.....51

Figure 3.2 DSC thermograms of block copolymers **P1-P4** during the first heating scan.....53

Figure 3.3 The optical texture of the mesophase (S_A) of **P1** observed by POM at 270 °C (cooling)54

Figure 3.4 X-ray diagrams of all polymers **P1-P5**.....55

Figure 3.5 Absorption (solid lines) and PL (dash lines) spectra of **P1** in solutions

(CHCl ₃ as solvent) and solid films.....	57
Figure 3.6 PL spectra of block copolymers P1-P4 in solution (CHCl ₃ as solvent)	58
Figure 4.1 DSC thermograms of polymers P1-P4 during the first heating scan at 5 °C/min.....	71
Figure 4.2 POM texture of the mesophase (S _A) of polymer P1 observed at 255 °C (cooling)	73
Figure 4.3 X-ray diffraction patterns of polymers P1 and P3	75
Figure 4.4 UV-visible absorption (solid lines) and PL (dash lines) spectra of monomers M1 and M2 in solutions (THF as solvent)	77
Figure 4.5 PL spectra of polymers P2 and P4 in solid films and solutions (THF as solvent)	78
Figure 4.6 PL spectra of polymer P2 in the solid state by spin-coating and quenching (by liquid N ₂) from 130 °C (the nematic phase)	79
Figure 4.7 Polarized PL spectra of aligned P2 solid film by quenching from 130 °C on a rubbing PI substrate, where PL _{//} is the parallel PL intensity as the polarizer is parallel to the rubbing direction, and PL _⊥ is the perpendicular PL intensity as the polarizer perpendicular to the rubbing direction.....	79
Figure 5.1 The schlieren texture (the nematic phase) of P1 observed by POM at 280°C (cooling).....	93
Figure 5.2 PL spectra of monomers (M1 and M2) and polymers (P1 and P3) in solutions.....	96
Figure 5.3 UV-visible absorption and PL spectra of P1 and P3 in solid films.....	96

Chapter 1

Introduction

1.1 Introduction to liquid crystals

The difference between crystals and liquids, the two most common condensed matter phases, is that the molecules in a crystal are ordered whereas in a liquid they are not. The order in a crystal is usually both positional and orientational, in that the molecules are constrained both to occupy specific sites in a lattice and to point their molecular axes in specific directions. The molecules in liquids, on the other hand, diffuse randomly throughout the sample container with the molecular axes tumbling wildly. Interestingly enough, many phases with more order than present in liquids but less order than typical of crystals also exist in nature. These phases are grouped together and called “*liquid crystals*”, since they share properties normally associated with both liquids and crystals.¹

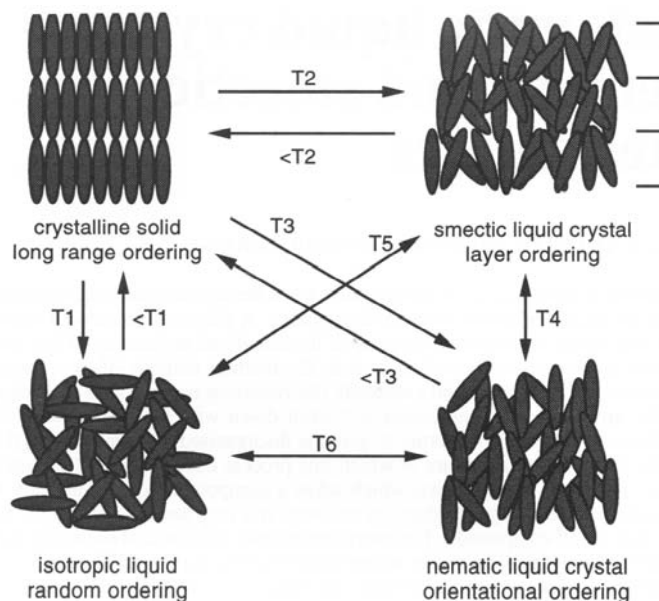
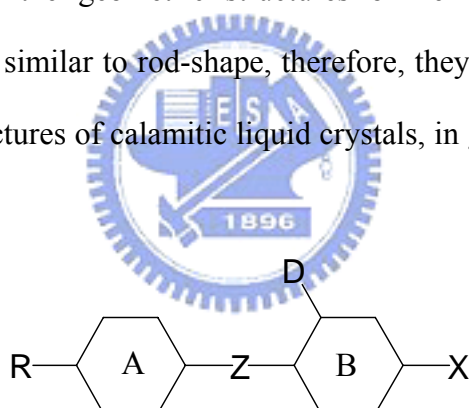


Figure 1.1 Possible melting sequences for a liquid crystalline material.¹

The liquid crystal can be divided into two categories: 1. lyotropic liquid crystal, the liquid crystalline molecule combines a hydrophobic group at one end with a hydrophilic group at the other end. Such amphiphilic molecules can form ordered structures at certain concentration in both polar and non-polar solvents. 2. Thermotropic liquid crystals, the liquid crystal phase is stable for a certain temperature interval. The most common types of thermotropic liquid crystalline molecule are rod-shaped molecule (calamitic liquid crystal) and disc-like molecules (discotic liquid crystal).¹

1.1.1 Calamitic liquid crystals

Generally speaking, the geometric structures of nematic and smectic liquid crystalline materials are similar to rod-shape, therefore, they are also called calamitic liquid crystals. The structures of calamitic liquid crystals, in general, can be described as follows:



R is side chain group, X is terminal group, and D is lateral substitution. Two or more saturated and unsaturated rings (A, B) are linked by linking group (Z), which is called core. A and B are usually consisted of cyclic rings. The temperature of mesophase will be promoted while the numbers of cyclic ring are increased. All of the following have been utilized for side chain groups (R):

1. alkyl group, C_nH_{2n+1}
2. alkoxy group, OC_nH_{2n+1}
3. alkenyl group, C_nH_{2n-1}
4. alkeneoxy group, OC_nH_{2n-1}

The length and flexibility of side chain have great effects on the transition temperature and mesophase of liquid crystals. The mesophase tends to form smectic phase from nematic phase while the length of side chain is increased.

The common linking groups have:

1. dimethylene group and methyleneoxy group
2. ester group
3. containing double bond groups, such as ethylene group, azo group, and imine group
4. acetylene group

Terminal unit is often a small polar substituent (e.g., CN, F, NCS, NO₂), which mainly decide dielectric constant (ϵ) and dielectric anisotropy ($\Delta\epsilon$). A wide range of different lateral substituents (e.g., F, Cl, CN, NO₂, CH₃, CF₃) have been incorporated into many different liquid crystal systems in many different environments. However, the fluoro substituent is the most useful lateral group because of its subtle combination of small size and high electronegativity. It can be thought that lateral substituent sticks out at the side of a molecule that will disrupt molecular packing and reduce liquid crystal phase stability. Figure 1.2¹ summaries the possibilities of lateral substitution.

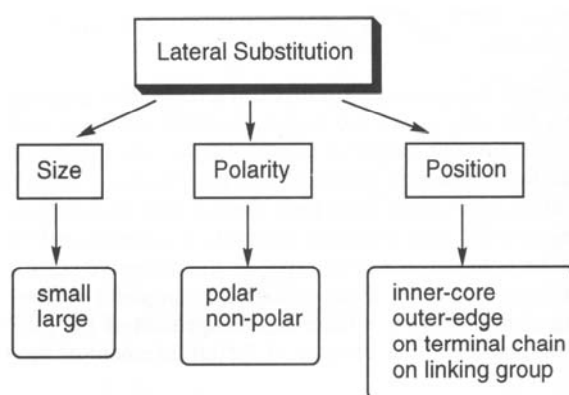


Figure 1.2 The important issues when considering lateral substitution.¹

1.2 Introduction to liquid crystalline (LC) block copolymer materials

In the past decade, many researchers focused on LC block copolymers type building and discussed their potential for the development of self-assembled materials. In general, there are two kinds of LC block copolymers, i.e. main-chain and side-chain LC block copolymers, where mesogenic groups connected along the backbones are main-chain copolymers, and pendent mesogenic groups attached to the backbones via flexible spacers are side-chain copolymers.(show in figure 1.3)

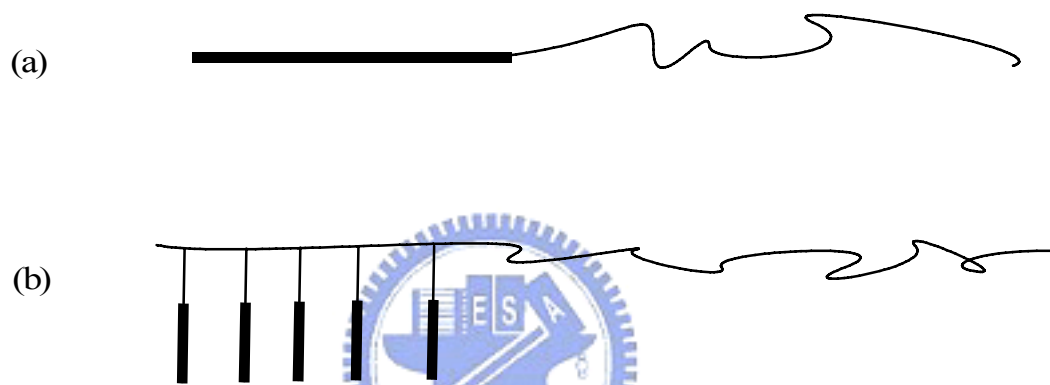


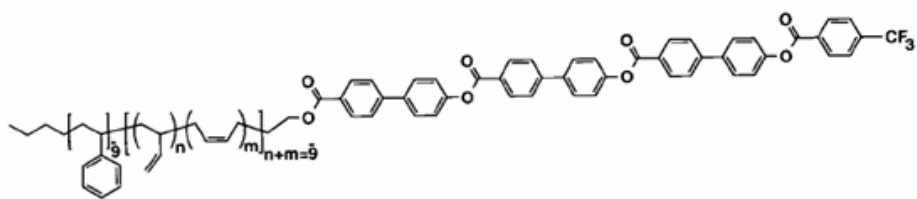
Figure 1.3 Schematic representations of two types of LC block copolymers (a) main-chain LC diblock copolymers (b) side-chain LC diblock copolymers.

1.2.1 Main-chain LC block copolymers

Rod-coil block systems based on mesogenic rods can provide a variety of supramolecular structures due to the effect of microphase separation and the molecular anisometry of rod block. Even though the molecular weight is very small, microphase separated structures can form due to large chemical differences between each block.

Stupp et al.² reported on rod-coil copolymers consisting of an extended mesogenic rod block and a monodisperse polyisoprene or poly(isoprene-block-styrene) coil blocks. These rod-coil copolymers self-assemble into ordered structures in terms of

varying rod and coil volume fractions as monitored by transmission electron microscopy and electron tomography. These supramolecular structures were discovered to vary from lamellar to micellar microphase-separation. The authors also presented an elegant approach to produce well-defined macromolecular objects converting supramolecular clusters by polymerization of cross-linkable group within a discrete supramolecular unit. The rod-coil triblock molecule synthesized by the authors is composed of a block of oligostyrene, a block of polymerizable oligobutadiene, and a rodlike block containing CF_3 end group (Molecule **1**) which has a large dipole moment (Figure 1.4). Thermal polymerization of rod-coil triblock molecules in liquid crystalline state produced high molar-mass products with a very narrow polydispersity within a range from 1.15 to 1.25 and molecular weight of approximately 70 000 as confirmed by GPC (Figure 1.5). Transmission electron microscopy (TEM) studies of triblock molecules revealed a solid state structure consisting of aggregates ~ 2 nm in diameter (Figure 1.6A)². Similar structures of 2 nm were observed for the isolated polymer object material (Figure 1.6B), which indicate that aggregation and rod packing were not altered by polymerization. The initial precursor undergoes a phase transition from the smectic to the isotropic state at 330°C (Figure 1.6C), whereas the polymerized objects form a highly birefringent melt at 160°C, and isotropization is never observed before chemical decomposition at 430°C (Figure 1.6D).



Molecule 1

Figure 1.4 The chemical structure of rod-coil LC triblock polymers (Molecule 1).²

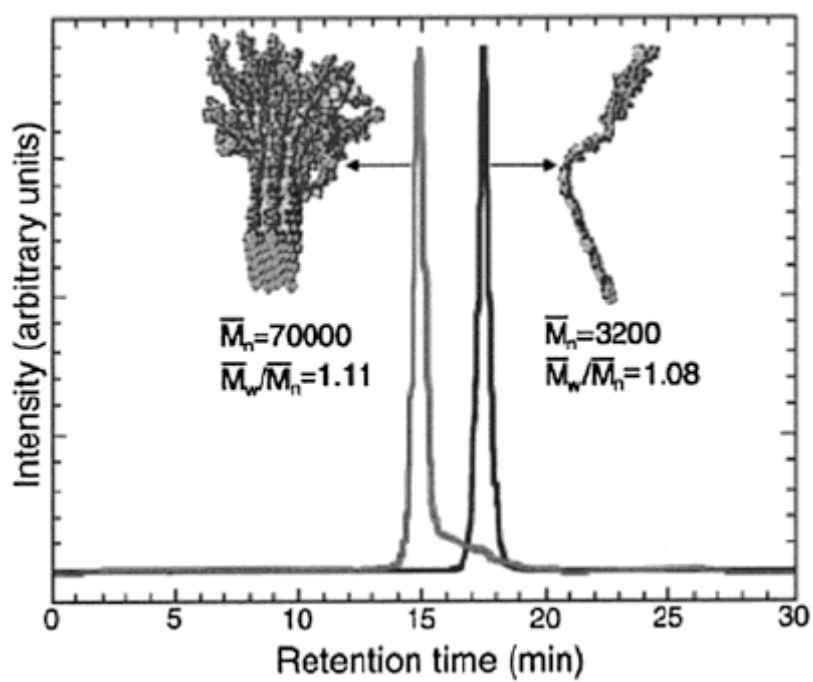


Figure 1.5 GPC traces of rod-coil triblock molecule 1 and macromolecular object.²

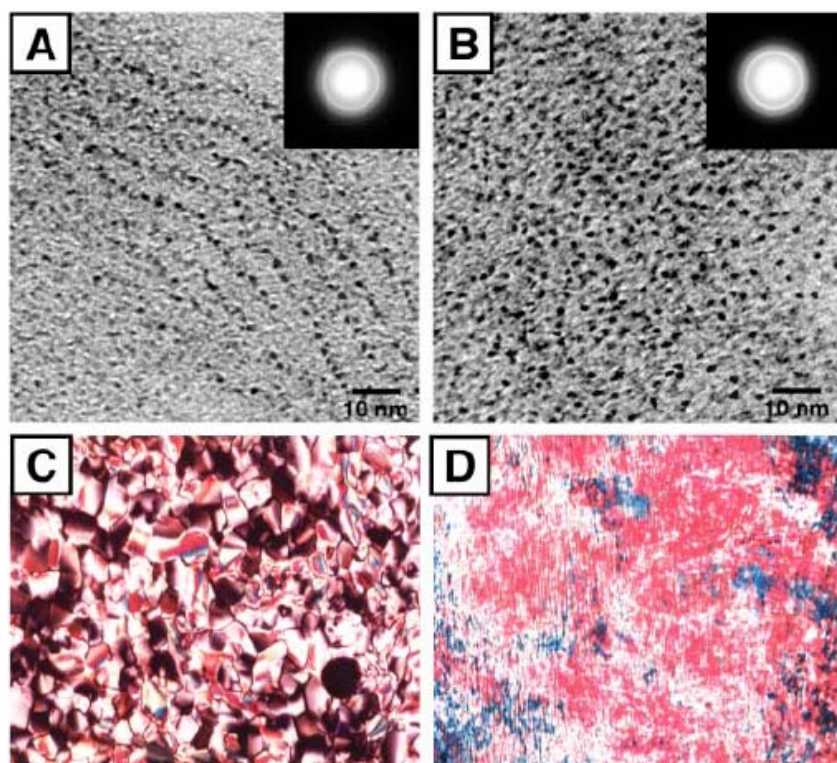


Figure 1.6 (A) A TEM micrograph at high magnification of a film that was formed by regularly sized and shaped supramolecular clusters composed of triblock molecules (B) A TEM micrograph at high magnification of a film that was formed by the isolated molecular objects. (C) An optical micrograph between crossed polarizers showing the smectic to isotropic phase transition at 330°C. (D) An optical micrograph between crossed polarizers showing the smectic texture of the macromolecular product at 420°C.²

Myongsoo Lee et al.³ also reported on small rod-coil systems with a mesogenic rod segment. Their molecules are based on flexible poly(ethylene oxide) or poly(propylene oxide) as a coil block. In a more systematic work on the influence of the coil length on phase behavior, the authors studied rod-coil molecules **2** with poly(propylene oxide) having different degrees of polymerization but the identical rod segment (Figure 1.7).

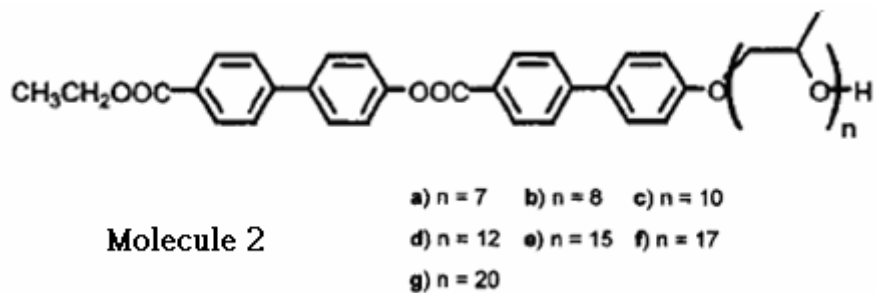


Figure 1.7 The chemical structure of Molecule 2.³

A dramatic structural change in the melt state of this rod-coil system was observed with variation in the coil length as determined by a combination of techniques consisting of differential scanning calorimetry (DSC), optical polarized microscopy, and X-ray scattering. Rod-coil molecules with 7 and 8 propylene oxide units exhibit layered smectic C and smectic A phases, while rod-coil molecules with 10 to 15 repeating units exhibit an optically isotropic cubic phase. This structure was identified by the X-ray scattering method to be a bicontinuous cubic phase with $Ia3d$ symmetry. Further increasing the coil length induces a hexagonal columnar mesophase as in the case of the molecules with 15 to 20 repeating units (Figure 1.8).

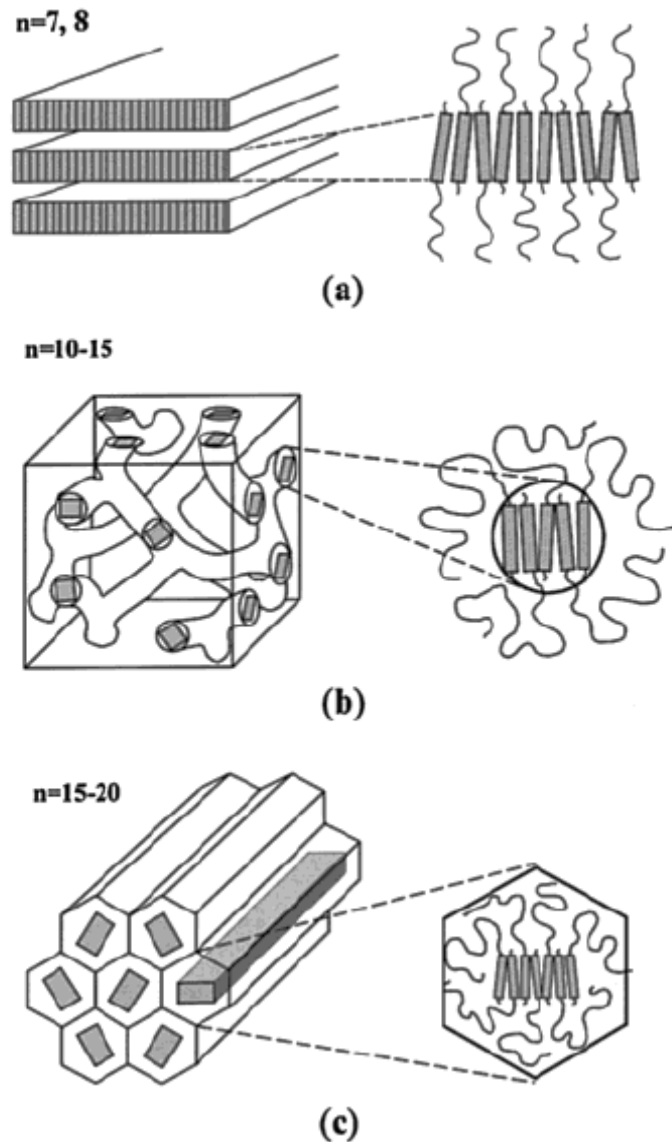


Figure 1.8 Schematic representations of supramolecular structures of rod-coil molecules **2**. (a) Smectic A (b) bicontinuous cubic phases (c) hexagonal columnar phases.³

1.2.2 Side-chain LC block copolymers

Side-chain liquid crystalline block copolymers offer great potential to serve in a wide array of commercial applications. Furthermore, they combine the thermotropic ordering of liquid crystals with the physics of block copolymer phase segregation. These copolymers can produce numbers of microphase separated nanostructures with cylinder, lamellar, sphere morphologies, etc.

Tomokazu Iyoda et al.⁴ design a novel series of multifunctional block copolymers, which contain both a defined length of poly-(ethylene glycol) (PEG) as the hydrophilic block and different length of poly(methacrylate) with an azobenzene unit as the hydrophobic, liquid crystalline, and photoisomerization block (**P1** and **P2**) (Figure 1.9). POM was used to identify the mesophases. On cooling of **P1e**, focal conic-fan shaped textures (Figure 1.10A) were observed in the temperature range 122-101 °C, suggesting a smectic A (SmA) phase. On further cooling below 100 °C, slight texture change but clear birefringence change were observed as shown in Figure 1.10B, suggesting a smectic C phase (SmC). On the further cooling below 74 °C, the color caused by the birefringence changed and the textures (Figure 1.10C) became obscure, indicating an other kind of smectic phase (SmX).

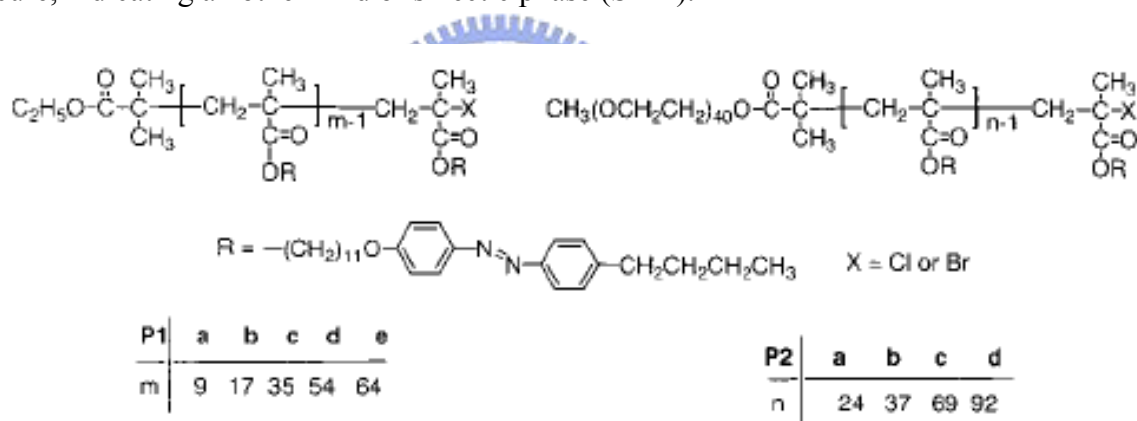


Figure 1.9 The chemical structure of side-chain LC polymers (**P1** and **P2**).⁴

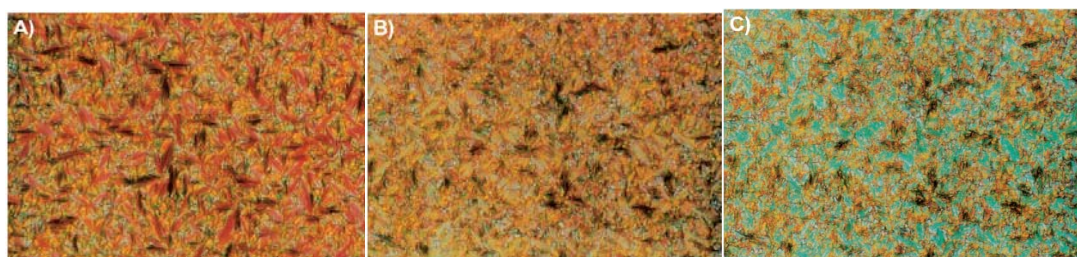


Figure 1.10 Typical polarized optical micrographs of **P1e** at (A) 115, (B) 90, and (C) 30 °C.⁴

L. Oriol et al.⁵ have undertaken the synthesis of a series of reactive LCs based on terphenyl derivatives. The terphenyl core has a calamitic structure that is compatible with mesomorphic ordering and is well known to give LCs that has high birefringence (Figure 1.11). These side-chain polymers exhibited smectic A and nematic phase but all polymers had poor solubilities to lead to unknown molecular weights.

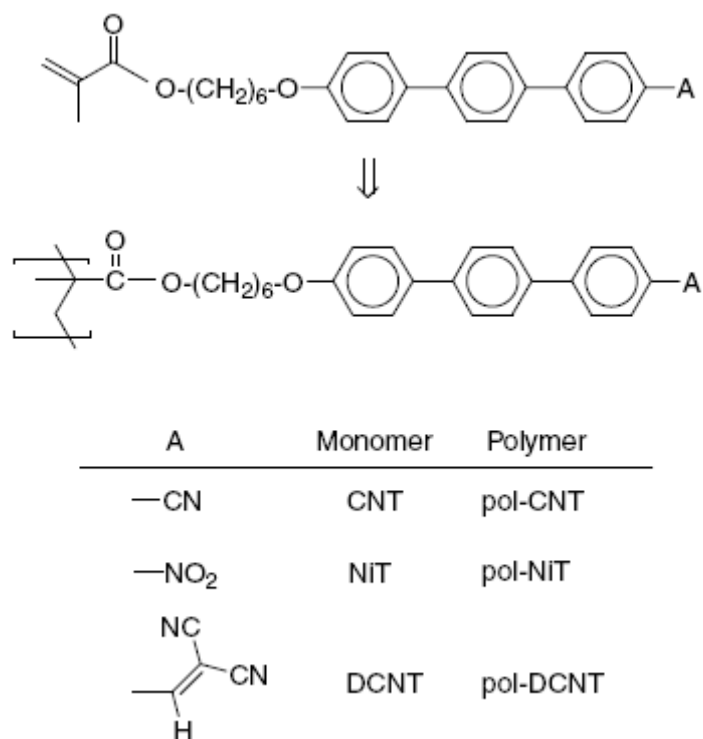


Figure 1.11 Terphenyl methacrylate monomers and derived side-chain polymers.⁵

Stupp et al. and Myongsoo Lee et al. reported on rod-coil copolymers consisting of different mesogenic rod block and a monodisperse polyisoprene, poly(isoprene-block-styrene) and poly(ethylene oxide) coil blocks. Hence, we have synthesized a novel conjugated aromatic rod containing a fluorene core symmetrically connected by thiophene and biphenyl groups on both sides through single bonds to form a long luminescent rod. After then, poly(ethylene oxide) flexible parts with different lengths (PEO, n = 17 and 44) were attached to one end of the luminescent core by ether linkage to form the luminescent main-chain rod-coil polymers.

Beside, side-chain LC polymers are often used in electro-optical applications, where different kinds of rigid cores, including azobenzene and biphenyl units, are used in mesogenic monomers. Therefore, a series of novel side-chain liquid crystalline block copolymers consisting of different flexible macroinitiators, including poly(ethylene oxide) (PEO), polystyrene (PS), and polymethacrylate with a pendent cyanoterphenyl, biphenyl-4-ylthiophene, biphenyl-4-ylfluorene, and 4,4'-bis-(biphenyl)fluorene units, were synthesized through atom transfer radical polymerization (ATRP).



Chapter 2

Synthesis and Characterization of Rod-Coil Polymers Based on Poly(ethylene oxide)s and Novel Luminescent Aromatic Cores

2.1 Introduction

In recent years, the study of the polymeric light-emitting diode (PLED) and liquid crystalline (LC) materials are widely surveyed. Generally, a combination of rigid cores and flexible chains is required for LC molecules, and a conjugated rigid core is a necessary segment for PLED materials. Therefore, in order to merge LC with PLED properties, the conjugated aromatic rings are designed as the rigid cores. The development of self-assembled materials has received a great attention due to their potential in the construction of well-defined supramolecular nanostructures. Rod-coil systems^{6,7} consisting of rigid rod and flexible coil segments are excellent candidates for creating well-defined supramolecular structures through a process of spontaneous organization. Theoretical works in some literatures⁸⁻¹⁰ have shown that various supramolecular structures such as nematic, smectic, and cylindrical phases depending on the relative volume fraction of blocks.

Stupp et al. reported on rod-coil copolymers consisting of an extended mesogenic rod block and a monodisperse polyisoprene¹¹ or poly(isoprene-block-styrene)¹² coil blocks. These rod-coil copolymers self-assemble into ordered structures in terms of varying rod and coil volume fractions as monitored by transmission electron microscopy and electron tomography. These supramolecular structures were discovered to vary from lamellar to micellar microphase-separation. In addition to

above coils reported by Stupp, poly(ethylene oxide) and poly(propylene oxide) as the flexible coils were used by Lee and coworkers.^{13,14} Liquid-crystalline behavior of these kinds of rod-coil molecules is associated with the volume fraction of coil segments. The mesophases changed from the nematic phase to the hexagonal columnar phase by increasing ethylene oxide units. A rigid rod and an elongated flexible coil connected by covalent linkage may result in new supramolecular structures because of the incompatible segregation ability of individual segments.

In recent publications, Stupp et al. also reported amphiphiles consisting of a well-defined oligo(*p*-phenylene vinylene) (OPV) trimer asymmetrically end-substituted with a hydrophobic alkyl chain and a hydrophilic poly(ethylene glycol) (PEG). They tuned the solubility and mesophase structure by controlling the length of the PEG block.¹⁵ Besides the mesogenic rod block, Lee et al. also reported the luminescent rod-coil systems containing three biphenyl groups linked by double bonds¹⁶ or penta-*p*-phenylene¹⁷ as the conjugated rigid rods. So far, rod-coil diblock systems containing poly(ethylene oxide) coils and luminescent conjugated aromatic rods have been described in a few literatures. Therefore, in this paper we have synthesized a novel conjugated aromatic rod containing a fluorene core symmetrically connected by thiophene and biphenyl groups on both sides through single bonds to form a long luminescent rod. After then, poly(ethylene oxide) flexible parts with different lengths (PEO, $n = 17$ and 44) were attached to one end of the luminescent core by ether linkage to form the luminescent rod-coil polymers. Besides, analogous derivative containing symmetric alkoxy flexible parts were synthesized and characterized. POM, DSC, and XRD data show that all investigated materials possess mesomorphism. Their PL and EL properties are also studied in this research.

2.2 Experimental Section

2.2.1 Materials

Chemicals and solvents were reagent grades and purchased from Aldrich, ARCROS, TCI, and Lancaster Chemical Co. Dichloromethane and THF were distilled to keep anhydrous before use. The other chemicals were used without further purification. Pyridine was dried by refluxing over calcium hydride.

2.2.2 Measurements.

¹H NMR spectra were recorded on a Varian Unity 300 MHz spectrometer using CDCl₃ solvent. Elemental analyses were performed on a HERAEUS CHN-OS RAPID elemental analyzer. Transition temperatures were determined by differential scanning calorimetry (Perkin-Elmer Pyris 7) with a heating and cooling rate of 10 °C/min. Gel permeation chromatography (GPC) analysis was conducted on a Waters 1515 separation module using polystyrene as a standard and THF as an eluant. UV-vis absorption spectra were recorded in dilute chloroform solutions (10⁻⁶ M) on a HPG1103A spectrophotometer, and fluorescence spectra were obtained on a Hitachi F-4500 spectrophotometer. Fluorescence quantum yields were determined by comparing the integrated PL density of a reference 9,10-diphenylanthracene in toluene with a known quantum yield (ca. 5 x 10⁻⁵ M, quantum yield = 1) and 9,10-DPA/PMMA film (quantum yield = 0.83).²⁸ Cyclic voltammetry (CV) was performed at a scanning rate of 100 mV/s on a BAS 100 B/W electrochemical analyzer, which was equipped with a three-electrode cell. Pt wire was used as a counter electrode, and an Ag/AgCl was used as a reference electrode in the CV measurement. The concentrations of polymer solutions in dichloromethane were 10⁻² M as a working electrode with ferrocene as a standard in acetonitrile, and 0.1 M tetrabutylammonium hexafluorophosphate (TBAPF₆) was used as a supporting

electrolyte. The textures of mesophases were studied using a polarizing optical microscope (POM, Model: Leica DMLP) equipped with a hot stage.

A series of double-layer EL devices with the configuration of PVK:emitters(100:8 by weight)/TPBI(30 nm)/MgAg(50 nm)/Ag(100 nm) were made by spin-coating the rod-coil diblock molecules blended with PVK onto indium-tin oxide (ITO) glass substrates. The solutions (30 mg/ml) of light-emitting materials in 1,2-dichloroethane were spin-coated on glass slides precoated with indium tin oxide (ITO) with sheet resistances of $\sim 20 \Omega/\text{square}$ and with an effective individual device area of 3.14 mm^2 . The ITO glasses were routinely cleaned by ultrasonic treatment in detergent solutions and diluted water, followed by through rinsing in acetone and then ethanol. After drying, the ITO glasses were kept in oxygen plasma for 3 min before being loaded into the vacuum chamber. The spin coating rate was 3000 rpm for 40 s, and the thickness of the emitting layer was about 60 nm. One layer of magnesium and silver alloy (ca. 10:1, 50 nm) was deposited thermally as a cathode at a rate of 0.1-0.3 $\text{\AA}/\text{s}$ under a pressure of $\sim 2 \times 10^{-5}$ torr in an Ulvac Cryogenic deposition system, which was capped with 100 nm of silver. The current-voltage-luminescence properties were measured in ambient conditions with a Keithley 2400 Source meter and a Newport 1835C Optical meter equipped with an 818ST silicon photodiode.

2.2.3 Synthesis.

The rigid cores of these aromatic conjugated molecules containing fluorene, thiophene, and biphenyl groups connected by single bonds were synthesized via Suzuki coupling reaction.^{18,19} The flexible chains were different alkoxy and poly(ethylene oxide) groups (PEO, $n = 17$ and 44). The synthetic route is shown in scheme 2.1.

2, 7-Dibromofluorene (2). Fluorene (8.3 g, 50 mmol) was dissolved in 80ml of

dry dichloromethane and then bromide (5.1 ml, 100 mmol) was added to react. The reaction mixture was stirred at room temperature for 24 hrs, and a saturated aqueous sodium bisulfite solution was added to quench bromide. The solution was extracted with water and dichloromethane and the organic layer was dried over magnesium sulfate, and the solvent was removed by rotavapor. The compound was purified by recrystallization from hexane to yield white crystals (12.5 g, 77 %). ¹H NMR (ppm, CDCl₃), δ: 3.84 (s, 2H), 7.48 (d, *J* = 8.2 Hz, 2H), 7.58 (d, *J* = 8.0 Hz, 2H), 7.64 (s, 2H)

2, 7-Dibromo-9, 9-diethylfluorene (3). A mixture of the compound **2** (12.5 g, 38.7 mmol) and potassium-tert-butoxide (13 g, 116 mmol) was dissolved in THF to reflux 1 hr, and then it was ethyl bromide (7.2 ml, 96.9 mmol) was added dropwise and reacted for additional 12 hrs. After reaction, THF was removed, and the solution was extracted with diethyl ether and water, and the organic layer was dried over magnesium sulfate. The solvent was removed by rotavapor, and the crude product was purified by column chromatography (silica gel, hexane eluent) to yield a white solid (12.5 g, 85 %). ¹H NMR (ppm, CDCl₃), δ: 0.29 (t, *J* = 5.4 Hz, 6H), 2.07 (m, 4H), 7.42 (s, 2H), 7.44 (d, *J* = 8.8 Hz, 2H), 7.51 (d, *J* = 8.8 Hz, 2H)

2-Thioiphenboronic Acid (4). 2-Bromothiophene (10 g, 61.3 mmol) was treated with magnesium (1.72 g, 79.5 mmol) in 200 mL of dry THF under nitrogen. The reaction mixture was refluxed for 7 hrs to form Grignard reagent and then the Grignard solution was added dropwise to trimethyl borate solution (12.75 g, 122.7 mmol in 30 ml of dry THF) at -78°C. The mixture solution was allowed to warm up to room temperature overnight. The final solution was acidified with 10 % HCl solution (100 ml) and stirred for 2 hrs at room temperature. The solution was washed with saturated sodium carbonate solution and water and then THF was removed. The crude product was extracted by diethyl ether and the organic layer was dried over

magnesium sulfate. After removing the solvent by rotavapor, The solid was recrystallized from ethyl acetate to obtain a white solid (4.72 g, 61 %). ¹H NMR (ppm, d₆-DMSO): δ 7.15 (dd, *J* = 4.8, 3.3 Hz, 1 H), 7.66 (d, *J* = 3.3 Hz, 1 H), 7.72 (d, *J* = 4.8 Hz, 1 H), 8.17 (s, 2 H).

2,7-Bis(thien-2-yl)-9,9-diethylfluorene (5). The compound **3** (5 g, 13.2 mmol), the compound **4** (5.05 g, 39.4 mmol),

tetrakis(triphenylphosphine)palladium(0) were reacted in DME (100 ml) for 10 mins, and then 100mL of 2 M aqueous Na₂CO₃ solution was added. The reaction mixture was refluxed for 48 hrs. The cooled solution was washed with dilute hydrochloric acid (10 %) and water, and dried over magnesium sulfate. The final solution was purified by column chromatography (silica gel, CH₂Cl₂/hexane 1:2) to yield a light green solid (4.2 g, 83 %). ¹H NMR (ppm, d₆-DMSO), δ: 0.26 (t, *J* = 7.4 Hz, 6 H), 2.11 (q, *J* = 7.4 Hz, 4 H), 7.15 (dd, *J* = 5.1, 3.7 Hz, 2 H), 7.54 (d, *J* = 5.1 Hz, 1 H), 7.55 (d, *J* = 5.1 Hz, 1 H), 7.60 (d, *J* = 3.7 Hz, 1 H), 7.61 (d, *J* = 3.7 Hz, 1 H), 7.64 (d, *J* = 7.8 Hz, 1 H), 7.64 (d, *J* = 3.7 Hz, 1 H), 7.72 (s, 2 H), 7.84 (d, *J* = 7.8 Hz, 2 H)

2,7-Bis(bromothien-2-yl)-9,9-diethylfluorene (6). *N*-Bromosuccinimide (2.5 g, 14.3 mmol, freshly purified by recrystallization from water) and the compound **5** (2.4 g, 6.22 mmol) was stirred in chloroform (25 mL) and glacial acetic acid (25 mL). The solution was heated under reflux for 1 hr, and warm up to room temperature. Sequentially, the solution washed with water (100 mL), HCl (150 ml, 20 %), and saturated aqueous sodium bisulfite solution and dried over magnesium sulfate. The final solution was purified by column chromatography (silica gel, CH₂Cl₂/hexane 1:1) to yield a light green solid (2.7 g, 80 %). ¹H NMR (ppm, d₆-DMSO), δ: 0.24 (t, *J* = 7.2 Hz, 6 H), 2.10 (q, *J* = 7.2 Hz, 4 H), 7.27 (d, *J* = 3.9 Hz, 2 H), 7.46 (d, *J* = 3.9 Hz, 2 H), 7.58 (d, *J* = 8.1 Hz, 2 H), 7.69 (s, 2 H), 7.85 (d, *J* = 8.1 Hz, 2 H).

4-Bromo-4'-octoxybiphenyl. 1-Bromooctane (11.6 g, 60 mmol), 4-bromo-4'-hydroxybiphenyl (10 g, 40 mmol), and potassium carbonate (16.6 g, 120 mmol) was dissolved in butan-2-one (100 mL) and reacted under reflux for 24 hrs. After cooling to room temperature, the potassium salt was filtered off. The solvent was removed by rotavapor and the crude product was recrystallized from petroleum ether (bp 35-60 °C) to yield a white solid (19.5 g, 54 mmol).²⁰ ¹H NMR (ppm, CDCl₃), δ : 0.89 (t, J = 6.9 Hz, 3H), 1.29-1.47 (m, 10 H), 1.80 (quintet, J = 6.6 Hz, 2H), 3.98 (t, J = 6.6 Hz, 2 H), 6.99 (d, J = 6.9 Hz, 2H), 7.40-7.54 (m, 6H).

4'-Octoxybiphenyl-4-ylboronic Acid (7). 4-Bromo-4'-octoxybiphenyl (10 g, 28 mmol) was treated with magnesium (1.0 g, 42 mmol) in 250ml of dry THF under nitrogen. The reaction mixture was refluxed for 10 hrs to form Grignard reagent and then it was added dropwise to trimethyl borate solution (8.6 g, 83 mmol) at -78°C. The mixture solution was allowed to cool to room temperature overnight. The final solution was acidified with 10 % HCl solution (100 mL) and stirred for 45 mins at room temperature. The solution was washed with saturated sodium carbonate solution and water and then THF was removed. The crude product was extracted by diethyl ether and the organic layer was dried over magnesium sulfate. After removing the solvent by rotavapor, the resulting solid was washed with petroleum ether and briefly dried on filter to obtain a white solid (5.2 g, 54 %).²⁰ ¹H NMR (ppm, d₆-DMSO), δ : 0.85 (t, J = 7.2 Hz, 3 H), 1.24-1.41 (m, 10 H), 1.71 (quintet, J = 6.6 Hz, 2H), 3.98 (t, J = 6.6 Hz, 2 H), 6.99 (d, J = 6.9 Hz, 2 H), 7.56-7.62 (m, 4 H), 7.83 (d, J = 6.3 Hz, 2 H), 8.03 (s, 2 H).

FOC₈ (8). The compound **6** (2.7 g, 5.0 mmol), 4'-octoxybiphenyl-4-ylboronic acid (**7**) (4.0 g, 12.2mmol), and tetrakis(triphenylphosphine)palladium(0) were reacted in THF (180 mL) for 10 mins, and then 100 mL of 2 M aqueous Na₂CO₃ solution was added. The reaction mixture was refluxed for 48 hrs. The cooled solution was washed

with dilute hydrochloric acid (10 %) and water, and dried over magnesium sulfate. The final solution was purified by column chromatography (silica gel, CH₂Cl₂) to yield a yellow-green solid (2.9 g, 62 %). ¹H NMR (ppm, CDCl₃), δ: 0.40 (t, *J* = 7.3 Hz, 6 H), 1.24-1.47 (m, 30 H), 2.11 (q, *J* = 7.3 Hz, 4 H), 3.99 (t, *J* = 6.6 Hz, 4 H), 6.97 (d, *J* = 8.7 Hz, 4 H), 7.33 (d, *J* = 3.9 Hz, 2 H), 7.36 (d, *J* = 3.9 Hz, 2 H), 7.53-7.71 (m, 18 H). Element analysis for C₆₅H₇₀O₂S₂: Calc. C, 82.41; H, 7.45; Found C, 82.35; H, 7.42%. LRMS (FAB+) Calc. 946.5; Found 946.5.

FOH (9), FOC₈ (8) (2.6 g, 2.7 mmol) was dissolved in dry chloroform (100 mL) under nitrogen and then boron tribromide (2.1g, 8.2 mmol) was added dropwise and reacted at -78°C. The mixture was allowed to warm up to room temperature and reacted for 24 hrs. The solution was washed with sodium hydroxide (1 M, 50 ml) to basification. Then, the solution was acidified with 10 % HCl and stirred for 4 hrs. Finally, the suspension was filtered off and purified by column chromatography (silica gel, ethyl acetate) to yield a green solid (1.5 g, 76 %). ¹H NMR (ppm, d₆-DMSO), δ: 0.29 (t, *J* = 7.2 Hz, 6 H), 2.16 (q, *J* = 7.2 Hz, 4 H), 6.86 (d, *J* = 8.8 Hz, 4 H), 7.55 (d, *J* = 8.8 Hz, 4 H), 7.60 (d, *J* = 3.9 Hz, 2 H), 7.64-7.78 (m, 14 H), 7.87 (d, *J* = 8.1 Hz, 2 H), 9.60 (s, 2 H).

FOC₁₆ (10), FOHOC₈ (11), and FOHOC₁₆ (12). Compounds **10-12** were synthesized using the same procedure, so a representative example is described for **FOC₁₆ (10)**. **FOH (9)** (300 mg, 0.41 mmol) and potassium carbonate (115 mg, 0.83 mmol) were dissolved in DMF (20 mL) and then 1-bromohexadecane (218 mg, 0.87 mmol) was added in solution to react for 24 hrs by reflux. After cooling to room temperature, the solution was extracted with dichloromethane and water, and the organic layer was dried over magnesium sulfate. The final solution was purified by column chromatography (silica gel, CH₂Cl₂) to yield a yellow-green solid (312 mg, 71%). ¹H NMR (ppm, CDCl₃), δ: 0.40 (t, *J* = 7.3 Hz, 6 H), 1.21-1.48 (m, 62 H), 2.11

(q, $J = 7.3$ Hz, 4 H), 3.99 (t, $J = 6.6$ Hz, 4 H), 6.97 (d, $J = 8.7$ Hz, 4 H), 7.33 (d, $J = 3.6$ Hz, 2 H), 7.37 (d, $J = 3.6$ Hz, 2 H), 7.53-7.71 (m, 18 H). Element analysis for $C_{81}H_{102}O_2S_2$: Calc. C, 83.02; H, 8.77%; Found C, 82.77; H, 8.53%. LRMS (FAB+) Calc. 1171.7; Found 1171.7.

FOHOC₈ (11). Yield, 50 %. 1H NMR (ppm, $CDCl_3$), δ : 0.40 (t, $J = 7.0$ Hz, 6H), 0.87 (t, $J = 6.6$ Hz, 3H), 1.28-1.42 (m, 10 H), 1.79 (m, $J = 6.9$ Hz, 2 H), 2.11 (q, $J = 7.2$ Hz, 4 H), 3.99 (t, $J = 6.2$ Hz, 2 H), 4.90 (s, 1 H), 6.89-6.98 (m, 4 H), 7.33-7.36 (m, 4 H), 7.50-7.70 (m, 18 H). Element analysis for $C_{57}H_{54}O_2S_2$: Calc. C, 81.97; H, 6.52; Found C, 81.76; H, 6.78%.

FOHOC₁₆ (12). Yield, 43 %. 1H NMR (ppm, $CDCl_3$), δ : 0.40 (t, $J = 7.5$ Hz, 6Hz), 0.87 (t, $J = 6.6$ Hz, 3 H), 1.25-1.46 (m, 26 H), 1.80 (m, $J = 7.5$ Hz, 2 H), 2.11 (q, $J = 7.5$ Hz, 4 H), 3.99 (t, $J = 6.6$ Hz, 2 H), 4.80 (s, 1 H), 6.90-6.98 (m, 4 H), 7.33-7.37 (m, 4 H), 7.50-7.70 (m, 18 H). Element analysis for $C_{65}H_{70}O_2S_2$: Calc. C, 82.41; H, 7.45; Found C, 82.1; H, 7.75%.

Methoxy poly(ethyleneoxy)ethyl tosylate (15, 16). Poly(ethylene oxide) monomethyl ether ($n = 17$, 5 g, 6.6 mmol) (**15**) was dissolved in dry pyridine (5 ml) under nitrogen and then a solution of toluene-*p*-sulfonyl chloride (1.4 g, 7.3 mmol) in 5 ml dry pyridine was added to the mixture. The mixture was reacted at room temperature under nitrogen for 24 hrs. The resulting solution was washed with water and extracted with dichloromethane. The solution of dichloromethane was dried over magnesium sulfate. The solvent was removed by rotavapor, and the crude product was purified by column chromatography (silica gel, ethyl acetate) to obtain a colorless liquid (4.8 g, 80 %). 1H NMR (ppm, $CDCl_3$), δ : 2.37 (s, 3 H), 3.38 (s, 3 H), 3.50 - 4.07 (m, 68H), 7.31 (d, $J = 8.0$ Hz, 2H), 7.77 (d, $J = 8.0$ Hz, 2H).

Poly(ethylene oxide) monomethyl ether ($n = 44$) (16) Yield, 66 %. 1H NMR (ppm, $CDCl_3$), δ : 2.31 (s, 3H), 3.37 (s, 3H), 3.54- 4.02 (m, 176H), 7.11 (d, Ar-H, $J =$

7.8 Hz, 2H), 7.74 (d, Ar-H, $J = 8.1$ Hz, 2H).

Polymers. FOC₈PEO₁₇ (17), FOC₁₆PEO₁₇ (18), FOC₈PEO₄₄ (19), and FOC₁₆PEO₄₄ (20). Polymers **17-20** were synthesized using the same procedure, so a representative example is described for **FOC₈PEO₁₇ (17)**. **FOHOC₈ (11)** (150 mg, 0.18 mmol), potassium carbonate (75 mg, 0.53 mmol), and methoxy poly(ethyleneoxy)ethyl tosylate **15** (244 mg, 0.27 mmol) were refluxed in DMF for 24 hrs. After cooling to room temperature, the solution was extracted with dichloromethane and water, and the organic layer was dried over magnesium sulfate. The final solution was purified by column chromatography (silica gel, CH₂Cl₂/methanol 5:1) to obtain **FOC₈PEO₁₇ (17)** (yellow solid, 126 mg, 45 %). ¹H NMR (ppm, CDCl₃), δ : 0.39 (t, $J = 7.5$ Hz, 6H), 0.87 (t, $J = 6.6$ Hz, 3H), 1.27-1.46 (m, 10 H), 1.77 (m, $J = 6.9$ Hz, 2 H), 2.10 (q, $J = 7.5$ Hz, 4 H), 3.39 (s, 3 H), 3.51-3.75 (m, 64 H), 3.87 (t, $J = 5.1$ Hz, 2H), 3.99 (t, $J = 6.6$ Hz, 2H), 4.17 (t, $J = 5.1$ Hz, 2H), 6.95-7.00 (m, 4H), 7.33-7.37 (m, 4H), 7.53-7.71 (m, 18H). LRMS (FAB+) Calc. 1552.8; Found 1552.8. Polydispersity index (PDI) = 1.09.

FOC₁₆PEO₁₇ (18). Yield, 34 %. ¹H NMR (ppm, CDCl₃), δ : 0.40 (t, $J = 7.2$ Hz, 6H), 0.87 (t, $J = 6.6$ Hz, 3H), 1.28-1.44 (m, 26 H), 1.78 (m, $J = 6.9$ Hz, 2H), 2.11 (q, $J = 7.5$ Hz, 4H), 3.39 (s, 3H), 3.50-3.75 (m, 64H), 3.86 (t, $J = 5.1$ Hz, 2H), 3.99 (t, $J = 6.6$ Hz, 2H), 4.17 (t, $J = 5.1$ Hz, 2H), 6.95-7.00 (m, 4 H), 7.33-7.37 (m, 4 H), 7.53-7.71 (m, 18 H). LRMS (FAB+) Calc. 1664.9; Found 1665.0. Polydispersity index (PDI) = 1.09.

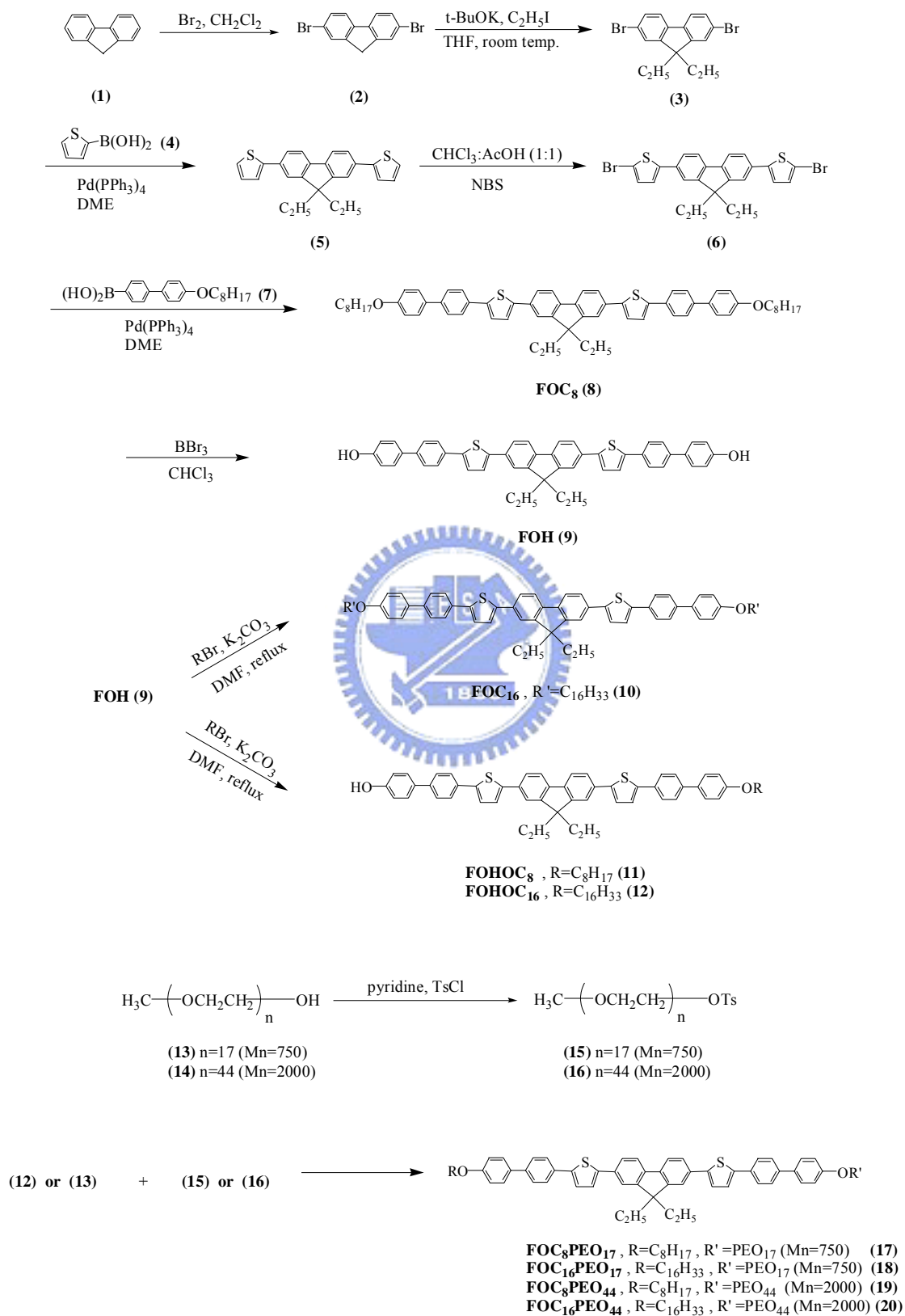
FOC₈PEO₄₄ (19). Yield, 41 %. ¹H NMR (ppm, CDCl₃), δ : 0.41 (t, $J = 7.5$ Hz, 6H), 0.85 (t, $J = 6.6$ Hz, 3H), 1.23-1.46 (m, 10 H), 1.77 (m, $J = 7.5$ Hz, 2H), 2.12 (q, $J = 7.5$ Hz, 4H), 3.36 (s, 3H), 3.52-3.71 (m, 172 H), 3.87 (t, $J = 4.7$ Hz, 2H), 3.99 (t, $J = 6.6$ Hz, 2H), 4.17 (t, $J = 5.1$ Hz, 2H), 6.95-7.00 (m, 4H), 7.34-7.37 (m, 4H), 7.53-7.71 (m, 18H). LRMS (FAB+) Calc. 2785.5; Found 2785.5. Polydispersity index

(PDI) = 1.10.

FOC₁₆PEO₄₄ (20). Yield, 35 %. ¹H NMR (ppm, CDCl₃), δ: 0.39 (t, *J* = 7.5 Hz, 6H), 0.86 (t, *J* = 6.9 Hz, 3H), 1.25-1.46(m, 26H), 1.79 (m, *J* = 7.5 Hz, 2H), 2.12 (q, *J* = 7.2 Hz, 4H), 3.36 (s, 3H), 3.51-3.75 (m, 172 H), 3.87 (t, *J* = 4.8Hz, 2H), 3.99 (t, *J* = 6.6 Hz, 2H), 4.17 (t, *J* = 4.8 Hz, 2H), 6.95-7.00 (m, 4H), 7.33-7.37 (m, 4H) , 7.53-7.71 (m, 18 H). LRMS (FAB+) Calc. 2897.6; Found 2897.6. Polydispersity index (PDI) = 1.09.



Scheme 2.1 Synthetic Routes of Synthesized Molecules

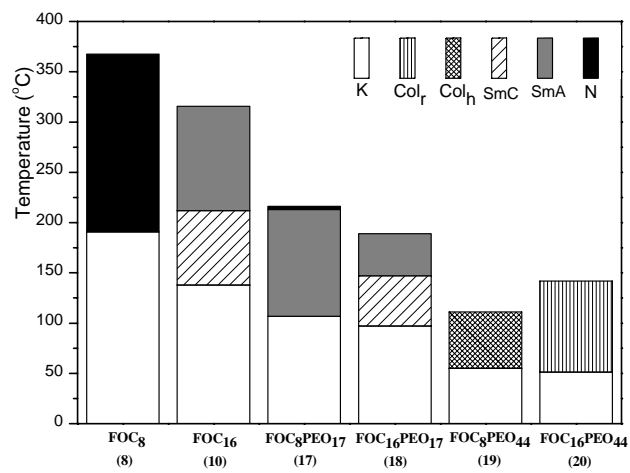


2.3 Results and Discussion

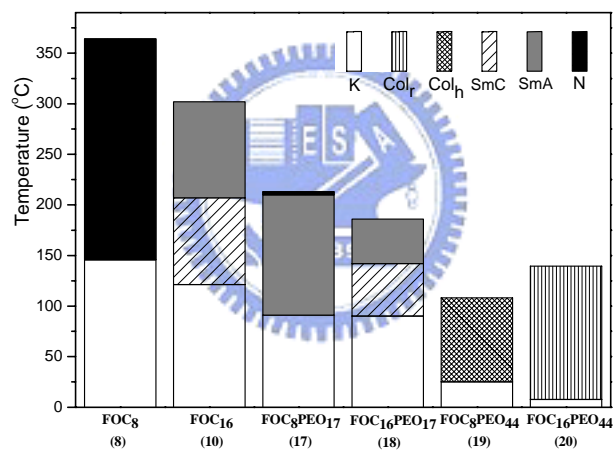
2.3.1. Thermal Properties

A series of conjugated aromatic molecules containing fluorene, thiophene, and biphenyl groups were synthesized successfully via Suzuki coupling reaction. These aromatic rings were connected by single bonds and alkoxy groups with different lengths ($-\text{OC}_8\text{H}_{17}$, and $-\text{OC}_{16}\text{H}_{33}$) were attached to the conjugated cores either on both sides or on one side of the molecules to form symmetrical and asymmetrical structures (as shown in scheme 2.1), respectively. The analogous derivatives containing alkoxy chains on both sides of the rigid cores are symmetrical molecules. Besides these alkoxy groups, two kinds of commercially available poly (ethylene oxide) monomethyl ethers ($n = 17$ and 44) were used as the other flexible chains to form rod-coil asymmetrical molecules.

As previous literatures showed that the phase behaviors of polymers, especially, those with low molecular weights, were influenced by polydispersity.²¹ Therefore, highly monodisperse polymers are important to investigate the representative phase behavior of rod-coil polymers. The rod-coil asymmetrical molecules containing poly(ethylene oxide) monomethyl esters as flexible chains showed polydispersity indexes (PDI) around 1.1 which were determined by GPC. The phase transition temperatures and enthalpies of all compounds were obtained from DSC traces (the second heating and first cooling scans) and summarized in Table 2.1. In addition, the phase diagrams of mesophases (during heating and cooling scans) are presented in Figure 1.1. Figure 2.2 shows that various characteristic textures of all corresponding mesophases observed by POM.



(a)



(b)

Figure 2.1 Phase diagrams of mesophases in all materials upon (a) heating, (b) cooling.

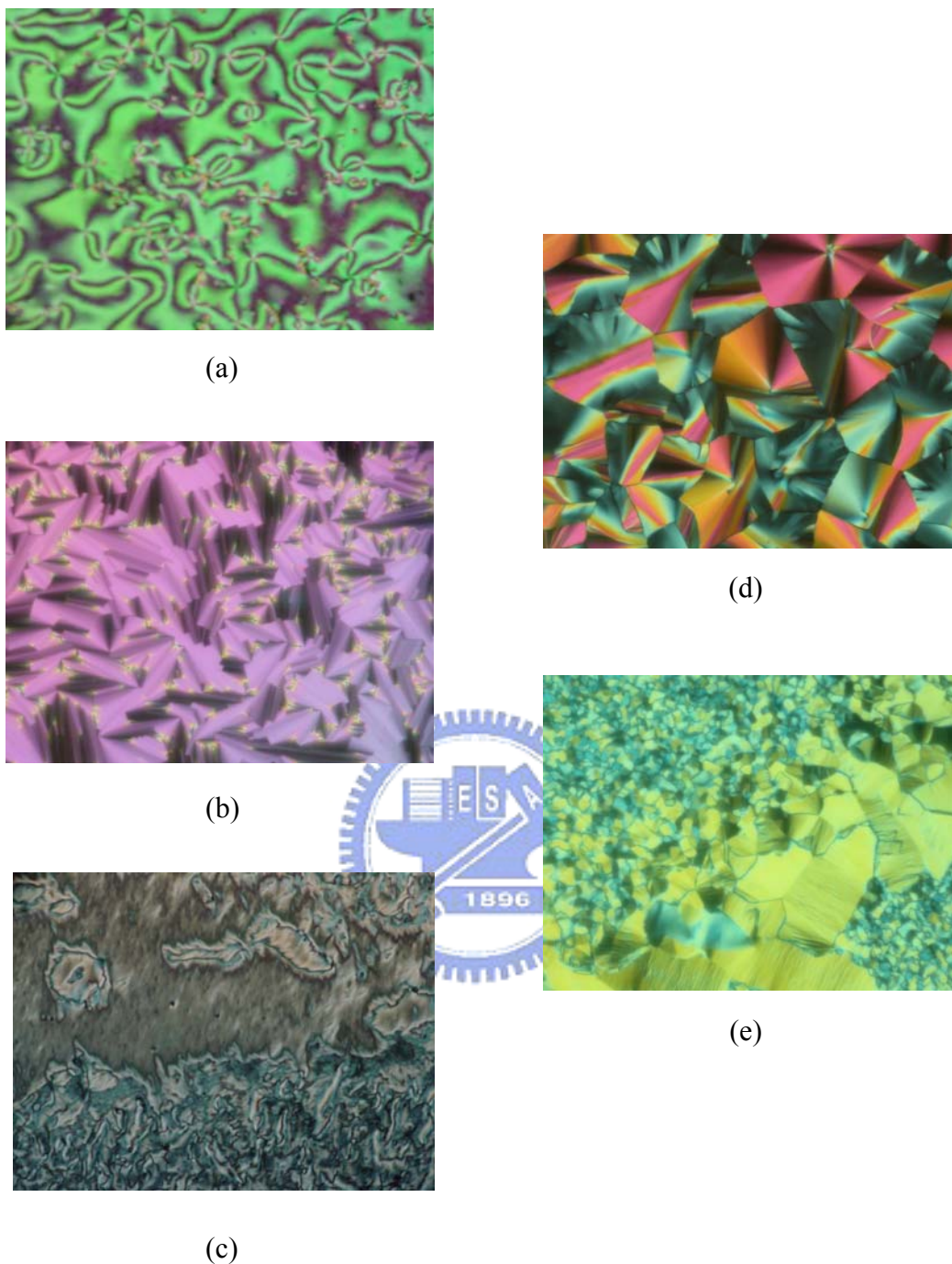


Figure 2.2 The optical textures of the mesophases observed by POM. (a) The nematic phase in **FOC₈ (8)** at 280°C (cooling). (b) The SmA phase in **FOC₈PEO₁₇ (17)** at 200°C (heating). (c) The SmC phase in **FOC₁₆ (10)** at 175°C (cooling). (d) The Col_h phase in **FOC₈PEO₄₄ (19)** at 115°C (cooling). (e) The Col_r phase in **FOC₁₆PEO₄₄ (20)** at 139°C (heating)

Table 2.1 Phase Behavior of Synthesized Molecules^{a,b}

Sample	Heating	Cooling
FOC₈ (8)	<i>K</i> 191.6 (25.6) <i>K'</i> 197.1 (5.1) <i>N</i> 368.5 (2.9) <i>I</i>	<i>I</i> 364.0 (-2.6) <i>N</i> 146.8 (-25.5) <i>K</i>
FOC₁₆ (10)	<i>K</i> 138.0 (7.5) <i>S_C</i> 212.2 (1.6) <i>S_A</i> 305 <i>I</i>	<i>I</i> 302 <i>S_A</i> 207.2 (-2.5) <i>S_C</i> 121.9 (-7.5) <i>K</i>
FOC₈PEO₁₇ (17)	<i>K</i> 107.2 (8.0) <i>S_A</i> 213.3 <i>N</i> 216.5 (0.1) <i>I</i>	<i>I</i> 213.0 (-0.1) <i>N</i> 210.2 <i>S_A</i> 91.0 (-5.7) <i>K</i>
FOC₁₆PEO₁₇ (18)	<i>K</i> 97.3 (3.6) <i>S_C</i> 147.5 (3.0) <i>S_A</i> 189.6 (2.6) <i>I</i>	<i>I</i> 186.2 (-2.8) <i>S_A</i> 142.3 (-2.3) <i>S_C</i> 90.8 (-2.3) <i>K</i>
FOC₈PEO₄₄ (19)	<i>K</i> 55.4 (112.5) <i>Col_h</i> 111.1 (1.3) <i>I</i>	<i>I</i> 108.5 (-1.2) <i>Col_h</i> 25.5 (-107.8) <i>K</i>
FOC₁₆PEO₄₄ (20)	<i>K</i> 51.5 (79.4) <i>Col_r</i> 141.6 (1.6) <i>I</i>	<i>I</i> 139.3 (-1.4) <i>Col_r</i> 7.8 (-68.9) <i>K</i>

^a Transition temperatures (°C) and enthalpies (in parentheses, kJ/mol) were determined by DSC (heating and cooling rate of 10°C/min).

^b **K** = crystalline; **S_A** = smectic A; **S_C** = smectic C; **N** = nematic; **Col_h** = hexagonal columnar phase. **Col_r** = rectangular columnar phase.

For symmetrical molecules, **FOC₈** and **FOC₁₆** exhibit the nematic and the smectic mesophases, respectively, which match the trends that the smectic phases are preferred in LC structures possessing longer flexible lengths. It is known that extending alkoxy chain length leads to the increasing lateral intermolecular interaction of flexible parts and the decreasing longitudinal interaction of rigid rods.²² As a result, **FOC₁₆** exhibits the smectic A and smectic C phases instead of the nematic phase in **FOC₈** (see Table 2.1 and Figure 2.1). In case of asymmetrical rod-coil molecules containing poly(ethylene oxide) of $n = 17$, both **FOC₈PEO₁₇** and **FOC₁₆PEO₁₇** display the smectic phases (see Table 2.1 and Figure 2.1), but **FOC₈PEO₁₇** reveals a short range of the nematic phase at high temperatures due to the shorter flexible octanoxo chain. Nevertheless, as temperature decreases, the immiscibility between the hydrophilic flexible chains and the hydrophobic rods leads to stronger lateral interaction of rigid rods and induces the smectic phases. By increasing the hydrophilic ethylene oxide units, the immiscibility increase and microphase-separation is enhanced to form more order columnar phases. For instance, **FOC₈PEO₄₄** and

FOC₁₆PEO₄₄ consisting of poly(ethylene oxide) of $n = 44$ exhibit two kinds of columnar phases, Col_h and Col_r (see Table 2.1 and Figure 2.1). The characterization of the columnar phases (i.e. Col_h and Col_r) are identified by POM, as shown in Figure 2.2(d) and 2.2(e), and can be further confirmed by X-Ray diffraction (XRD) measurements. It is not unusual for **FOC₈PEO₄₄** and **FOC₁₆PEO₄₄** to form highly order columnar phases because microphase separation between stiff rod and flexible coil segments occur as the number of ethylene oxide units increase.

In general, the melting temperatures (T_m) decrease with increasing the lengths of flexible chains, i.e. alkoxy chains in symmetrical molecules and ethylene oxide units in asymmetrical molecules. Besides, the trend of the isotropization temperature (T_i) is similar to that of T_m . In terms of symmetrical molecules, **FOC₈** and **FOC₁₆**, they have lower viscosity at mesophasic temperatures and thus to have well-organized mesomorphic textures, i.e. the nematic, smectic A, and smectic C phases shown in Figure 2.2(a), 2.2(b), and 2.2(c), owing to their lower molecular weights compared with analogous rod-coil compounds. Because of the higher flexibility of ethylene oxide units, rod-coil polymers possess lower transition temperatures of T_m and T_i than their corresponding symmetrical molecules. Accordingly, the transition temperatures and the nature of the mesophases of rod-coil molecules are dependent on the lengths of the flexible chains in alkoxy and poly(ethylene oxide) units.

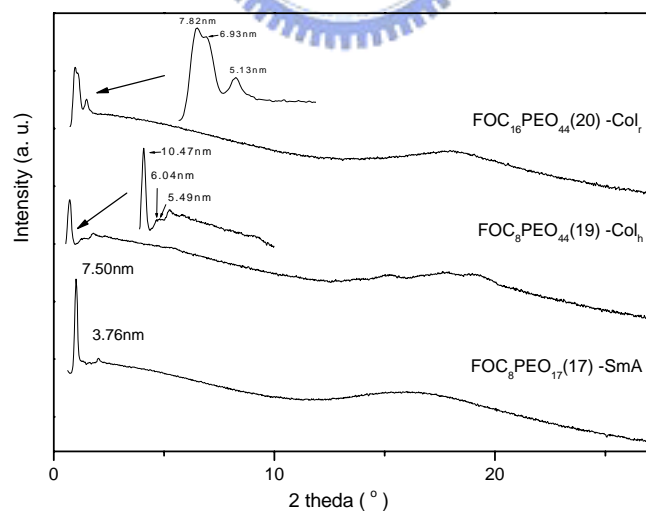
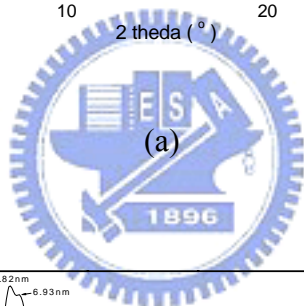
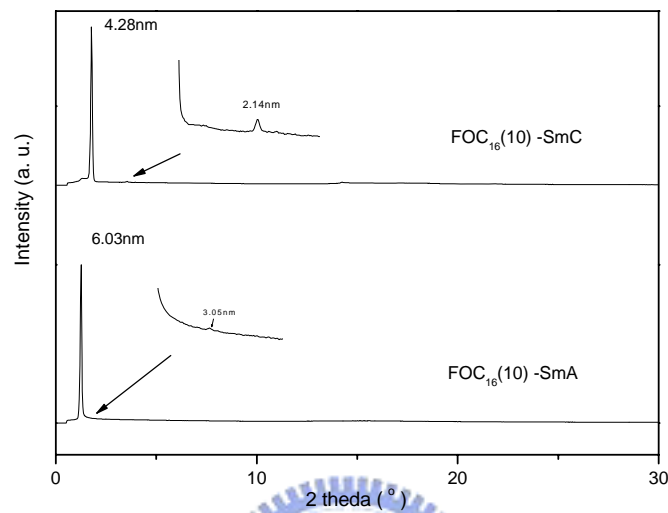
2.3.2 X-ray Investigation

In order to elucidate the structure of the mesophases, X-Ray diffraction (XRD) measurements were carried out at the temperature ranges of mesophases for compounds **FOC₁₆**, **FOC₈PEO₁₇**, **FOC₈PEO₄₄**, and **FOC₁₆PEO₄₄**. As shown in Figure 2.3(a), the XRD patterns of **FOC₁₆** indicate the layer d-spacing at 270°C and 150°C are 6.03 nm and 4.28 nm, respectively. In addition, the layer d-spacing values

in the ratio of 1:1/2 indicate a lamellar order exists in the mesophases. With regard to the fully-extended molecular length (L) of 5.91 nm by the molecular modeling calculation, it suggests that the d-spacing value of 6.03 nm corresponds to the monolayer SmA phase of **FOC₁₆** at 175°C. Upon cooling to 115°C, the layer d-spacing, i.e. 4.28 nm, is shorter than the theoretical molecular length (L = 5.91 nm), so it implies a tilted SmC phase with a tilt angle of 43° (by θ calculation of $d = L \times \cos\theta$) to the layer normal.⁴ In Figure 2.3(b), **FOC₈PEO₁₇** possessing the layer d-spacing, 7.50 nm (L = 7.60 nm by the molecular modeling calculation) obtained from the XRD pattern, also shows the monolayer SmA phase, which is longer than that of **FOC₁₆** due to the longer flexible chains of poly(ethylene oxide) with n = 17 than those of alkoxy chains.

As shown in the middle pattern of Figure 2.3(b), compound **FOC₈PEO₄₄** in the mesophase displays reflection peaks at $d_1 = 10.47$ nm, $d_2 = 6.04$ nm, and $d_3 = 5.49$ nm in the small angle region, and the ratio of the d-layer spacing values is about 1: $(1/3)^{1/2}$: $(1/2)$, and the lattice parameter calculates for $a = 12.09$ nm. Furthermore, a typical pseudo focal-conic texture was clearly observed by POM as shown in Figure 2.2(d), which is the characteristic of the hexagonal columnar phase (Col_h). On the top XRD pattern of Figure 2.3(b), the small angle region of **FOC₁₆PEO₄₄** exhibits strong coupling twin peaks (at $d_1 = 7.82$ nm and $d_2 = 6.93$ nm) along with a weaker peak (at $d_3 = 5.13$ nm), which correspond to the rectangular lattice constants: $a = 15.64$ nm, $b = 7.75$ nm. This type of diffraction pattern with two stronger peaks or one additional weaker peak at small-angles corresponds to the rectangular columnar arrangement (Col_r).²³⁻²⁵ Besides the evidence of the XRD data, the mosaic texture of **FOC₁₆PEO₄₄** in Figure 2.2(e) supported by POM can be recognized as the rectangular columnar phase (Col_r). Therefore, in addition to the characteristic textures of mesophases observed by POM, the types of the mesophases and the molecular arrangements can

be further proved and analyzed by the results of XRD measurements, which are strongly dependent on the lengths of the flexible alkoxy and poly (ethylene oxide) units.



(b)

Figure 2.3 X-ray diffraction data (a) SmA (270°C) and SmC (150°C) phases of $\text{FOC}_{16}(\text{10})$ (b) SmA (120°C) phase of $\text{FOC}_8\text{PEO}_{17}(\text{17})$, Col_h (50°C) phase of $\text{FOC}_8\text{PEO}_{44}(\text{19})$ and Col_r (30°C) phase of $\text{FOC}_{16}\text{PEO}_{44}(\text{20})$.

2.3.3 Photoluminescent (PL) and Electroluminescent (EL) Properties

The photophysical properties of all luminescent compounds were studied by photoluminescence (PL) and UV-visible absorption spectra in dilute chloroform solutions and thin films. The optical properties of all compounds are summarized in Table 2.2. Due to the identical rigid cores, all synthesized materials in solutions have almost the same maximum absorption wavelength around 400nm in solutions and 390nm in films. Similar to the absorption spectra, the maximum PL wavelength of all compounds are around 448 nm in solutions and 496 nm in films, respectively. Compared with the maximum PL wavelength in solutions, the materials in thin films exhibit red-shifted PL emission owing to the π - π^* aggregation of the rigid cores. It is unexpected that the maximum absorption wavelength in solid state (390nm) is more blue-shifted than in solution (400nm). In terms of the onset wavelengths (λ_{onset}) of UV-visible absorption spectra, it exhibits that the λ_{onset} is around 469 nm in films and 446 nm in solutions. Therefore, the optical band gaps (calculated by the equation: $E^{\text{onset}} = 1240 / \lambda_{\text{onset}}$) in film are smaller than in solutions and this is because of the π - π^* aggregation of the rigid cores in films. Figure 2.4(a) shows an example of the UV-Visible and PL spectra of the rod-coil molecule, **FOC₈PEO₄₄**. In figure 2.4(b), the influence of the flexible chain lengths in PL spectra are compared. It shows that the intensity of the shorter wavelength peak at 464 nm grows as the flexible chains increase because the flexible chains of poly(ethylene oxide)s seem to be as solid solvents to insulate the intermolecular aggregation. Moreover, in order to realize the relation of two peaks between 464 nm and 496 nm, figure 2.5(a) shows the normalized photoluminescence excitation (PLE) spectra of **FOC₈PEO₁₇** in the same film monitored the emissions at 464 nm and 496 nm. The patterns of PLE spectra monitored at 464 nm and 496 nm almost coincide with each other. It demonstrated that the shorter wavelength peak at 464 nm is a vibronic peak but not the

non-aggregated molecular emission. The joined flexible chains of poly(ethylene oxide)s in molecule change the state of the whole molecular aggregation which lead to change the distribution of the emission energy in PL spectra. Therefore, we suppose that the two peaks in PL spectra at 464 nm and 496 nm are the nature emission of the materials but not the co-existence of aggregated and non-aggregated emissions. Besides the insulation of the molecules, we believe that bulky poly(ethylene oxide) chains would influence the conformation of the rigid cyclic backbone.²⁶ For these reasons, we might predict that the peak at 464nm will continue growing and the peak at 496nm decreasing as keeping on poly(ethylene oxide) length increase. Finally, it will be a blue-shifted spectrum. Furthermore, this prediction might be proved by the EL spectra of our PLED devices (the emitter were doped in PVK which behaves as a solid solvent) in figure 2.6(a). Figure 2.6(a) shows the EL spectra of analogous compounds and the maximum EL wavelengths are around 462 nm which correspond to the growing peak at 464nm and decreasing peak at 496nm in figure 2.4(b). Figure 2.5(b) displays the PL spectra of **FOC₈PEO₄₄** in solid state and in Col_h phase (50°C). At mesomorphic temperature, the molecule, **FOC₈PEO₄₄**, was self-assembled to highly order Col_h phase and it lead to the aggregation of the rigid cores. Hence, the PL spectra in solid state are red-shifted and the shorter wavelength peak at 464 nm became a shoulder.

Table 2.2 Absorption and Photoluminescence Spectral Data of Synthesized Molecules

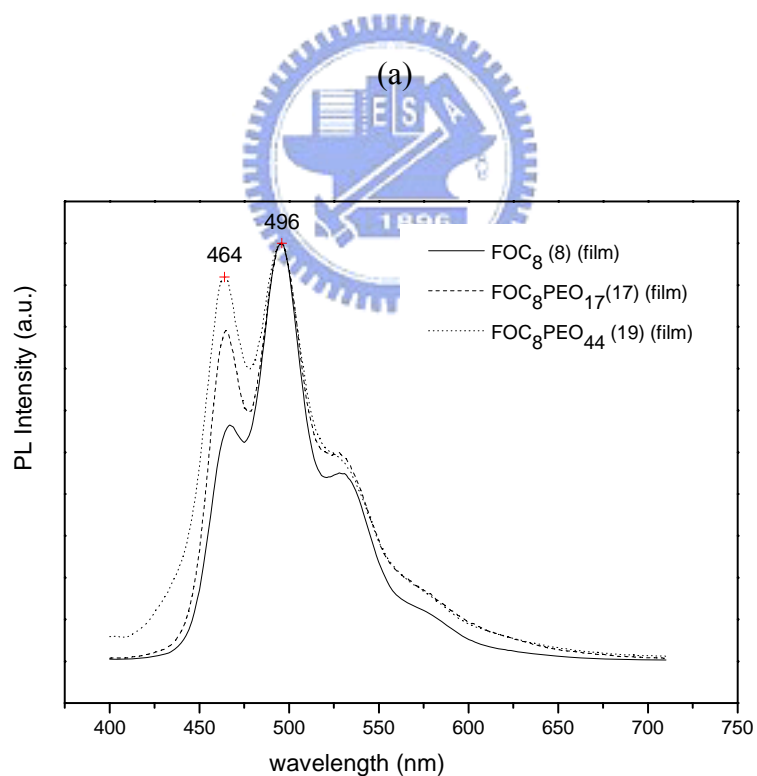
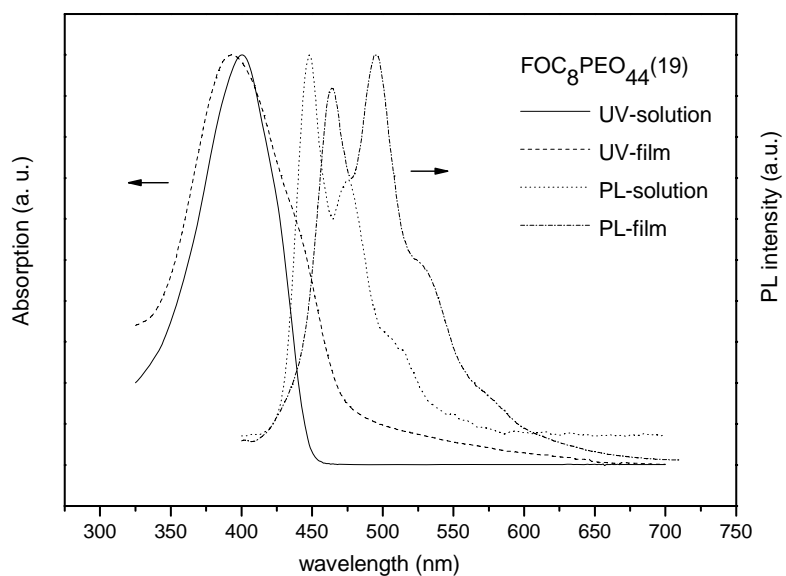
Sample	absorption λ_{\max} (nm)		PL emission λ_{\max} (nm)		Φ (solution) ^b	Φ (film) ^c
	solution ^a	film	solution ^a	film		
FOC₈ (8)	401	382	447	496	0.69	0.36
FOC₁₆ (10)	400	382	448	498	0.70	0.38
FOC₈PEO₁₇ (17)	400	387	448	496	0.71	0.43
FOC₁₆PEO₁₇ (18)	400	386	448	497	0.70	0.42
FOC₈PEO₄₄ (19)	400	393	448	496	0.72	0.47
FOC₁₆PEO₄₄ (20)	401	390	448	497	0.71	0.47

^a Absorption and PL emission spectra were recorded in dilute CHCl₃ solutions at room temperature.

^b PL quantum yield in CHCl₃ and 9,10-Diphenylanthrance is the reference of quantum yield.

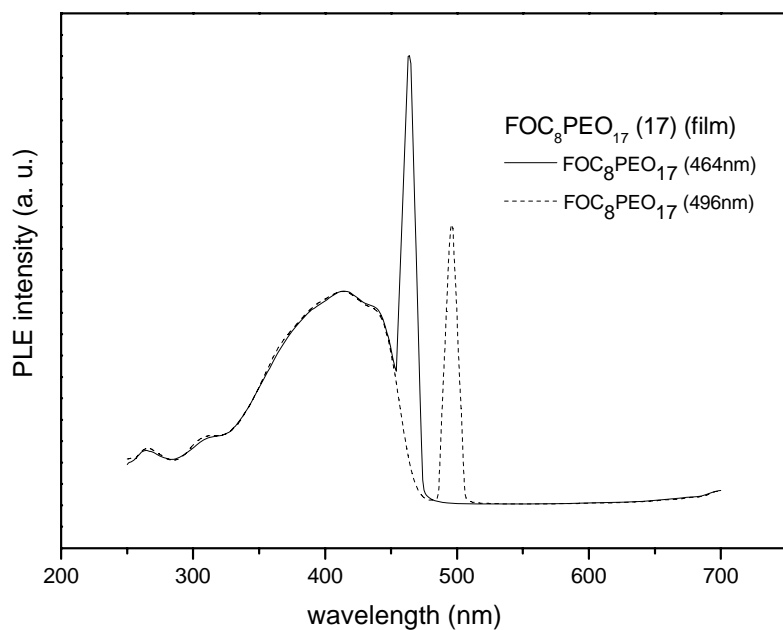
^c Solid film of 9,10-Diphenylanthrance blended in PMMA is the reference of quantum yield.



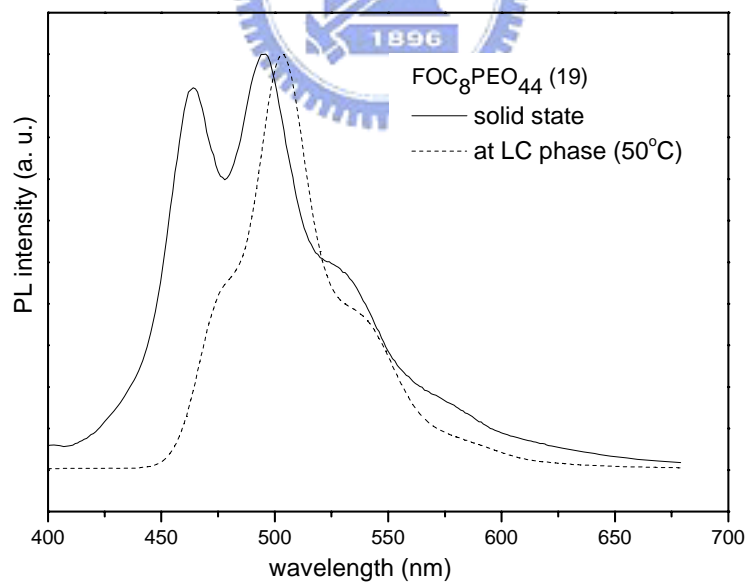


(b)

Figure 2.4 (a) Absorption and PL spectra of **FOC₈PEO₄₄ (19)** in solutions (CHCl₃ as solvent) and films. (b) PL spectra of films of materials contain different flexible chains.



(a)



(b)

Figure 2.5 (a) PLE spectra of **FOC₈PEO₁₇ (17)** film monitored at 464 nm and 496 nm respectively (normalized at 412 nm). (b) PL spectra of **FOC₈PEO₄₄ (19)** in solid state and at 50°C (Col_h phase).

To fit the energy band structures of PLED devices, it is necessary to determine the

energy levels of the highest occupied molecular orbital (HOMO) and the lowest unoccupied molecular orbital (LUMO) in each component, which were carried out by CV measurements to investigate the redox behavior of the molecules in solutions (CH₂Cl₂ as solvent). The potential values estimated here were based on the reference energy level of ferrocene (4.8 eV below the vacuum level) according to the following equation:²⁷ $E^{\text{HOMO}}/E^{\text{LUMO}} = [-(E^{\text{onset}} - 0.45) - 4.8]$ eV. The onset potentials were determined from the intersection of two tangents drawn at the rising and background currents of the cyclic voltammogram. A crude estimation of the LUMO levels of reduction compounds were deduced from the HOMO values and the optical band gaps. The HOMO and LUMO energies are summarized in Table 2.3. As expected, HOMO and LUMO energies are almost similar on account of the identical rigid cores.

Table 2.3 HOMO and LUMO Energies, and Electrochemical Properties

Sample	$E^{\text{ox/onset}}$ (eV)	E^{HOMO} (eV) ^a	E^{LUMO} (eV) ^b	$E^{\text{opt.}}$ (eV) ^c
FOC₈ (8)	0.83	-5.49	-2.71	2.78
FOC₈PEO₁₇ (17)	0.83	-5.5	-2.72	2.78
FOC₈PEO₄₄ (20)	0.81	-5.48	-2.7	2.78

^a HOMO energies were obtained from the cyclic voltammetry.

^b LUMO energies were deduced from HOMO values and optical band gaps.

^c Optical band gaps were obtained from the UV-Visible spectra.

Due to the poor film quality of the synthesized molecules, the emitters were doped into PVK to fabricate PLED devices. A series of double-layered EL devices with the configuration of PVK:emitters(100:8 by weight)/TPBI(30 nm)/MgAg(50 nm)/Ag(100 nm) were made by spin-coating of PVK blended with the synthesized emitters (100:8 by weight) onto indium-tin oxide (ITO) glass substrates, and their EL data are demonstrated in Table 2.4. In Figure 2.5(a), It is reasonable to expect that the maximum EL wavelengths around 462 nm (they are not optimized devices) because

the emitters are doped into PVK which behaves as a solid solvent. The current-voltage and luminescence-voltage, i.e. EL response, curves of one typical PLED device (PVK:FOC₈(100:8 by weight)/TPBI /MgAg/Ag) is displayed in Figure 2.5(b). All these devices show turn-on voltages for current and turn-on voltages for light from 8 to 10 V, and their attainable maximum luminances are from 1045 to 2871 cd/m².

Table 2.4 EL Data of PLED Devices^a

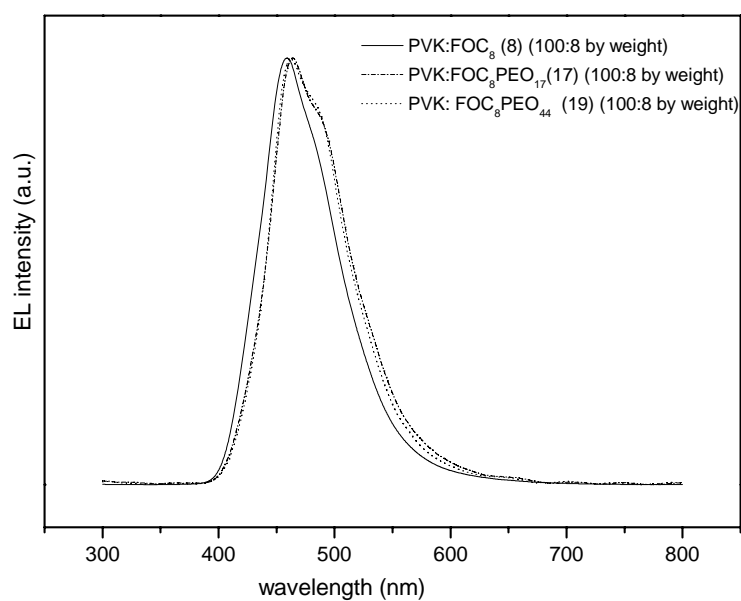
Sample	$\lambda_{\text{max, EL}}$ (nm)	V_{on} (V) ^b	V_{on} (V) ^c	Max. Luminance (cd/m ²)	Φ_{F} (%)
FOC₈ (8)	460	9.5	9.5	2871	0.23
JFOC₈PEO₁₇ (17)	464	8	8	2126	0.39
FOC₈PEO₄₄ (20)	462	10	10	1045	0.38

^a PVK:emitters(100:8 by weight)/TPBI(30 nm)/MgAg(50 nm)/Ag(100 nm).

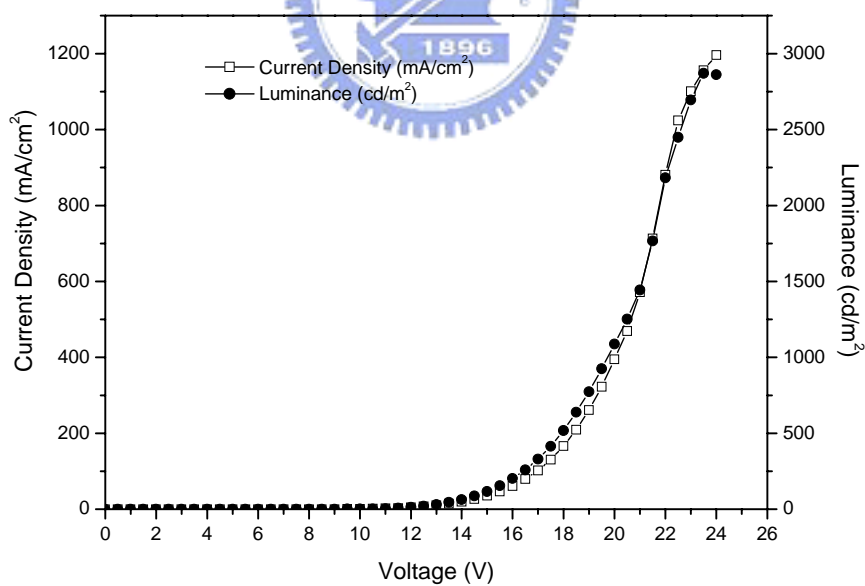
^b V_{on} is the turn on voltage of current.

^c V_{on} is the turn on voltage of light.





(a)



(b)

Figure 2.6 (a) Normalized EL spectra of PLED devices, PVK:emitters(100:8 by weight)/TPBI(30 nm)/MgAg(50 nm)/Ag(100 nm). (b) Current-voltage and luminescence-voltage characteristics of the PLED device, PVK:FOC₈(100:8 by weight)/TPBI (30 nm)/MgAg (50 nm)/Ag (100 nm).

2.4 Conclusion

A novel conjugated aromatic core containing direct-coupled fluorene, thiophene, and biphenyl groups via Suzuki coupling reaction was synthesized in this study. The rigid hydrophobic core was combined with two different lengths of poly(ethylene oxide)s as hydrophilic flexible chains. It is interesting that the increasing flexible chains lead to different mesophases (and molecular arrangements) and decrease the phase transition temperatures of T_m and T_i . The XRD patterns and optical textures by POM have proved their mesophasic structures and molecular arrangements. The melting points of the commercial poly(ethylene oxide)s with $M_n=750$ and 2000 are 30°C and 52°C , respectively. Hence, LC segregation might be influenced with poly(ethylene oxide)s. Besides mesophasic properties, the PL and EL properties of all rod-coil polymers and analogous derivatives are also investigated.



Chapter 3

Synthesis and Characterization of Liquid Crystalline Block

Copolymers with Cyanoterphenyl Moieties by ATRP

3.1 Introduction

In recent years, many research groups have concentrated on the synthesis of liquid crystalline (LC) block copolymers and characterization of their phase behavior and morphology.²⁹⁻³⁴ These kinds of liquid crystalline (LC) block copolymers were synthesized via different types of living free-radical polymerization.³⁵⁻³⁸ The interest in this type of materials resides in the combined properties of two (or more than two) completely different polymers which are chemically bonded to each other. The macrophase separation takes place due to the segregation of different polymer chains. Regarding LC properties, the combination of rigid cores and flexible chains is required for the LC molecular design. In general, there are two kinds of LC block copolymers, main-chain and side-chain LC block copolymers. Mesogenic groups are connected along the polymer backbones as main-chain copolymers, and pendent mesogenic groups are attached to the polymer backbones via flexible spacers as side-chain copolymers.

Side-chain LC polymers are often used in electro-optical applications, where different kinds of rigid cores, including azobenzene^{4, 39-40} and biphenyl units⁴¹⁻⁴⁶, are used in mesogenic monomers. In previous studies, the aromatic cores in conjugation with a terminal cyano group have high values of birefringence and reasonable viscosities. Moreover, they are chemically and photochemically stable. Cyanoterphenyl derivatives have been used in a wide range of nematic mixtures possessing high thermal, chemical and photochemical stabilities.⁴⁷ Therefore, a series

of novel side-chain liquid crystalline block copolymers consisting of different flexible macroinitiators, including poly(ethylene oxide) (PEO), polystyrene (PS), and poly(ethylene oxide)-b-polystyrene, and polymethacrylate with a pendent cyanoterphenyl group, were synthesized through atom transfer radical polymerization (ATRP). Furthermore, thermal, mesomorphic, and PL properties of all polymers were also investigated in this study.

3.2 Experimental Section

3.2.1 Measurements

¹H NMR spectra were recorded on a Varian unity 300 MHz spectrometer using CDCl₃ and d₆-DMSO solvents. Elemental analyses were performed on a HERAEUS CHN-OS RAPID elemental analyzer. Transition temperatures were determined by differential scanning calorimetry (DSC) (Perkin–Elmer, model: Diamond) with a heating and cooling rate of 5 °C/min. The mesophases were studied using a polarizing optical microscope (POM) (Leica, model: DMLP) equipped with a hot stage. Thermogravimetric analysis (TGA) was conducted on a Du Pont Thermal Analyst 2100 system with a TGA 2950 thermogravimetric analyzer with a heating rate of 10°C/min under nitrogen. Gel permeation chromatography (GPC) analysis was conducted on a Waters 1515 separation module with chloroform as the eluant against a polystyrene calibration curve. UV-visible absorption spectra were recorded in dilute chloroform solutions (10⁻⁶ M) on a HP G1103A spectrophotometer. Photoluminescence (PL) spectra were obtained on a Hitachi F-4500 spectrophotometer. Polymer solid films were spin-coated on quartz substrates from chloroform solutions with a concentration of 1 mg/mL.

3.2.2 Materials

Chemicals and solvents were reagent grade and purchased from Aldrich, ACROS, TCI, and Lancaster Chemical Co. Dichloromethane and THF were distilled to kept anhydrous before use. Pyridine was dried by refluxing over calcium hydride. The other chemicals were used without further purification.

3.2.3 Synthesis

Scheme 3.1 summarizes the steps involved in the synthesis, with details of each step given below.

4-Bromo-4'-octoxybiphenyl (2). 1-Bromooctane (11.6 g, 60 mmol), 4-bromo-4'-hydroxybiphenyl (10 g, 40 mmol), and potassium carbonate (16.6 g, 120 mmol) were dissolved in butan-2-one (100 mL) and reacted under reflux for 24 h. After cooling to room temperature, the potassium salt was filtered off. The solvent was removed by rotavapor and the crude product was recrystallized from petroleum ether (bp: 35-60 °C) to yield a white solid (13.5 g, 93%). ¹H NMR (ppm, CDCl₃), δ: 0.89 (t, *J* = 6.9 Hz, 3H), 1.29-1.47 (m, 10 H), 1.80 (quintet, *J* = 6.6 Hz, 2H), 3.98 (t, *J* = 8.6 Hz, 2H), 6.99 (d, *J* = 8.8 Hz, 2H), 7.40-7.54 (m, 6H).⁴⁸

4'-Octoxybiphenyl-4-ylboronic Acid (3). 4-Bromo-4'-octoxybiphenyl (**2**) (5 g, 13.8 mmol) was dissolved in THF (200 mL) and then n-Butyllithium (8.9 mL, 2.5 M, 22.1 mmol) was added dropwise at -78 °C to react. The reaction mixture was maintained under these conditions for one more 1 h. Furthermore, it was added dropwise to trimethyl borate solution (3.5 g, 33.2 mmol) at -78 °C. The solution was allowed to cool to room temperature overnight. The final solution was acidified with 10 % HCl solution (100 mL) and stirred for 45 mins at room temperature. The solution was washed with saturated sodium carbonate solution and water, and the THF was removed. The crude product was extracted by diethyl ether and the organic layer was dried over magnesium sulfate. After removing the solvent by rotavapor, the

resulting solid was washed with petroleum ether and briefly dried on filter to obtain a white solid (6.0 g, 80%). ¹H NMR (ppm, d₆-DMSO), δ: 0.85 (t, *J* = 7.2 Hz, 3H), 1.24-1.41 (m, 10H), 1.71 (quintet, *J* = 6.6 Hz, 2H), 3.98 (t, *J* = 6.6 Hz, 2H), 6.99 (d, *J* = 8.8 Hz, 2H), 7.56-7.62 (m, 4H), 7.83 (d, *J* = 8.8 Hz, 2H), 8.03 (s, 2H).⁴⁸

4-Octoxy-4''-cyanoterphenyl (5). Compound **4** (2.3 g, 12.8 mmol), compound **3** (5.0 g, 15.3 mmol), and tetrakis(triphenylphosphine)palladium(0) (740 mg, 0.64 mmol) were reacted in THF (100 mL) for 10 mins, and then 100mL of 2 M aqueous Na₂CO₃ solution was added. The mixture was reacted and refluxed for 48 h. After reaction, the cooled solution was washed with dilute hydrochloric acid (10%) and water, and dried over magnesium sulfate. The final solution was purified by column chromatography (silica gel, CH₂Cl₂/hexane 1:1) to yield a white solid (4.7 g, 83%). ¹H NMR (ppm, CDCl₃), δ: 0.87 (t, *J* = 6.6 Hz, 3H), 1.26-1.46 (m, 10 H), 1.80 (quintet, *J* = 6.9 Hz, 2H), 3.99 (t, *J* = 6.6 Hz, 2H), 6.98 (d, *J* = 9.0 Hz, 2H), 7.54 (d, *J* = 9.0 Hz, 2H), 7.62 (m, 4H), 7.71 (m, 4H).

4-Hydroxyl-4''-Cyanoterphenyl (6). 4-Octoxy-4''-cyanoterphenyl (**5**) (3.7 g, 9.5 mmol) was dissolved in dry chloroform (150 mL) under nitrogen and then boron tribromide (4.8 g, 19.1 mmol) was added dropwise and reacted at -78 °C. The mixture was allowed to warm up to room temperature and reacted for 24 h. The solution was washed with sodium hydroxide (1 M, 50 mL). Then, the solution was acidified with 10% HCl and stirred for 4 h. Finally, the suspension was filtered off and purified by column chromatography (silica gel, ethyl acetate) to yield a white solid (2.37 g, 92%). ¹H NMR (ppm, d₆-DMSO), δ: 6.86 (d, *J* = 8.4 Hz, 2H), 7.55 (d, *J* = 8.7 Hz, 2H), 7.71 (d, *J* = 8.4 Hz, 2H), 7.79 (d, *J* = 8.7 Hz, 2H), 7.91 (m, 4H), 9.63 (s, 1H).

4-(6-Hydroxyhexyloxy)-4''-cyanoterphenyl (7). 4-Hydroxyl-4''-Cyanoterphenyl (**6**) (2.4 g, 8.7 mmol), 6-chloro-1-hexanol (2.1 g, 11.3 mmol), K₂CO₃ (3.6 g, 26.1 mmol) and less KI (20 mg) were dissolved in 200 mL of DMF and refluxed overnight.

The reaction mixture was then cooled and poured into 200 mL of water and stirred for 2 h. The crude product was extracted with ethyl acetate and the organic layers were washed with a saturated aqueous solution of NaCl and water, and then the organic layer was dried over magnesium sulfate. After removing the solvent by rotavapor, the residue was recrystallized from absolute ethanol to give a colorless solid (2.6 g, 80%). ¹H NMR (ppm, d₆-DMSO), δ: 1.28-1.70 (m, 8H), 3.44 (m, 2H), 3.99 (t, *J* = 6.6 Hz, 2H), 4.32 (t, *J* = 5.0 Hz, 1H), 7.00 (d, *J* = 8.6 Hz, 2H), 7.62 (d, *J* = 8.6 Hz, 2H), 7.71 (d, *J* = 8.4 Hz, 2H), 7.80 (d, *J* = 8.4 Hz, 2H), 7.90 (m, 4H).

4-(6-Methacryloyloxyhexyloxy)-4''-cyanoterphenyl (8). 4-(6-Hydroxyhexyloxy)-4''-cyanoterphenyl (**7**) (2.6 g, 7.0 mmol), triethylamine (2.1 g, 21 mmol), and 2,6-di-tertbutyl-4-methylphenol (200 mg, as a thermal inhibitor) were dissolved in 150 mL of anhydrous THF under a nitrogen atmosphere and then methacryloyl chloride (2.2 g, 21 mmol) was added dropwise. The reaction mixture was heated under reflux overnight and then cooled and poured into 200 mL of an aqueous solution of NH₄Cl (10%). The crude product was extracted with CH₂Cl₂. The resulting organic layer was washed with a saturated solution of NaCl and water, and the organic layer was dried over magnesium sulfate. After removing the solvent by rotavapor, the resulting solid was purified by column chromatography using hexane/ethyl acetate (7:3) as an eluant to yield a colorless solid (2.3 g, 75%). ¹H NMR (ppm, CDCl₃), δ: 1.46 -1.53 (m, 4H), 1.62-1.74 (m, 2H), 1.82 (m, 2H), 1.93 (s, 3H), 4.00 (t, *J* = 6.3 Hz, 2H), 4.15 (t, *J* = 6.6 Hz, 2H), 5.53 (m, 1H), 6.09 (m, 1H), 6.97 (d, *J* = 8.7 Hz, 2H), 7.55 (d, *J* = 8.7 Hz, 2H), 7.64 (m, 4H), 7.71 (m, 4H). Element analysis for C₂₉H₂₉NO₃: Calc. C, 79.24; H, 6.65; N, 3.19; Found C, 79.30; H, 6.71; N, 3.05.

Macroinitiator (II). A solution of 1.8 g (7.7 mmol) of 2-bromo-2-methylpropionyl chloride in 10 mL of dry THF was added to a mixture of 1.1 g (10 mmol) of

triethylamine and 10 g (5 mmol) of PEG methyl ether with an M_n of 2000 g mol^{-1} in 30 mL of THF at 0 °C, and then the mixture was stirred for 18 h. After the mixture was filtered, half of the solvent was evaporated, and the PEG macroinitiator was precipitated into cold ether. After dissolution in ethanol, the solution was stored in refrigerator to recrystallize to yield a white solid. Yield: 55%. $^1\text{H NMR}$ (ppm, CDCl_3), δ : 1.94 (s, 6H), 3.38 (s, 3H), 3.54-3.76 (m, 174H), 4.33 (dd, 2H).

Preparation of Macroinitiators *I2*, *I3* and *I4*

Polymerization of macroinitiator *I3*. In a Schlenk flask, 3.46 mg of *N,N,N',N',N''*-pentamethyldiethylenetriamine (PMDETA, 0.02 mmol), 14.3 mg of CuBr (0.1 mmol), and 5.5 g of styrene (52.8 mmol) were added and stirred for 30 min. 74 mg of 1-(1-bromoethyl)benzene (0.4 mmol) was added, and the mixture was immediately frozen in liquid nitrogen under vacuum. After several freeze-thaw cycles, the flask was sealed under vacuum and put in an oil bath at 100 °C for 20 h. After the reaction, the content was dissolved in chloroform. After being concentrated, the chloroform solution was precipitated into methanol. The precipitation was repeated three times. The final product was dried at 50 °C under vacuum. $M_n = 10337 \text{ g mol}^{-1}$ and PDI (M_w/M_n) = 1.28 (by GPC).

The macroinitiators (*I2* and *I4*) were synthesized by using analogous procedures via ATRP and the information of M_n and PDI for *I2* and *I4* are listed below.

Macroinitiator, *I2*: $M_n = 1016 \text{ g mol}^{-1}$ and PDI (M_w/M_n) = 1.11 (by GPC).

Macroinitiator, *I4*: $M_n = 27474 \text{ g mol}^{-1}$ and PDI (M_w/M_n) = 1.35 (by GPC).

Preparation of Homopolymer and Block Copolymers

Block copolymers (*P1-P4*) and homopolymer (*P5*) were synthesized by using the analogous procedure except for the utilization of different initiators (see Scheme 3.2).

Preparation of polymer *P1* (polymerization of monomer *8* with macroinitiator *II*). 4 mg (0.04 mmol) of CuCl, 20 mg (0.01 mmol) of *II*, and 440 mg (1 mmol) of

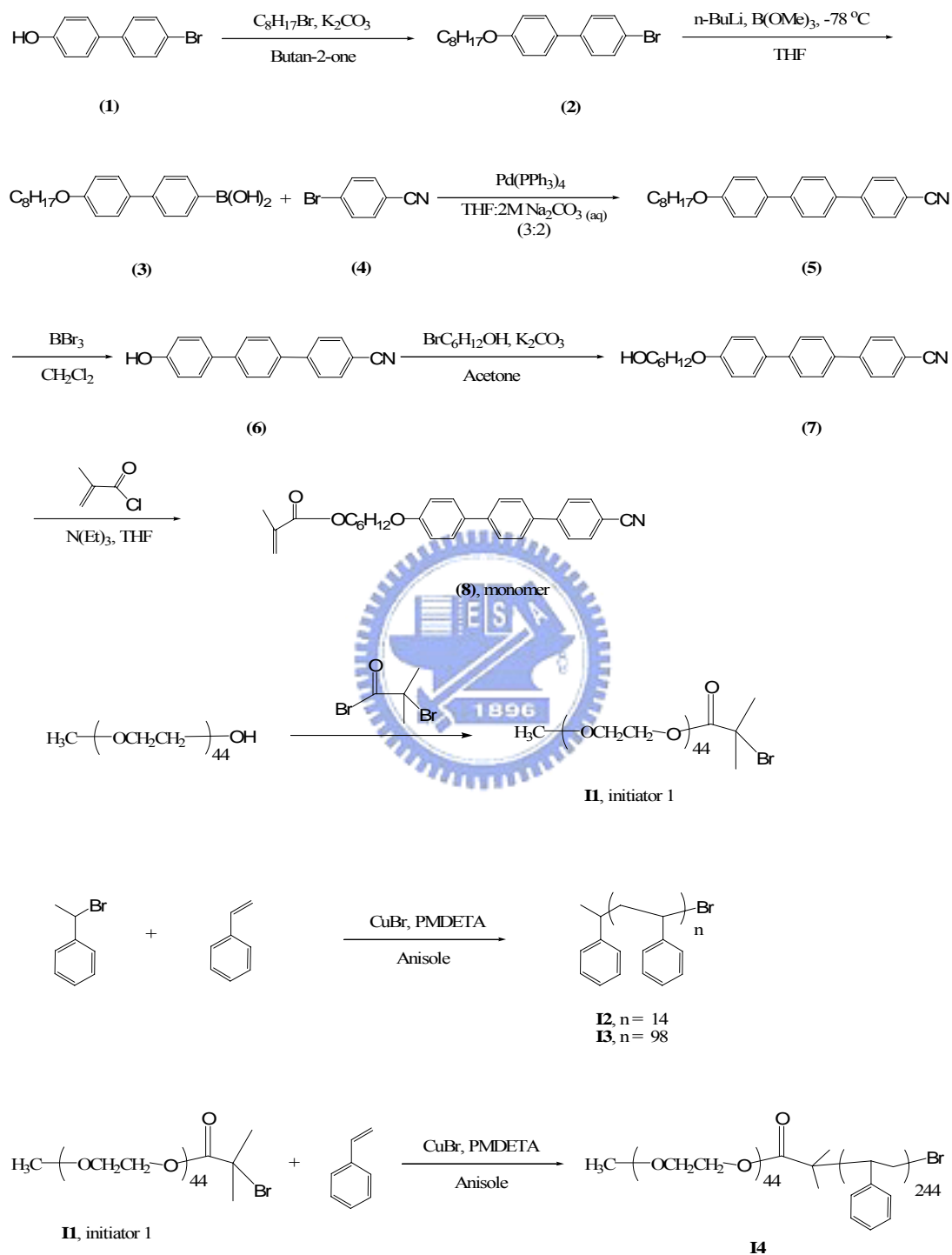
monomer (**8**) were mixed under nitrogen. 11 μL (23 mg, 0.1 mmol) of 1,1,4,7,10,10-hexamethyltriethylenetetramine (HMTETA) in 6 mL of anisole was added through a syringe. The mixture was degassed three times using the freeze-pump-thaw procedure and sealed under vacuum. After stirring for 30 min at room temperature, the mixture was reacted in a preheated 80 °C oil bath for 12 h. The solution was passed through a neutral Al_2O_3 column with THF as an eluant to remove the catalyst. The white filtrate was concentrated under reduced pressure and reprecipitated twice into methanol. The white product of polymer was collected by filtration and dried under vacuum. Yield: 150 mg (34 %). $M_n = 10258 \text{ gmol}^{-1}$ and PDI (M_w/M_n) = 1.17 (by GPC).

P2: Yield: 158 mg (33 %). $M_n = 9772 \text{ gmol}^{-1}$ and PDI (M_w/M_n) = 1.28 (by GPC, the soluble part of the polymer).

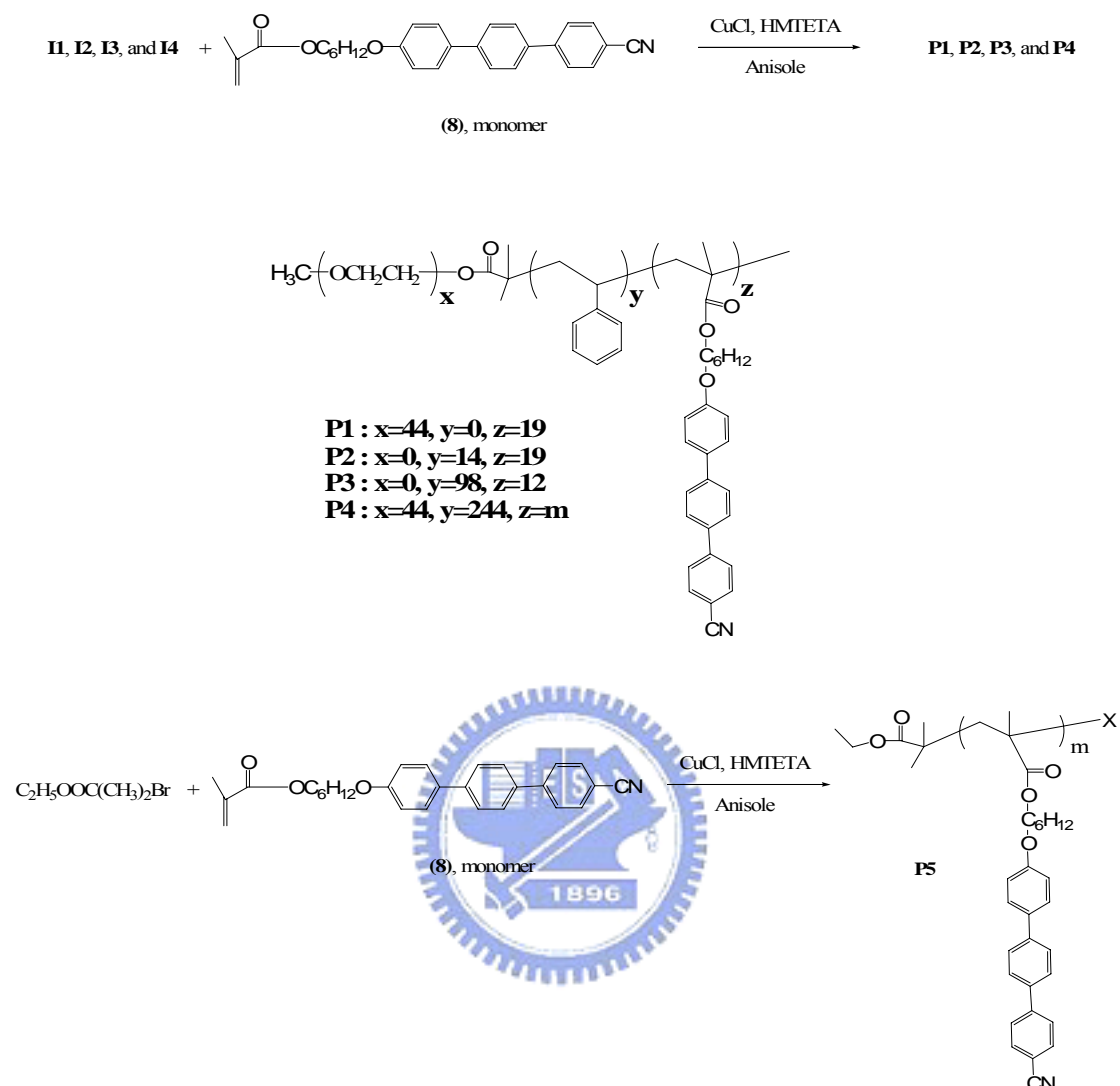
P3: Yield: 206 mg (32 %). $M_n = 15632 \text{ gmol}^{-1}$ and PDI (M_w/M_n) = 1.34 (by GPC, the soluble part of the polymer).

P4 and **P5**: No data obtained due to poor solubilities of longer cyanoterphenyl blocks.

Scheme 3.1 Synthetic routes of monomers and macroinitiators



Scheme 3.2 Synthetic routes of polymers



3.3 Results and Discussion

3.3.1 Synthesis and Characterization

Atom transfer radical polymerization (ATRP) has proven to be a very powerful polymerization technique for the preparation of block copolymers from a wide variety of monomers.^{49, 50} In this work, macroinitiators, including poly(ethylene oxide) (**I1**),⁴ polystyrenes (**I2** and **I3**),³⁴ and poly(ethylene oxide)-b-polystyrene (**I4**), were used to copolymerize cyanoterphenyl methacrylate monomers to produce LC cyanoterphenyl block copolymers. GPC measurements indicated that all macroinitiators (**I1-I4**) and

the diblock copolymers (**P1-P3**) with extended molecular weights had narrow polydispersities. Due to poor solubilities of longer cyanoterphenyl blocks in **P4** and **P5**, no GPC data were obtained for these polymers. The number-average molecular weights (M_n) of macroinitiators (**I2**, **I3**, and **I4**) determined by GPC are 1016, 10337, and 27474 g mol^{-1} with polydispersities (PDI) = 1.11, 1.28, and 1.35, respectively. The precursor of **I1** was purchased from the commercially available poly(ethylene oxide) ($M_n=2000 \text{ g mol}^{-1}$) with PDI = 1.04. The cyanoterphenyl homopolymer (**P5**) exhibited poor solubility in conventional organic solvents so as not to characterize and process into films.⁵ Figure 3.1 shows the NMR spectra of block copolymers **P1**, **P3** and **P4**, where the NMR spectrum of **P2** is omitted due to its similarity with that of **P3**. In Table 3.1, the number-average molecular weights (M_n) of the diblock copolymers containing LC cyanoterphenyl blocks (**P1-P3**) were determined by GPC, in which chloroform was used as an eluant. The triblock copolymer **P4** also exhibited poor solubility in conventional organic solvents. Though the flexible chains of PEO and PS blocks was the longest one in **P4**, it suggested that the molecular weight of LC cyanoterphenyl block might be polymerized to such a high degree of polymerization to induce poor solubility.

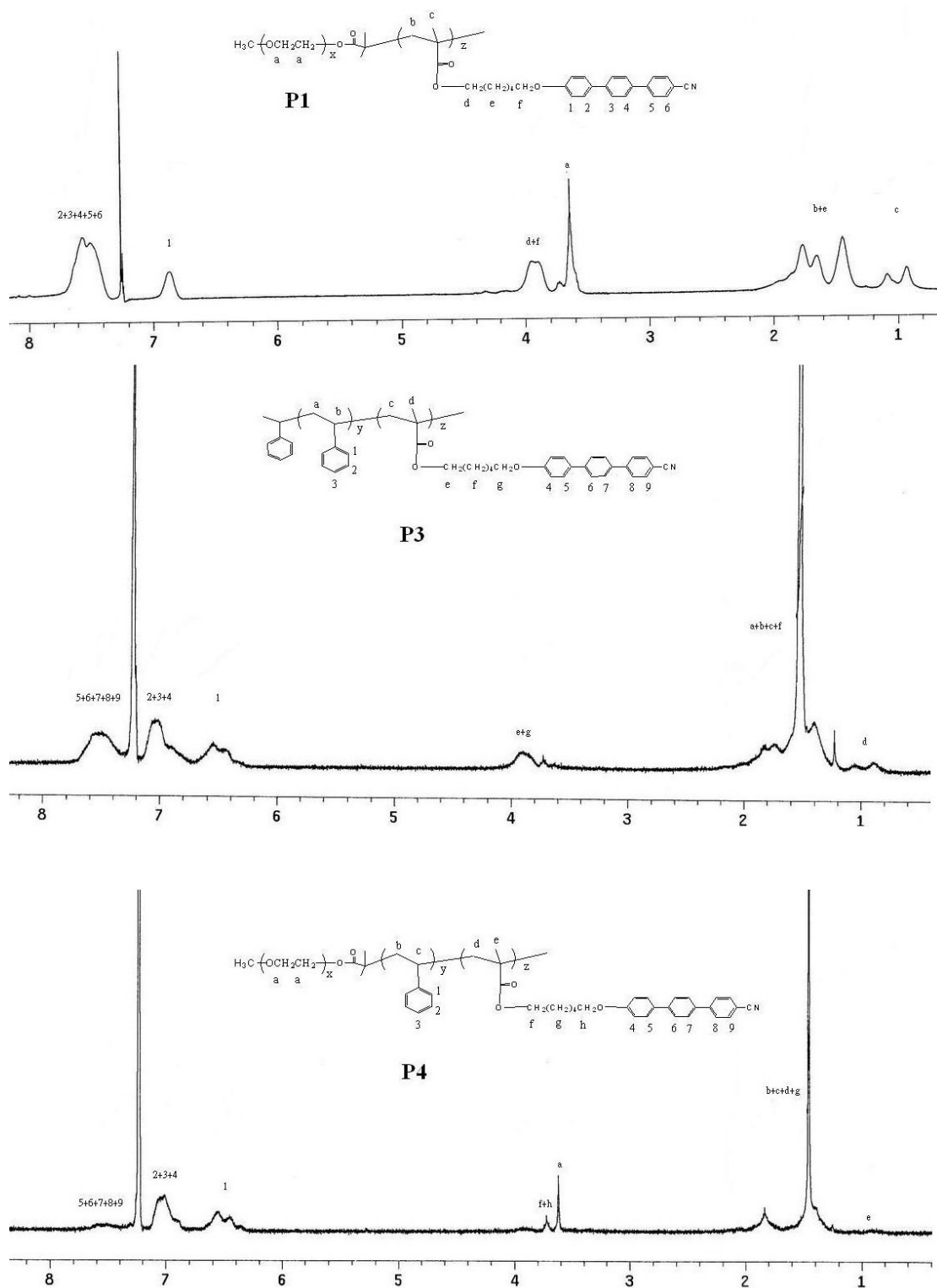


Figure 3.1 ^1H NMR spectra of block copolymers *P1*, *P3*, and *P4*.

Table 3.1 Molecular Weights and Thermal Properties of Block Copolymers **P1-P4**

Sample	M_n (g mol ⁻¹)	M_w (g mol ⁻¹)	PDI (M_w/M_n)	Td (°C) ^a	Tg (°C) ^b
P1	10258	11996	1.17	325.0	162.9
P2	9772	11308	1.28	347.5	111.7
P3	15632	18110	1.34	341.6	98.4
P4	-	-	-	326.3	82.7 and 153.7

^a Temperature of 5% weight loss measured by TGA under nitrogen.

^b The glass transition temperatures (°C) were determined by DSC (with a heating and cooling rate of 5 °C /min).

3.3.2 Thermal Properties and X-ray Investigation

The average molecular weights and polydispersity indices of these macroinitiators (**II-IV**) and block copolymers (**P1-P3**) were obtained by GPC. The thermal stability of polymers (**P1-P4**) under an atmosphere of nitrogen was evaluated by thermogravimetric analysis (TGA), which indicates that Td (the degradation temperature of 5% weight loss in nitrogen) ≥ 325 °C for all polymers (shown in Table 3.1). The mesomorphism was characterized by polarizing optical microscopy (POM) and differential scanning calorimetry (DSC). The phase transition temperatures and enthalpies of all polymers are summarized in Table 2. Regarding these results, all block copolymers (**P1-P4**) possessed the smectic A phase, which also existed in the cyanoterphenyl homopolymer (the same structure as **P5**) in a previous study.⁵ The DSC thermograms are displayed in Figure 3.2. To avoid thermal decomposition, these polymers were heated up to about 250 °C (with a heating rate of 5 °C/min) and their melting temperatures were not observed even over 250 °C. All block copolymers revealed clearing temperatures (Tc) around 275~300 °C where thermal decomposition occurred. Figure 3.3 showed that a fan-shaped texture of the corresponding smectic A phase of **P1** observed by POM at 270 °C (cooling).

Table 3.2 Phase Behavior of Block Copolymers *P1-P4*^{a,b}

Sample	T (°C)	T _c (°C) ^c
P1	K 173.8 (9.8) S_A	~ 300
P2	K 152.5 (4.1) S_A	~ 300
P3	K 181.6 (7.0) S_A	~ 275
P4	K 191.1 (4.7) S_A	~ 300

^a Transition temperatures (°C) and enthalpies (in parentheses, kJ/mol) were determined by DSC (a heating rate of 5 °C /min).

^b **K** = crystalline; **S_A** = smectic A

^c T_c : the clearing (isotropization) temperature which was observed by polarizing optical microscopy (POM).

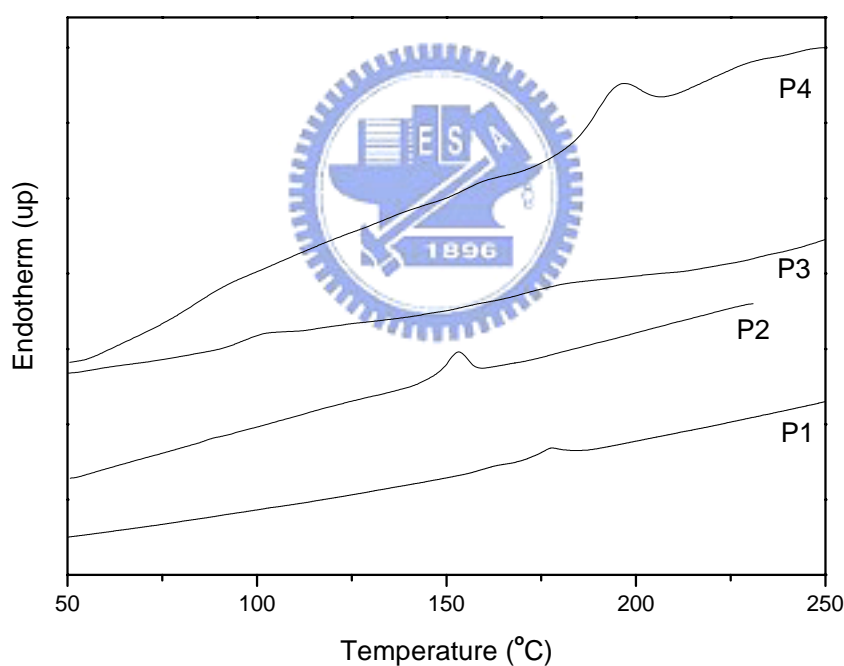


Figure 3.2 DSC thermograms of block copolymers *P1-P4* during the first heating scan.



Figure 3.3 The optical texture of the mesophase (S_A) of **P1** observed by POM at 270 °C (cooling).

Because it is not easy to observe the glass transition temperatures (T_g) of these block copolymers, T_g values were detectable by liquid nitrogen quenching of polymers in the first heating scans of DSC measurements (with a heating rate of 5 °C/min). At this rate, the DSC results can indicate T_g values of all block copolymers more clearly and their T_g values are in the range of 82 to 163 °C referred to Table 3.1. For all block copolymers in Figure 3.2, **P3** and **P4** can easily reveal the glass transition temperatures (T_g s), but T_g s of **P1** and **P2** could not be observed due to the low T_g of PEO block in **P1** and the short block of polystyrene in **P2**. The glass transition temperature (T_g) of **P3** (at 98 °C) was mostly contributed from the polystyrene block with PS repeating units of 98.^{51, 52} However, two glass transition temperatures (at 83 and 154 °C) were present in **P4**, which are attributed to the immiscibility between the more extended polystyrene block (with PS repeating units of 244 and $T_g = 83$ °C) and the LC cyanoterphenyl block (with $T_g = 154$ °C). The lower T_g of the more extended polystyrene block (with PS repeating units of 244 and $T_g = 83$ °C) in **P4** in comparison with the higher T_g of the shorter polystyrene block (with PS repeating units of 98 and $T_g = 98$ °C) in **P3** is due to the plasticizer effect of PEO block in the triblock copolymer **P4**. Hence, this situation may serve as evidence

for the microphase separation morphology of the triblock copolymer **P4**.⁵³

In order to elucidate the structures of the mesophases, X-ray diffraction (XRD) measurements were carried out at the temperature ranges of mesophases for polymers **P1-P5**. As shown in Figure 3.4, the XRD patterns of polymers **P1-P5** are almost identical and their layer d-spacing values are around 37 Å. In addition, the layer d-spacing values in the ratio of 1:1/2 indicate a lamellar order exists in the mesophases, and the XRD data are summarized in Table 3.3. Furthermore, a fan-shaped texture is clearly observed by POM as shown in Figure 3.3, which is a characteristic texture of the smectic A phase. According to the molecular modeling calculation, the layer d-spacing value of coplanar structure in monomer (**8**) is around 35.6 Å (the layer d-spacing value around 37 Å by XRD patterns). Therefore, a possible layer structures of block copolymers **P1-P5** is suggested to be interdigitated packing of rods. From this evidence, the layer structures of all polymers, **P1-P5**, have little relationship with respect to the flexible blocks, such as PS and PEO blocks.

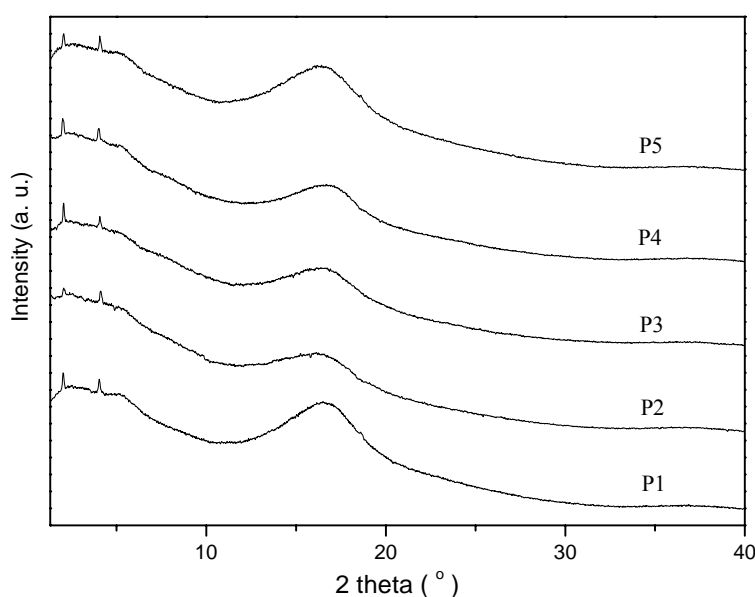


Figure 3.4 X-ray diagrams of all polymers **P1-P5**.

Table 3.3 XRD Diffraction Data of All Polymers **P1-P5** at 190 °C

Sample	d-Spacing (Å) ^a
P1	$d_{001} = 37.45$
	$d_{002} = 18.82$
P2	$d_{001} = 36.70$
	$d_{002} = 18.45$
P3	$d_{001} = 37.27$
	$d_{002} = 18.73$
P4	$d_{001} = 38.03$
	$d_{002} = 18.91$
P5	$d_{001} = 36.90$
	$d_{002} = 18.45$

^aThe theoretical d-spacing value is 35.6 Å for all polymers **P1-P5**.

3.3.3 Optical Properties

The photophysical properties of all block polymers **P1-P4** containing luminescent cyanoterphenyl blocks were studied by photoluminescence (PL) and UV-visible absorption spectra in dilute chloroform solutions and solid films. The optical properties of all polymers are summarized in Table 3.4. Due to the identical rigid cores of luminescent cyanoterphenyl blocks, all synthesized polymers in solutions have almost the same maximum absorption wavelength around 310 nm and emit blue light at approximately $\lambda_{\text{max,PL}} = 435$ nm in solid films.

Figure 5 shows an example of UV-visible and PL spectra of diblock copolymer **P1**. Compared with the maximum PL wavelength in solutions, the materials in solid films exhibit red-shifted PL emission owing to the π - π^* aggregation of the rigid cores (luminescent cyanoterphenyl blocks). In terms of PL wavelengths of all block copolymers in dilute solutions, Figure 3.6 indicates that **P2** and **P4** are more red-shifted than **P1** and **P3**. The red-shifted PL emission in **P4** might result from a large molecular weight in LC cyanoterphenyl block with higher aggregation of

emitting cyanoterphenyl moieties. In contrast to *P1* and *P3*, *P2* has shorter flexible polystyrene chains resulting in a stronger π - π^* aggregation effect of the cyanoterphenyl blocks.

Table 3.4 Absorption and Photoluminescence Spectral Data of Block Copolymers *P1-P4*.

Sample	$\lambda_{\max, \text{Abs}}$ (nm)		$\lambda_{\max, \text{PL}}$ (nm)	
	solution ^a	film	solution ^a	film
<i>P1</i>	310	309	403	427
<i>P2</i>	312	314	416	435
<i>P3</i>	310	308	404	434
<i>P4</i>	312	310	431	438

^a Absorption and PL emission spectra were recorded in dilute CHCl_3 solutions at room temperature.

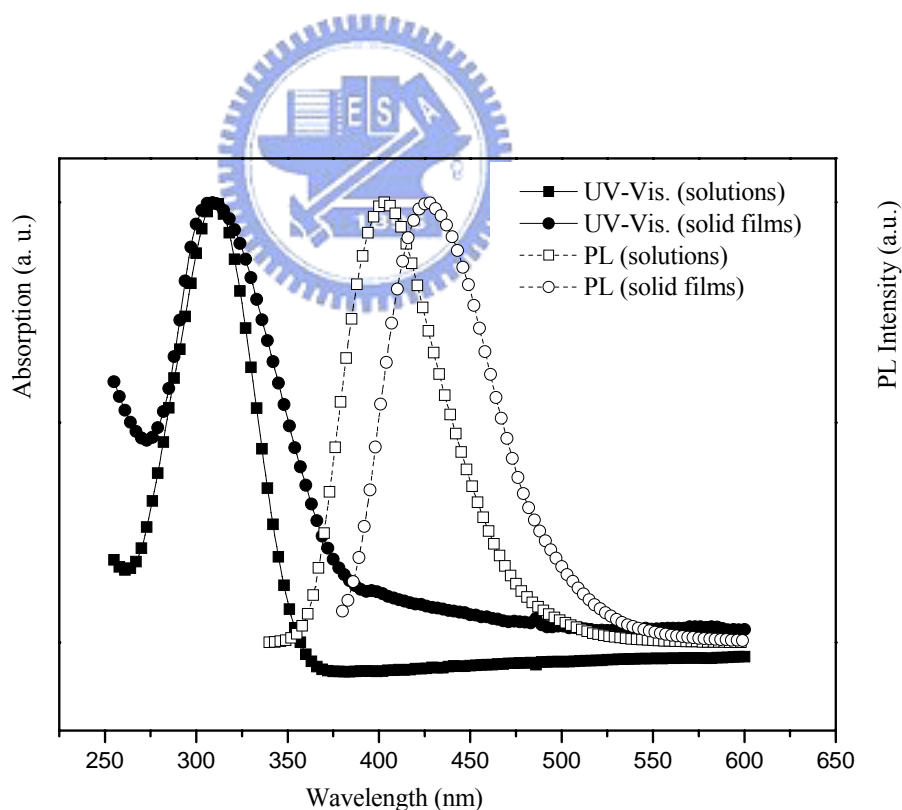


Figure 3.5 Absorption (solid lines) and PL (dash lines) spectra of *P1* in solutions (CHCl_3 as solvent) and solid films.

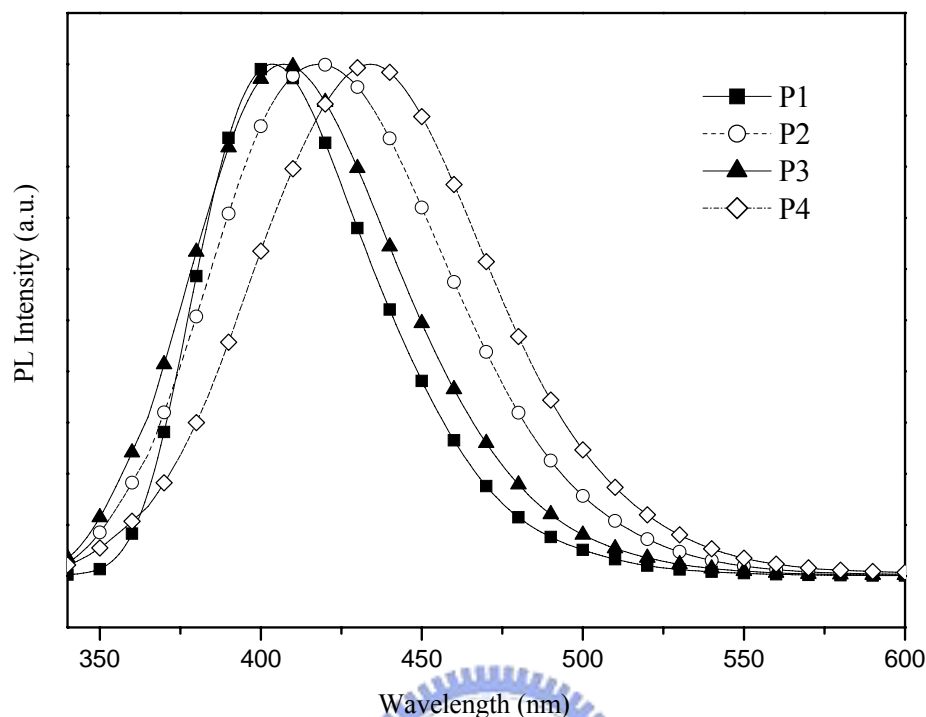


Figure 3.6 PL spectra of block copolymers *P1-P4* in solution (CHCl_3 as solvent).

3.4 Conclusion

Atom transfer radical polymerization (ATRP) was employed to fabricate block copolymers composed of different macroinitiators and liquid crystalline cyanoterphenyl-based polymethacrylate blocks. Thermal and XRD investigations indicate that all polymers exhibit the interdigitated packing smectic A phase which have little relationship with respect to the flexible PS and PEO blocks. In terms of PL wavelengths of all block copolymers in dilute solutions, *P2* and *P4* are more red-shifted than *P1* and *P3*, which might be due to the π - π^* aggregation effect of the cyanoterphenyl blocks in block copolymers.

Chapter 4

Synthesis and characterization of side-chain liquid crystalline homopolymers and block copolymers containing biphenyl-4-ylthiophene and biphenyl-4-ylfluorene pendants

4.1 Introduction

A wide variety of liquid crystalline (LC) copolymers^{31, 33, 54-58} with optimized structures have been developed in recent years. In addition, numerous liquid crystalline (LC) block copolymers consisting of mesogenic blocks and isotropic blocks were synthesized via different types of living free-radical polymerization^{35-36, 38, 59} and their phase behavior and morphology were characterized. In general, there are two kinds of LC block copolymers, i.e. main-chain and side-chain LC block copolymers, where mesogenic groups connected along the backbones are main-chain copolymers (such as copolyesters composed of *p*-hydroxybenzoic acid and poly(ethylene terephthalate), etc.)⁶⁰⁻⁶², and pendant mesogenic groups attached to the backbones via flexible spacers are side-chain copolymers.

Among these LC copolymers, side-chain LC copolymers have attracted significant interests because of their liquid crystalline behavior as low molecular mass pendant mesogens and their easy processing characteristic as polymers. Furthermore, side-chain LC polymers are often used in electro-optical applications due to their lower viscosities and easier alignment tendencies than those of main-chain LC polymers. Several kinds of rigid cores, including azobenzene^{4, 36-37} and biphenyl units⁴¹⁻⁴⁶, were applied to mesogenic groups of side-chain LC polymers. In previous researches⁶³, side-chain LC polymers containing cyanoterphenyl units were also

reported to possess mesogenic phases and high stabilities in thermal, chemical, and photochemical properties, but they had poor solubilities. Herein, in order to improve solubility, a series of new mesogenic homopolymers and block copolymers composed of methacrylates containing pendent biphenyl-4-ylthiophene (**M1**) and biphenyl-4-ylfluorene (**M2**) groups were synthesized by atom transfer radical polymerization (ATRP), where block copolymers **P3** and **P4** were produced from styrene-macroinitiator (**SMi**). Furthermore, the thermal, mesogenic, and photoluminescent (PL) properties of all polymers were also investigated in this study.

4.2 Experimental Section

4.2.1 Measurements

¹H NMR spectra were recorded on a Varian unity 300 MHz spectrometer using CDCl₃ and d₆-DMSO solvents. Elemental analyses were performed on a HERAEUS CHN-OS RAPID elemental analyzer. Transition temperatures were determined by differential scanning calorimetry (DSC) (Perkin–Elmer, model: Diamond) with heating and cooling rates of 5 °C/min. The mesomorphic properties were studied using a polarizing optical microscope (POM) (Leica, model: DMLP) equipped with a hot stage. Thermogravimetric analysis (TGA) was conducted on a Du Pont Thermal Analyst 2100 system with a TGA 2950 thermogravimetric analyzer at a heating rate of 10 °C/min under nitrogen. Gel permeation chromatography (GPC) analysis was conducted on a Waters 1515 separation module with chloroform as the eluant against a polystyrene calibration curve. UV-visible absorption spectra were recorded in dilute THF solutions (10⁻⁶ M) on a HP G1103A spectrophotometer. Photoluminescence (PL) spectra were obtained on a Hitachi F-4500 spectrophotometer.

4.2.2 Materials

Unless otherwise specified, chemicals and solvents were reagent grade and

purchased from Aldrich, ACROS, TCI, and Lancaster Chemical Co. Dichloromethane and THF were distilled to keep anhydrous before use. Pyridine was dried by refluxing over calcium hydride. The other chemicals were used without further purification.

4.2.3 Synthesis

The synthetic routes of monomers (**M1** and **M2**) and the macroinitiator (**SMi**) are shown in Scheme 4.1. Their synthetic details were described as follows:

4-Bromo-4'-octoxybiphenyl (2). 1-Bromooctane (11.6 g, 60 mmol), 4-bromo-4'-hydroxybiphenyl (**1**) (10 g, 40 mmol), and potassium carbonate (16.6 g, 120 mmol) were dissolved in butan-2-one (100 mL) and reacted under reflux for 24 h. After cooling to room temperature, the potassium salt was filtered off. The solvent was removed by rotavapor and the crude product was recrystallized from petroleum ether (bp: 35-60 °C) to yield a white solid (13.5 g, 93%). ¹H NMR (ppm, CDCl₃), δ: 0.89 (t, *J* = 6.9 Hz, 3H), 1.29-1.47 (m, 10 H), 1.80 (quintet, *J* = 6.6 Hz, 2H), 3.98 (t, *J* = 8.6 Hz, 2H), 6.99 (d, *J* = 8.8 Hz, 2H), 7.40-7.54 (m, 6H) ⁶³.

4'-Octoxybiphenyl-4-ylboronic Acid (3). 4-Bromo-4'-octoxybiphenyl (**2**) (5 g, 13.8 mmol) was dissolved in THF (200 mL) and then n-butyllithium (8.9 mL, 2.5 M, 22.1 mmol) was added dropwise to react at -78 °C. The reaction mixture was maintained under this condition for 1 h. Furthermore, it was added dropwise to trimethyl borate solution (3.5 g, 33.2 mmol) at -78 °C. The solution was allowed to cool to room temperature overnight, and the final solution was acidified with 100 mL of 10 % HCl solution and stirred for 45 min at room temperature. Subsequently, the solution was washed with saturated sodium carbonate solution and water, and then THF was removed. The crude product was extracted by diethyl ether and the organic layer was dried over magnesium sulfate. After removing the solvent by rotavapor, the resulting solid was washed with petroleum ether and briefly dried on filter to obtain a white solid (6.0 g, 80%). ¹H NMR (ppm, d₆-DMSO), δ: 0.85 (t, *J* = 7.2 Hz, 3H),

1.24-1.41 (m, 10H), 1.71 (quintet, $J = 6.6$ Hz, 2H), 3.98 (t, $J = 6.6$ Hz, 2H), 6.99 (d, $J = 8.8$ Hz, 2H), 7.56-7.62 (m, 4H), 7.83 (d, $J = 8.8$ Hz, 2H), 8.03 (s, 2H) ⁶³.

2-(4'-Octoxy-biphenyl-4-yl)-thiophene (6). Compound **4** (3 g, 18.5 mmol), compound **3** (7.9 g, 24.1 mmol), and tetrakis(triphenylphosphine)palladium(0) (1.07 g, 0.93 mmol) were reacted in THF (200 mL) for 10 min, and then 130 mL of 2 M aqueous Na₂CO₃ solution was added. The mixture was reacted and refluxed for 48 h. After reaction, the cooled solution was washed with dilute hydrochloric acid (10%) and water, and dried over magnesium sulfate. The final solution was purified by column chromatography (silica gel, CH₂Cl₂/hexane 1:1) to yield a white solid (4.8 g, 71%). ¹H NMR (ppm, CDCl₃), δ : 0.87 (t, $J = 6.9$ Hz, 3H), 1.27-1.45 (m, 10H), 1.81 (quintet, $J = 6.3$ Hz, 2H), 3.97 (t, $J = 6.6$ Hz, 2H), 6.92 (d, $J = 9.6$ Hz, 2H), 7.06 (dd, $J = 3.6$ Hz, 1H), 7.26 (d, $J = 5.4$ Hz, 1H), 7.31 (d, $J = 3.6$ Hz, 1H), 7.51 (m, 4H), 7.63 (d, $J = 8.7$ Hz, 2H).

2-(4'-Octoxy-biphenyl-4-yl)-9,9-diethyl-9H-fluorene(7). Compound **7** was synthesized by means of analogous procedures of compound **6** via Suzuki coupling reaction. Yield: 71%. ¹H NMR (ppm, CDCl₃), δ : 0.34 (t, $J = 6.6$ Hz, 6H), 0.85 (t, $J = 6.9$ Hz, 3H), 1.27-1.45 (m, 10H), 1.83 (quintet, $J = 6.6$ Hz, 2H), 2.09 (m, 4H), 3.98 (t, $J = 6.3$ Hz, 2H), 6.96 (d, $J = 8.7$ Hz, 2H), 7.29-7.35 (m, 3H), 7.54-7.75 (m, 10H).

2-(4'-Hydroxyl -biphenyl-4-yl)-thiophene (8). 2-(4'-Octoxy-biphenyl-4-yl)-thiophene (**6**) (4.6 g, 12.6 mmol) was dissolved in dry chloroform (150 mL) under nitrogen and then boron tribromide (6.4 g, 25.2 mmol) was added dropwise to react at -78 °C. The mixture was allowed to warm up to room temperature and reacted for 24 h. The solution was washed with sodium hydroxide (1 M, 50 mL) and then the solution was acidified with 10% HCl and stirred for 4 h. Finally, the suspension was filtered off and purified by column chromatography (silica gel, ethyl acetate) to yield a white solid (2.8 g, 89%). ¹H NMR (ppm, d₆-DMSO), δ : 6.85 (d, $J = 8.4$ Hz, 2H),

7.14 (dd, $J = 3.9$ Hz, 1H), 7.50 (d, $J = 4.0$ Hz, 1H), 7.54 (d, $J = 3.6$ Hz, 1H), 7.60 (m, 4H) 7.68 (d, $J = 8.4$ Hz, 2H), 9.56 (s, 1H).

2-(4'-Hydroxyl-biphenyl-4-yl)-9,9-diethyl-9H-fluorene (9). Compound **9** was synthesized through analogous procedures of compound **8**. Yield: 87%. ^1H NMR (ppm, $\text{d}_6\text{-DMSO}$), δ : 0.35 (t, $J = 7.2$ Hz, 6H), 2.07 (m, 4H), 6.58 (s, 1H), 6.94 (d, $J = 8.4$ Hz, 2H), 7.31-7.33 (m, 3H), 7.50-7.76 (m, 10H).

2-(4'-(6-Hydroxyhexyloxy)-biphenyl-4-yl)-thiophene (10). Compound **8** (2.5 g, 9.9 mmol), 6-chloro-1-hexanol (2.3 g, 12.9 mmol), K_2CO_3 (4.1 g, 29.7 mmol), and KI (20 mg) were dissolved in 200 mL of DMF to reflux overnight. The reaction mixture was then cooled and poured into 200 mL of water and stirred for 2 h. The crude product was extracted with ethyl acetate and the organic layers were washed with a saturated aqueous solution of NaCl and water, and then the organic layer was dried over magnesium sulfate. After removing the solvent by rotavapor, the residue was recrystallized from absolute ethanol to give a colorless solid (2.4 g, 69%). ^1H NMR (ppm, $\text{d}_6\text{-DMSO}$), δ : 1.22-1.70 (m, 8H), 3.39 (m, 2H), 3.99 (t, $J = 6.4$ Hz, 2H), 4.35 (t, $J = 5.1$ Hz, 1H), 7.00 (d, $J = 9.0$ Hz, 2H), 7.14 (dd, $J = 3.9$ Hz, 1H), 7.53 (d, $J = 4.8$ Hz, 1H), 7.55 (d, $J = 3.6$ Hz, 1H), 7.64 (m, 4H) 7.70 (d, $J = 8.7$ Hz, 2H).

2-(4'-(6-Hydroxyhexyloxy)-biphenyl-4-yl)-9,9-diethyl-9H-fluorene(11).

Compound **11** was synthesized via analogous procedures of compound **10**. Yield: 80%. ^1H NMR (ppm, CDCl_3), δ : 0.35 (t, $J = 7.2$ Hz, 6H), 1.41-1.83 (m, 8H), 2.10 (m, 4H), 3.65 (m, 2H), 4.00 (t, $J = 6.4$ Hz, 2H), 6.97 (d, $J = 9.0$ Hz, 2H), 7.30-7.35 (m, 3H), 7.54-7.76 (m, 10H).

M1. 2-(4'-(6-Hydroxyhexyloxy)-biphenyl-4-yl)-thiophene (**10**) (2.0 g, 5.7 mmol), triethylamine (5.7 g, 57 mmol), and 2,6-di-tertbutyl-4-methylphenol (100 mg, as a thermal inhibitor) were dissolved in 150 mL of anhydrous THF under a nitrogen atmosphere and then methacryloyl chloride (1.8 g, 17.1 mmol) was added dropwise.

Afterward, the reaction mixture was heated under reflux overnight and then cooled to pour into 200 mL of aqueous NH_4Cl solution (10%). The crude product was extracted with CH_2Cl_2 . The resulting organic layer was washed with a saturated solution of NaCl and water, and the organic layer was dried over magnesium sulfate. After removing the solvent by rotavapor, the resulting solid was purified by column chromatography using dichloromethane as an eluant to yield a colorless solid (1.9 g, 81%). ^1H NMR (ppm, CDCl_3), δ : 1.45 -1.50 (m, 4H), 1.67-1.84 (m, 4H), 1.93 (s, 3H), 3.99 (t, $J = 6.5$ Hz, 2H), 4.15 (t, $J = 6.6$ Hz, 2H), 5.53 (s, 1H), 6.09 (s, 1H), 6.96 (d, $J = 9.0$ Hz, 2H), 7.07 (dd, $J = 3.6$ Hz, 1H), 7.26 (d, $J = 5.1$ Hz, 1H), 7.32 (d, $J = 3.6$ Hz, 1H), 7.54 (m, 4H) 7.64 (d, $J = 8.7$ Hz, 2H). Element analysis for $\text{C}_{26}\text{H}_{28}\text{O}_3\text{S}$: Calc. C, 74.25; H, 6.71; Found C, 74.43; H, 6.76. HRMS (EI) m/z : Calc. 420.1759; Found 420.1754.

M2. Monomer **M2** was synthesized by analogous procedures of **M1**. Yield: 83%. ^1H NMR (ppm, CDCl_3), δ : 0.36 (t, $J = 6.9$ Hz, 6H), 1.45 -1.56 (m, 4H), 1.67-1.83 (m, 4H), 1.94 (s, 3H), 2.06 (m, 4H), 4.01 (t, $J = 6.3$ Hz, 2H), 4.16 (t, $J = 6.6$ Hz, 2H), 5.54 (s, 1H), 6.09 (s, 1H), 6.98 (d, $J = 8.7$ Hz, 2H), 7.32-7.36 (m, 3H), 7.55-7.77 (m, 10H). Element analysis for $\text{C}_{39}\text{H}_{42}\text{O}_3$: Calc. C, 83.83; H, 7.58; Found C, 83.52; H, 7.54. HRMS (EI) m/z : Calc. 558.3134; Found 558.3126.

Polymerzation of macroinitiator SMi. In a Schlenk flask, N,N,N',N',N'' -pentamethyldiethylenetriamine (PMDETA, 3.46 mg, 0.5 mmol), CuBr (14.3 mg, 0.25 mmol), and styrene (6.8 g, 65 mmol) were added and stirred for 30 min. Ethyl 2-bromo-2-methylpropanoate (195 mg, 1 mmol) was added, and the mixture was immediately frozen in liquid nitrogen under vacuum. After several freeze-thaw cycles, the flask was sealed under vacuum and put in an oil bath at 100°C to react for 20 h. After reaction, the content was dissolved in chloroform. After being concentrated, the chloroform solution was precipitated into methanol and the

precipitation was repeated for three times. The final product was dried at 50 °C under vacuum. Yield: 75%. The number-average molecular weight measured by GPC was $M_n = 6196 \text{ gmol}^{-1}$ with PDI (M_w/M_n) = 1.11.

Preparation of Homopolymer (P1 and P2) and Block Copolymers (P3 and P4)

According to analogous procedures as shown in Scheme 4.2, homopolymers (**P1** and **P2**) and block copolymers (**P3** and **P4**) were synthesized by utilization of initiators **12** and **SMi**, respectively.

Preparation of polymer P1. *N,N,N',N',N''*-pentamethyldiethylenetriamine (PMDETA, 8.7 mg, 0.05 mmol), CuBr (3.6 mg, 0.025 mmol), and **MI** (210.3 mg, 0.5 mmol) were added and stirred for 30 min. Ethyl 2-bromo-2-methylpropanoate (1.95 mg, 0.01 mmol) was added, and the mixture was immediately frozen in liquid nitrogen under vacuum. The mixture was degassed three times using the freeze-pump-thaw procedure and sealed under vacuum. After stirring for 30 min at room temperature, the mixture was reacted at 100 °C in a preheated oil bath for 24 h. The mixture was reprecipitated more than twice in methanol and then washed by acetone. The white product of polymer was collected by filtration and dried under vacuum. Yield: 80 mg (36%).

P2: Yield: 75 mg (27%). ¹H NMR (ppm, CDCl₃), δ: 0.31 (broad), 0.93 (broad), 1.53-1.93 (broad), 2.02 (broad), 3.97 (broad), 6.91 (broad), 7.29 (broad), 7.54 (broad). The number-average molecular weight measured by GPC is $M_n = 5103 \text{ gmol}^{-1}$ with PDI (M_w/M_n) = 1.25.

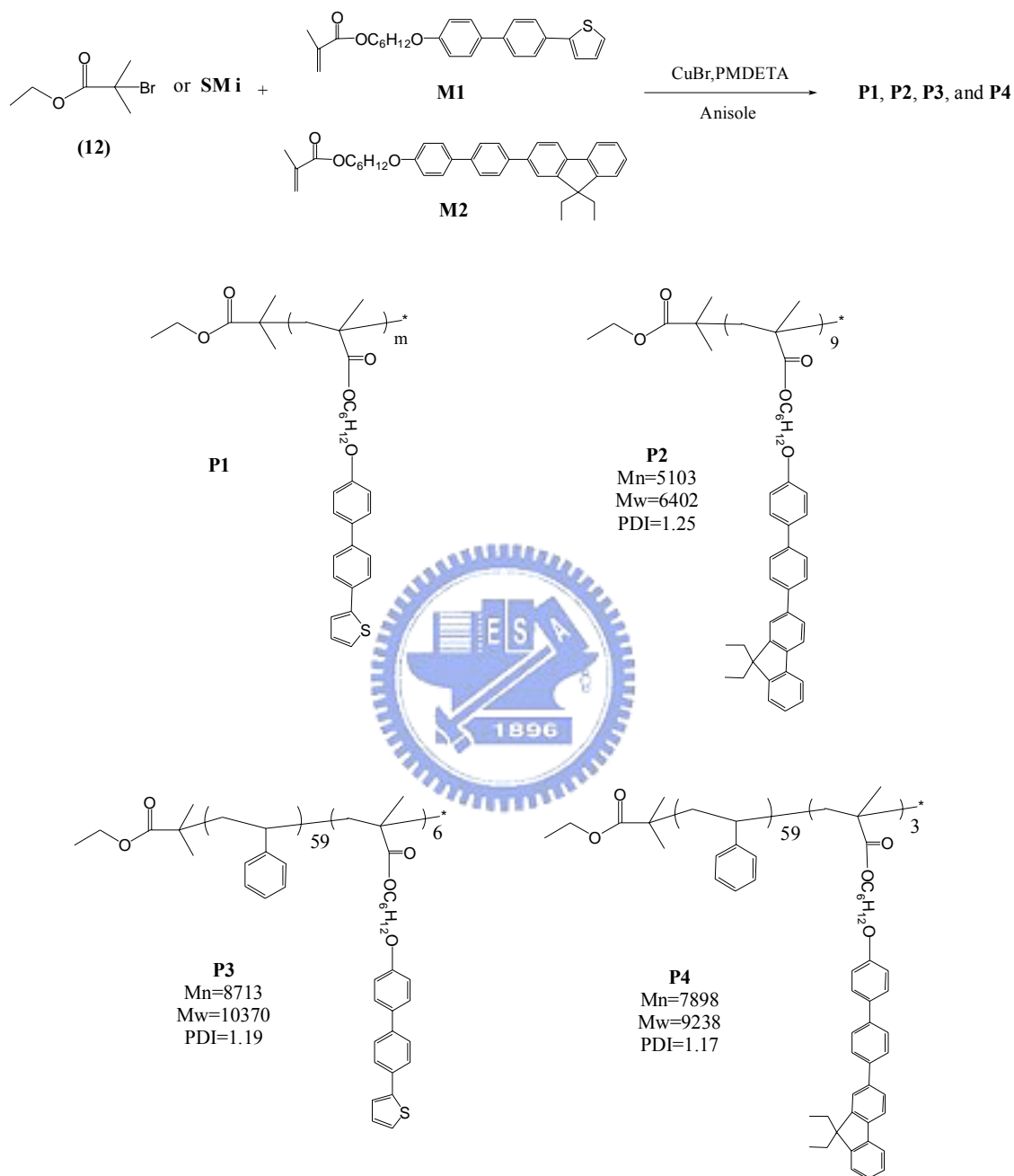
P3: (monomer/ initiator=30/1). Yield: 110 mg (40 %). ¹H NMR (ppm, CDCl₃), δ: 0.96 (broad), 1.41-1.93 (broad), 3.99 (broad), 6.55 (broad), 7.06 (broad), 7.31 (broad), 7.59 (broad). The number-average molecular weight of the soluble part in the polymer

measured by GPC is $M_n = 8713 \text{ gmol}^{-1}$ with PDI (M_w/M_n) = 1.19.

P4: (monomer/ initiator=30/1). Yield: 100 mg (29 %). ^1H NMR (ppm, CDCl_3), δ : 0.30 (broad), 0.85 (broad), 1.40-1.84 (broad), 2.03 (broad), 3.98 (broad), 6.55 (broad), 7.02 (broad), 7.30 (broad), 7.58 (broad). The number-average molecular weight measured by GPC is $M_n = 7898 \text{ gmol}^{-1}$ with PDI (M_w/M_n) = 1.17.



Scheme 4.2 Synthetic routes of homopolymers (**P1** and **P2**) and block copolymers (**P3** and **P4**).



4.3 Results and discussions

4.3.1 Synthesis and Characterization

Atom transfer radical polymerization (ATRP) has been proven to be a very

powerful polymerization technique for the preparation of block copolymers from various monomers.^{47, 49-50, 63} In this work, the styrene-macroinitiator (**SMi**) was used to copolymerize with methacrylate monomers containing biphenyl-4-ylthiophene (**M1**) and biphenyl-4-ylfluorene (**M2**) pendants to produce diblock copolymers. The number-average molecular weights (M_n) as well as PDI values of homopolymer (**P2**) and diblock copolymers (**P3** and **P4**) containing biphenyl-4-ylthiophene and biphenyl-4-ylfluorene LC blocks determined by GPC (THF as an eluant) are shown in Table 4.1. It indicates that all of the macroinitiator (**SMi**), homopolymer (**P2**), and diblock copolymers (**P3** and **P4**) with extended molecular weights had small PDI values by ATRP. Due to the poor solubility of longer biphenyl-4-ylthiophene units in **P1**, homopolymer **P1** was unable to be characterized, including the molecular weight. According to the number-average molecular weight (M_n) of homopolymer **P2**, i.e. 5103 g mol^{-1} with a PDI value of 1.25, homopolymer **P2** contains only about 9 units of biphenyl-4-ylfluorene monomer (**M2**). In addition, the number-average molecular weight (M_n) of macroinitiator (**SMi**) determined by GPC was 6196 g mol^{-1} (containing about 59 styrene monomer units) with a PDI value of 1.11, so diblock copolymers **P3** and **P4** only contain about 6 and 3 units of methacrylate monomers consisting of biphenyl-4-ylthiophene (**M1**) and biphenyl-4-ylfluorene (**M2**) pendants, respectively, as shown in the chemical structures of Scheme 4.2.

Table 4.1 Molecular weight and thermal properties of polymers **P1-P4**

Sample	M_n (gmol ⁻¹)	M_w (gmol ⁻¹)	PDI (M_w/M_n)	Td (°C) ^a	Tg (°C) ^b
P1 ^c	- ^c	- ^c	- ^c	315.2	187.2
P2	5103	6402	1.25	337.9	81.3
P3 ^d	8713	10370	1.19	349.0	91.3
P4 ^d	7898	9238	1.17	333.1	90.6

^a Temperature of 5% weight loss measured by TGA under nitrogen.

^b The glass transition temperatures (°C) were determined by DSC (with a heating and cooling rate of 5 °C /min).

^c The molecular weight was undetermined due to polymer **P1** is insoluble in most organic solvents.

^d The number-average molecular weight (M_n) of macroinitiator **SMi** determined by GPC was 6196 gmol⁻¹ with a PDI value of 1.11.

4.3.2 Thermal and mesogenic properties

The thermal stabilities of polymers (**P1-P4**) under an atmosphere of nitrogen were evaluated by thermogravimetric analysis (TGA), which indicate that the values of Td (the degradation temperature of 5% weight loss in nitrogen) ≥ 315 °C for all polymers (as shown in Table 4.1). Due to the unclear glass transition temperatures (Tg) of these block copolymers, Tg values were only detectable during the first heating scans of DSC measurements (with a heating rate of 5 °C/min) by following the quench of polymers (from 200 °C) in liquid nitrogen. By this quenching process, the Tg values of all polymers in DSC measurements were demonstrated more clearly in the range of 81 to 187 °C as shown in Table 4.1 and Figure 4.1. Comparing polymers **P1** and **P2**, they exhibited glass transition temperatures (Tgs) at 187 and 81 °C, correspondingly. **P1** was more rigid than **P2** due to without any lateral flexible chains on the pendants of **P1** and thus to have poorer solubility. Therefore, the Tg value of **P1** was higher than that of **P2**. However, the Tg values of block copolymers **P3** and **P4** were comparable (around 91 °C), which were mostly contributed from the

flexible blocks of polystyrene (PS) ⁵¹⁻⁵² due to the longer block, i.e. larger molecular weight, of PS originated from macroinitiator **SMi**.

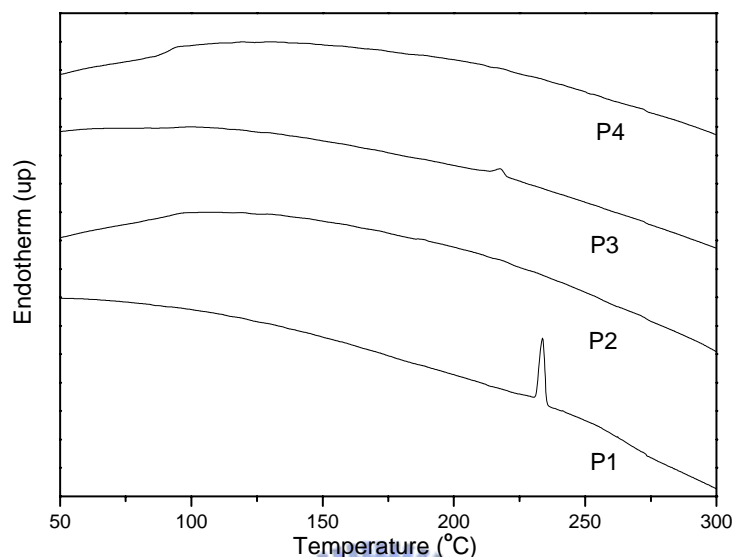


Figure 4.1 DSC thermograms of polymers **P1-P4** during the first heating scan at 5 °C/min.

The mesogenic properties of all polymers were characterized by polarizing optical microscopy (POM) and differential scanning calorimetry (DSC). The phase transition temperatures and enthalpies of polymers **P1-P4** are summarized in Table 4.2 and their DSC thermograms are displayed in Figure 4.1. To avoid thermal decomposition, these polymers were only heated up to about 300 °C (with a heating rate of 5 °C/min). Since both monomers, i.e. biphenyl-4-ylthiophene monomer (**M1**) and biphenyl-4-ylfluorene monomer (**M2**), possess the smectic A and nematic phases, respectively, polymers **P1-P4** indeed inherit the LC properties from their constituents (**M1** and **M2**). Regarding their mesomorphism, homopolymer **P1** and block copolymer **P3** which contain biphenyl-4-ylthiophene units possessed the smectic A phase. **P2** and **P4** were amorphous polymers with $T_g = 81$ and 91 °C, respectively.

Homopolymer **P2** showed a stable glass-forming nematic phase, but **P4** did not possess any mesogenic phase due to a less monomer content (**M2**) of biphenyl-4-ylfluorene units in the copolymer composition of **P4**. Figure 4.2 showed a fan-shaped focal conic texture of homopolymer **P1** observed by POM (at 255 °C cooling), which is a characteristic texture of the smectic A phase. In addition, their smectic phases had been further confirmed by X-ray diffraction (XRD) measurements (will be described later). Because of no lateral flexible chains on the thiophene pendants of **P1** and **P3**, rigid rods of LC blocks generate stronger transverse interaction and thus to induce the smectic phases in polymers **P1** and **P3**. Interestingly, even though block copolymer **P3** contains only about 6 biphenyl-4-ylthiophene monomer units (**M1**) and 59 styrene monomer units, **P3** still can sustain its mesogenic property ascribed to the rigid thiophene pendants of the short block (6 monomer units). Regarding homopolymer **P2**, the lateral diethyl groups on 9 position of fluorene pendants, which separate the rigid cores of the side-chains, cause the reduction of transverse interaction among rigid rods in **P2** and thus to favor the nematic phase. However, in contrast to polymers **P1-P3**, block copolymer **P4** contains only about 3 biphenyl-4-ylfluorene monomer units (**M2**) but with 59 styrene monomer units, so it led to no mesogenic phase in **P4** due to the less rigidity and shorter block of biphenyl-4-ylfluorene LC units. Moreover, polymers **P1** and **P3** with thiophene pendent groups revealed higher isotropization temperatures (T_i around 270 °C) than polymers **P2** and **P4** with fluorene pendent groups (T_i around 140 °C). Therefore, the comparison of isotropization temperatures in monomers **M1-M2** and polymers **P1-P4** additionally suggests that the rigidity of biphenyl-4-ylthiophene units is higher than that of biphenyl-4-ylfluorene units.

Table 4.2 Phase behavior of polymers **P1-P4**^{a,b,c}

Sample	Transition temperature (°C) and enthalpy (in parentheses, kJ/g)	Ti (°C) ^d
<i>P1</i>	K 235.4 (15.8) S_A	~ 270
<i>P2</i>	G 81.3 N	~ 140
<i>P3</i>	K 218.9 (4.1) S_A	~ 275
<i>P4</i>	G 90.6	~ 145

^a Transition temperatures (°C) and enthalpies (in parentheses, kJ/mol) were determined by DSC (a heating rate of 5 °C /min).

^b **G**= glass temperature; **K** = crystalline; **N** = nematic; **S_A** = smectic A

^c Transition temperatures of **M1** and **M2** are as follows:

M1 : **K** 185.3 °C (52.2 kJ/g) **S_A** with Ti = 245 °C; **M2** : **K** 60.4 °C (3.4 kJ/g) **N** with Ti = 98 °C.

^d Ti : all isotropization temperatures, including monomers **M1** and **M2**, were characterized by polarizing optical microscopy (POM).

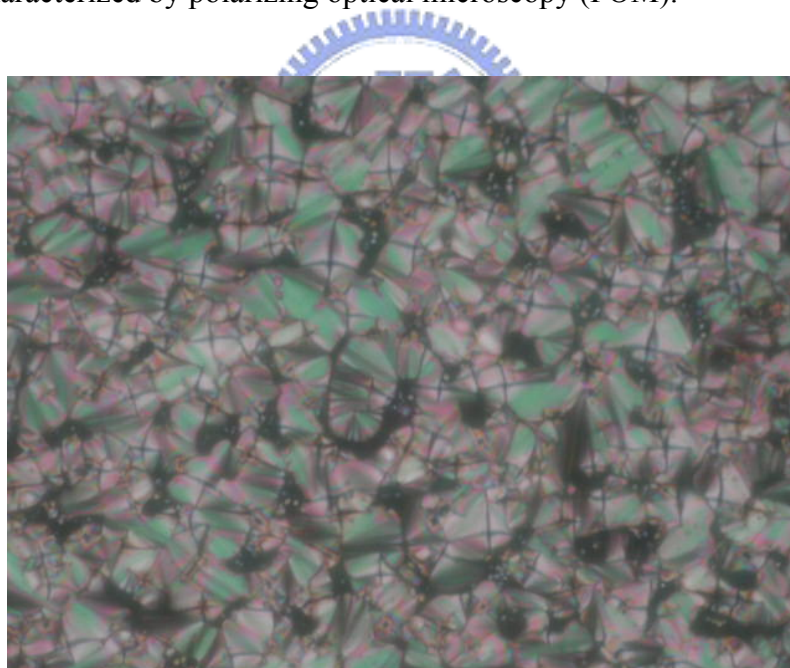


Figure 4.2 POM texture of the mesophase (**S_A**) of polymer **P1** observed at 255 °C (cooling).

4.3.3 X-ray Measurements

In order to elucidate the structures of the mesophases, X-ray diffraction (XRD) measurements were carried out in the temperature ranges of mesophases for polymers

P1–P4, and the XRD data are summarized in Table 4.3. Owing to no smectic phases in **P2** (only the nematic phase) and in **P4** (no mesophase), there are no any peaks in the XRD patterns of polymers **P2** and **P4**. As shown in Figure 4.3, the XRD patterns of polymers **P1** and **P3** are almost identical and their layer d-spacing values are around 29 Å, which were attributed to the layer d-spacing in the rigid blocks of biphenyl-4-ylthiophene units. In addition, the layer d-spacing values in the ratio of 1:1/2 indicate lamellar orders exist in the mesophases of **P1** and **P3**. According to the molecular modeling calculation, the layer d-spacing value of coplanar structure in **M1** is about 23.7 Å. Therefore, the layer d-spacing value of 29 Å by XRD measurements in polymers **P1** and **P3** were suggested to be interdigitated packing of biphenyl-4-ylthiophene units in rigid blocks. By this evidence, the layered structures of polymers **P1** and **P3** have little relationship with respect to the flexible blocks of polystyrene (PS).

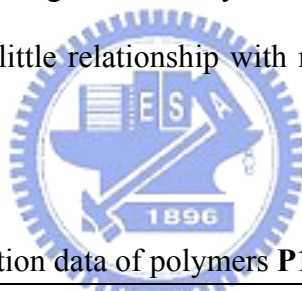


Table 4.3 XRD diffraction data of polymers **P1** and **P3**

Sample	Mesophase	Temperature (°C)	d-Spacing (Å) ^a
P1	S_A	255	d ₀₀₁ = 26.98 d ₀₀₂ = 13.68
P3	S_A	230	d ₀₀₁ = 26.86

^a The theoretical d-spacing value is 23.7 Å for polymers **P1** and **P3**.

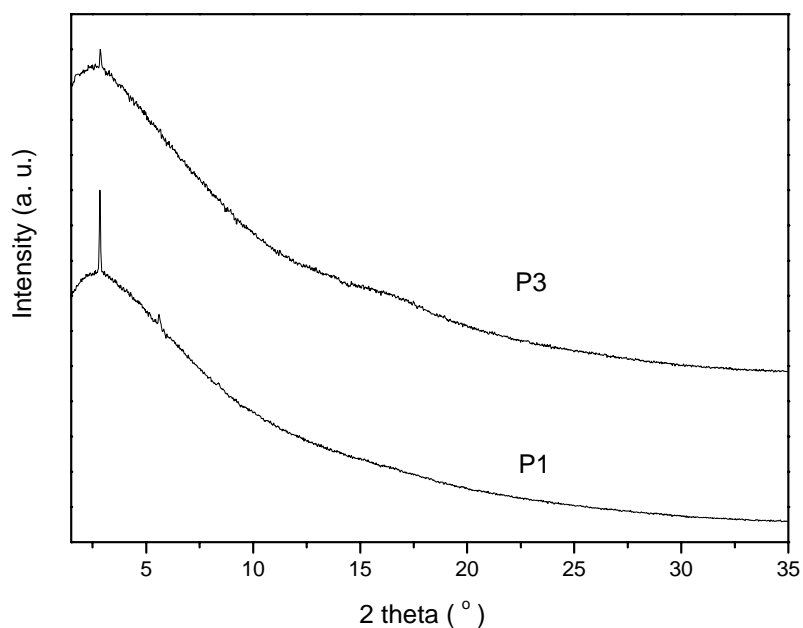


Figure 4.3 X-ray diffraction patterns of polymers **P1** and **P3**.

4.3.4 Photophysical Properties

The photophysical properties, including the UV-visible absorption and photoluminescence (PL) spectral data, of all polymers in THF solutions are summarized in Table 4.4. By reason of the identical rigid cores of luminescent biphenyl-4-ylthiophene units in monomer **M1** and polymers **P1** and **P3**, they have almost the same maximum absorption wavelength around 312 nm and emit blue light at approximately $\lambda_{\text{max,PL}} = 377$ nm in solutions. Comparably, monomer **M2** and polymers **P2** and **P4** have the identical rigid cores of luminescent biphenyl-4-ylfluorene units, therefore, they have almost the same values of the maximum absorption wavelength around 322 nm and the maximum PL wavelength ($\lambda_{\text{max,PL}}$) around 386 nm in solutions.

Table 4.4 UV-visible absorption and photoluminescence spectral data of monomers (**M1** and **M2**) and polymers (**P1-P4**)

Sample	$\lambda_{\max, \text{Abs}}$ (nm) ^a	$\lambda_{\max, \text{PL}}$ (nm) ^a	Φ (%) ^b
M1	312	375	17.5
M2	322	385	23.2
P1	313	377	15.3
P2	321	386	19.0
P3	312	378	15.8
P4	321	387	18.9

^a Absorption and PL spectra were recorded in dilute THF solutions at room temperature.

^b PL quantum yield in THF and 9,10-diphenylanthracene was the reference of the quantum yield.

Figure 4.4 shows the UV-visible absorption and PL spectra of monomers **M1** and **M2** in solutions. Compared with **M1**, monomer **M2** consisting of fluorene units result in longer maximum absorption wavelengths and PL wavelengths due to longer conjugation lengths in rigid cores. By the same reason, the maximum absorption and PL wavelengths of polymers **P2** and **P4** are more red-shifted than those of polymers **P1** and **P3**. Because of the less aggregated form originated from the lateral diethyl groups on fluorene pendants in **M2**, the quantum yield of biphenyl-4-ylfluorene monomer **M2** is higher than that of biphenyl-4-ylthiophene monomer **M1**. Accordingly, the quantum yields of polymers **P2** and **P4** are larger than those of polymers **P1** and **P3**.

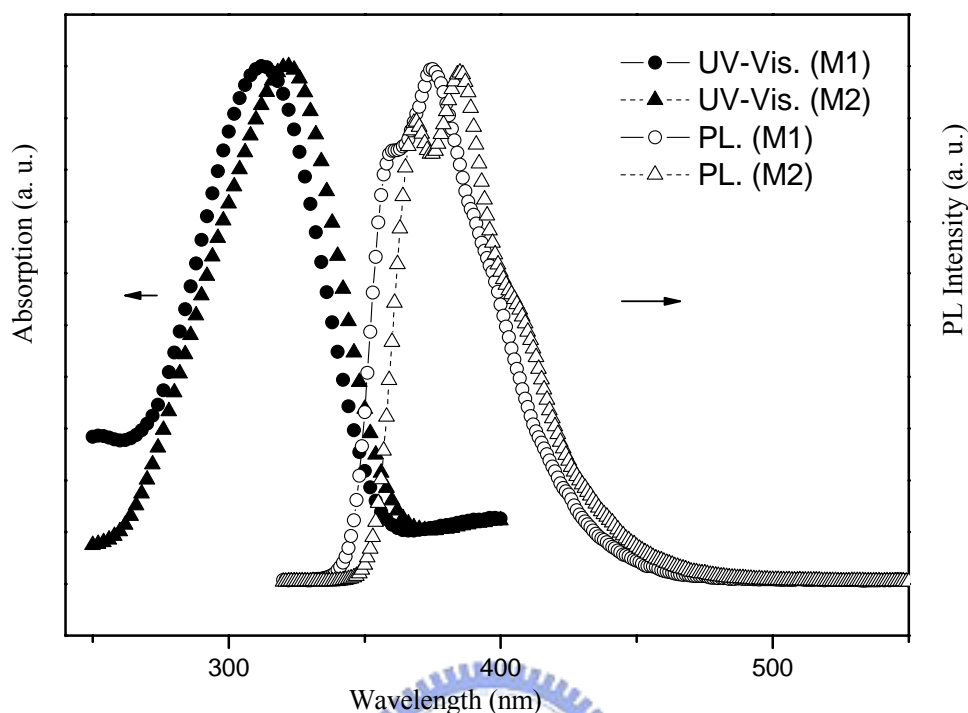


Figure 4.4 UV-visible absorption (solid lines) and PL (dash lines) spectra of monomers **M1** and **M2** in solutions (THF as solvent).

Due to the poor solubility of polymers **P1** and **P3** and lower molecular weights of monomers **M1** and **M2**, the photophysical properties of these compounds in solid films were not obtained. Compared with solutions, solid films of polymers **P2** and **P4** in Figure 4.5 exhibit red-shifted PL emissions around 396 nm owing to the π - π^* aggregation of the rigid cores. In addition, the differences of photophysical properties between polymers **P2** and **P4** (both in solutions and solid films) are trivial, so the flexible PS blocks did not reflect important contribution to the photophysical properties. Figure 4.6 displays the PL spectra of **P2** solid films by spin-coating and quenching (by liquid N₂) from 130 °C (the nematic phase). Due to the frozen nematic structure by quenching, **P2** was more orderly aligned and it led to aggregation of rigid

cores in Figure 4.6. Hence, the shorter wavelength peak at 376 nm in PL spectrum of **P2** solid film became a shoulder by quenching, which is similar to our previous report⁵⁶. In order to evaluate the effect of mesogenic structure on photoluminescence properties, polarized PL spectra (as shown in Figure 4.7) were measured from aligned **P2** solid film by quenching from 130 °C on a rubbing PI substrate. Polarization ratio ($PL_{//} / PL_{\perp}$) was about 1.43, where $PL_{//}$ is the maximum PL emission intensity as the polarizer is parallel to the rubbing direction, and PL_{\perp} is the maximum PL emission intensity as the polarizer is perpendicular to the rubbing direction. This result shows the effect of mesogenic alignment of **P2** on rubbing PI substrate can induce a polarized PL emission with a polarization ratio 1.43.

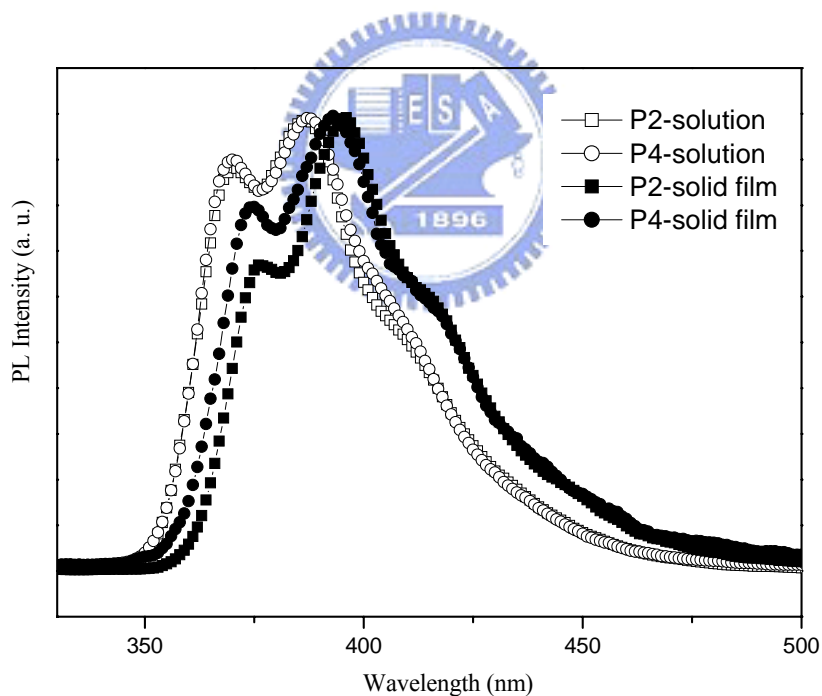


Figure 4.5 PL spectra of polymers **P2** and **P4** in solid films and solutions (THF as solvent).

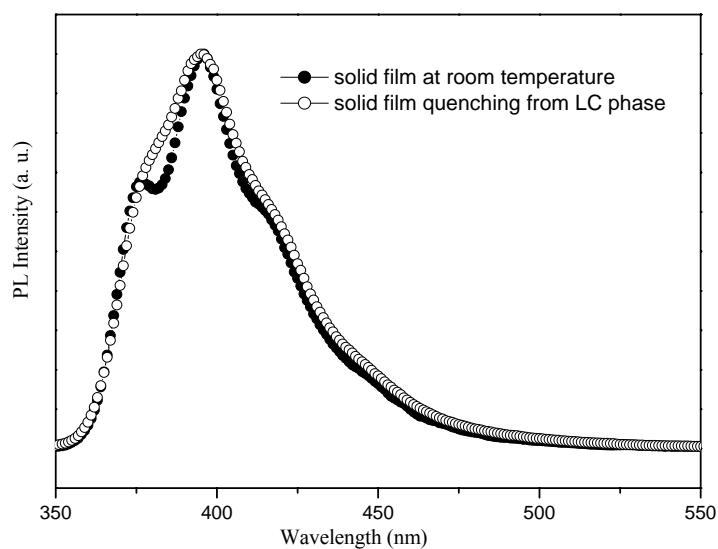


Figure 4.6 PL spectra of polymer **P2** in the solid state by spin-coating and quenching (by liquid N₂) from 130 °C (the nematic phase).

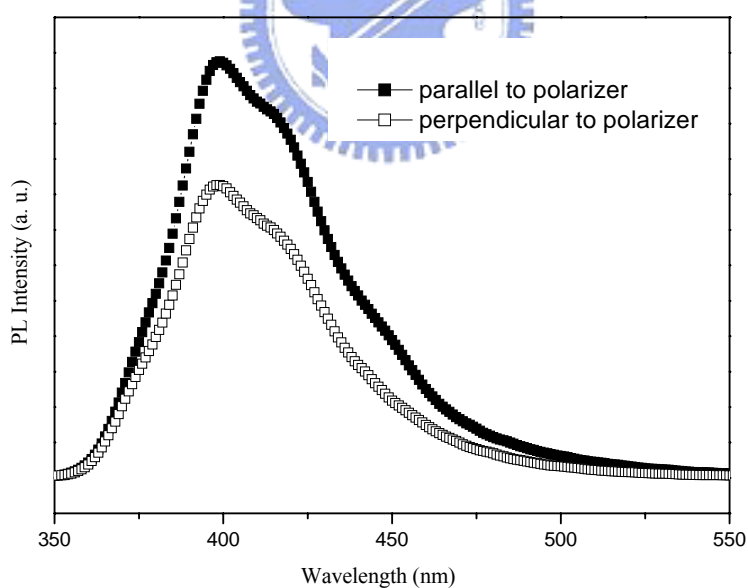
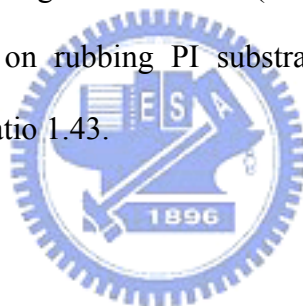


Figure 4.7 Polarized PL spectra of aligned **P2** solid film by quenching from 130 °C on a rubbing PI substrate, where PL_{//} is the parallel PL intensity as the polarizer is parallel to the rubbing direction, and PL_⊥ is the perpendicular PL intensity as the polarizer perpendicular to the rubbing direction.

4.4 Conclusion

Atom transfer radical polymerization (ATRP) was employed to fabricate block copolymers consisting of PS macroinitiators and liquid crystalline polymethacrylate blocks containing biphenyl-4-ylthiophene (**M1**) and biphenyl-4-ylfluorene (**M2**) units. Thermal and XRD investigations indicate that polymers **P1** and **P3** exhibited the interdigitated smectic A phase which has little relationship with respect to their flexible PS blocks. In terms of PL wavelengths of all block copolymers in dilute solutions, **P2** and **P4** are more red-shifted than **P1** and **P3**, which might be due to longer conjugation lengths of the lateral biphenyl-4-ylfluorene blocks in polymers **P2** and **P4**. The shorter wavelength peak at 376 nm in PL spectrum of **P2** solid film became a shoulder by quenching from 130 °C (the nematic phase). The effect of mesogenic alignment of **P2** on rubbing PI substrate can induce a polarized PL emission with a polarization ratio 1.43.



Chapter 5

Synthesis and Characterization of Liquid Crystalline Side-Chain Block Copolymers Containing Luminescent 4,4'-Bis(biphenyl)fluorene Pendants

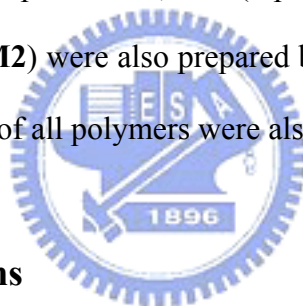
5.1 Introduction

During the past decade, there are several types of liquid crystalline (LC) block copolymers produced by living free-radical polymerizations.^{35-38, 64} Matyjaszewski's group⁶⁵ and Sawamoto and co-workers⁶⁶ independently developed transition metal catalyzed living free radical polymerization known as atom transfer radical polymerization (ATRP), which is typically initiated by an alkyl halide (R-X) and catalyzed by a transition metal complex, such as CuX/bpy. ATRP has been demonstrated to provide controlled polymerizations of styrenes, methacrylates, and acrylonitriles with variations of compositions and architectures.

Recently, ATRP were also used in the synthesis of side-chain LC block copolymers,^{34, 67-70} in which mesogenic pendent groups were grafted onto polymer backbones to form side-chain LC blocks. The interest in this type of materials resides in the cohesive properties of two (or more than two) completely different polymers which are chemically bonded to each other. The macrophase separation takes place due to the segregation of different polymer chains. In order to introduce luminescent properties into LC polymers, the combination of long conjugation rigid cores with flexible chains is required for the molecular design of luminescent LCs.⁷¹⁻⁷³ However, the microphase structures of side-chain LC polymers were influenced by the mesogenic groups, such as azobenzene^{4,39-40} and biphenyl⁴¹⁻⁴⁶ units, which were

frequently used in LC monomers.

In our previous studies^{58,63}, main-chain block copolymers containing conjugated fluorene, thiophene, and biphenyl backbones as well as side-chain block copolymers containing biphenyl-4-ylthiophene or cyanoterphenyl pendants possess the smectic A and columnar (Col_h and Col_r) phases, but side-chain block copolymers consisting of biphenyl-4-ylfluorene pendants possess the nematic phase. Herein, a series of a new mesogenic homopolymer and block copolymer (**P1** and **P2**), which were composed of styrene-macroinitiators (**SMi**) and methacrylates with pendent 4,4'-bis(biphenyl)fluorene (**M1**) groups, were synthesized through atom transfer radical polymerization(ATRP). In addition, random copolymer **P3** and block copolymer **P4** consisting of pendent 4,4'-bis(biphenyl)fluorene units (**M1**) and biphenyl-4-ylfluorene units (**M2**) were also prepared by ATRP. Furthermore, thermal, mesogenic, and PL properties of all polymers were also investigated in this study.



5.2 Experimental Sections

5.2.1 Measurements

¹H NMR spectra were recorded on a Varian unity 300 MHz spectrometer using CDCl₃ and d₆-DMSO solvents. Elemental analyses were performed on a HERAEUS CHN-OS RAPID elemental analyzer. Transition temperatures were determined by differential scanning calorimetry (DSC) (Perkin–Elmer, model: Diamond) with a heating and cooling rate of 5 °C/min. The mesogenic properties were studied using a polarizing optical microscope (POM) (Leica, model: DMLP) equipped with a hot stage. Thermogravimetric analysis (TGA) was conducted on a Du Pont Thermal Analyst 2100 system with a TGA 2950 thermogravimetric analyzer at a heating rate of 10°C/min under nitrogen. Gel permeation chromatography (GPC) analysis was conducted on a Waters 1515 separation module with chloroform as the eluant against

a polystyrene calibration curve. High-resolution electron impact mass data were obtained on a Finnigan-MAT-95XL. UV-visible absorption spectra were recorded in dilute THF solutions (10^{-6} M) on a HP G1103A spectrophotometer. Photoluminescence (PL) spectra were obtained on a Hitachi F-4500 spectrophotometer.

5.2.2 Materials

Chemicals and solvents were reagent grade and purchased from Aldrich, ACROS, TCI, and Lancaster Chemical Co. Dichloromethane and THF were distilled to keep anhydrous before use. Pyridine was dried by refluxing over calcium hydride. The other chemicals were used without further purification.

5.2.3 Synthesis

Atom transfer radical polymerization (ATRP) is very versatile and is tolerant for a wide range of functional groups present either in the monomers, solvents, or initiators.^{49,50, 63} Schemes 5.1 and 5.2 summarize the steps involved in the syntheses of the macroinitiator (**SMi**), monomers (**M1** and **M2**), and polymers (**P1-P4**), and the details of each step are given below.

4-Bromo-4'-octoxybiphenyl (2). 1-Bromooctane (11.6 g, 60 mmol), 4-bromo-4'-hydroxybiphenyl (10 g, 40 mmol), and potassium carbonate (16.6 g, 120 mmol) were dissolved in butan-2-one (100 mL) and reacted under reflux for 24 h. After cooling to room temperature, the potassium salt was filtered off. The solvent was removed by rotavapor and the crude product was recrystallized from petroleum ether (bp: 35-60 °C) to yield a white solid (13.5 g, 93%). ¹H NMR (ppm, CDCl₃), δ : 0.89 (t, $J = 6.9$ Hz, 3H), 1.29-1.47 (m, 10H), 1.80 (quintet, $J = 6.6$ Hz, 2H), 3.98 (t, J

= 8.6 Hz, 2H), 6.99 (d, $J = 8.8$ Hz, 2H), 7.40-7.54 (m, 6H).⁶³

4'-Octoxybiphenyl-4-ylboronic Acid (3). 4-Bromo-4'-octoxybiphenyl (**2**) (5 g, 13.8 mmol) was dissolved in THF (200 mL) and then n-butyllithium (8.9 mL, 2.5 M, 22.1 mmol) was added dropwise to react at -78 °C. The reaction mixture was maintained under this condition for 1 h. Furthermore, it was added dropwise to trimethyl borate solution (3.5 g, 33.2 mmol) at -78 °C. The solution was allowed to cool to room temperature overnight. The final solution was acidified with 100 mL of 10 % HCl solution and stirred for 45 min at room temperature. The solution was washed with saturated sodium carbonate solution and water, and then THF was removed. The crude product was extracted by diethyl ether and the organic layer was dried over magnesium sulfate. After removing the solvent by rotavapor, the resulting solid was washed with petroleum ether and briefly dried on filter to obtain a white solid (6.0 g, 80%). ¹H NMR (ppm, d₆-DMSO), δ : 0.85 (t, $J = 7.2$ Hz, 3H), 1.24-1.41 (m, 10H), 1.71 (quintet, $J = 6.6$ Hz, 2H), 3.98 (t, $J = 6.6$ Hz, 2H), 6.99 (d, $J = 8.8$ Hz, 2H), 7.56-7.62 (m, 4H), 7.83 (d, $J = 8.8$ Hz, 2H), 8.03 (s, 2H).⁶³

Compound 5. Compound **4** (2.0 g, 5.3 mmol), compound **3** (4.0 g, 12.3 mmol), and tetrakis(triphenylphosphine)palladium(0) (307 mg, 0.27 mmol) were reacted in THF (120 mL) for 10 min, and then 80 mL of 2 M aqueous Na₂CO₃ solution was added. The mixture was reacted and refluxed for 48 h. After reaction, the cooled solution was washed with dilute hydrochloric acid (10%) and water, and dried over magnesium sulfate. The final solution was purified by column chromatography (silica gel, CH₂Cl₂/hexane 1:1) to yield a white solid (3.3 g, 87%). ¹H NMR (ppm, CDCl₃), δ : 0.42 (t, $J = 6.9$ Hz, 6H), 0.89 (t, $J = 6.9$ Hz, 6H), 1.31-1.61 (m, 20H), 1.84 (m, 4H), 2.14 (q, $J = 7.3$ Hz, 4H), 4.01(t, $J = 6.0$ Hz, 4H), 6.98 (d, $J = 7.8$ Hz, 4H), 7.57-7.80 (m, 18H).

Compound 6.Compound **5** (3.3 g, 4.5 mmol) was dissolved in dry chloroform

(150 mL) under nitrogen and then boron tribromide (3.4 g, 13.6 mmol) was added dropwise to react at -78 °C. The mixture was allowed to warm up to room temperature and reacted for 24 h. The solution was washed with sodium hydroxide (1 M, 50 mL), and then the solution was acidified with 10% HCl and stirred for 4 h. Finally, the suspension was filtered off and purified by column chromatography (silica gel, ethyl acetate) to yield a white solid (2.4 g, 94%). ¹H NMR (ppm, d₆-DMSO), δ: 0.29 (t, *J* = 7.2 Hz, 6H), 2.16 (q, *J* = 7.2 Hz, 4H), 6.87 (d, *J* = 8.4 Hz, 4H), 7.5 (d, *J* = 8.7 Hz, 4H), 7.70 (m, 6H), 7.79 (m, 6H), 7.91 (d, *J* = 7.8 Hz, 2H), 9.63 (s, 2H).

Compound 7.Compound **6** (2.2 g, 3.94 mmol) and potassium carbonate (1.09 mg, 7.88 mmol) were dissolved in 50 mL of DMF and then 1-bromooctane (760 mg, 3.94 mmol) was added in solution to react for 24 h by reflux. After cooling to room temperature, the solution was extracted with dichloromethane and water, and the organic layer was dried over magnesium sulfate. The final solution was purified by column chromatography (silica gel, CH₂Cl₂) to yield a white solid (1.3 g, 54%). ¹H NMR (ppm, CDCl₃), δ: 0.43 (t, *J* = 7.2 Hz, 6H), 0.90 (t, *J* = 6.6 Hz, 3H), 1.25-1.48 (m, 10H), 1.82 (m, 2H), 2.14 (q, *J* = 6.9 Hz, 4H), 4.01 (t, *J* = 6.6 Hz, 2H), 4.90 (s, 1 H), 6.92-7.01 (m, 4H), 7.53-7.67 (m, 12H), 7.73-7.80 (m, 6H).

Compound 8.Compound **7** (1.2 g, 1.80 mmol), 6-bromo-1-hexanol (421 mg, 2.33 mmol), K₂CO₃ (740 mg, 5.4 mmol), and KI (20 mg) were dissolved in 80 mL of DMF to reflux overnight. The reaction mixture was then cooled and poured into 200 mL of water and stirred for 2 h. The crude product was extracted with ethyl acetate and the organic layer as washed with a saturated aqueous solution of NaCl and water, and then the organic layer was dried over magnesium sulfate. After removing the solvent by rotavapor, the residue was recrystallized from absolute ethanol to give a colorless solid (1.1 g, 80%). ¹H NMR (ppm, CDCl₃), δ: 0.43 (t, *J* = 7.2 Hz, 6H), 0.88 (t, *J* = 6.0 Hz, 3H), 1.31-1.86 (m, 20H), 2.15 (m, 4H), 3.67 (m, 2H), 4.01 (m, 4H),

7.00 (m, 4H), 7.57-7.80 (m, 18H).

M1. Compound **8** (1.1 g, 1.4 mmol), triethylamine (1.4 g, 14.3 mmol), and 2,6-di-tertbutyl-4-methylphenol (30 mg, as a thermal inhibitor) were dissolved in 100 mL of anhydrous THF under a nitrogen atmosphere and then methacryloyl chloride (448 mg, 4.3 mmol) was added dropwise. The reaction mixture was heated under reflux overnight and then cooled to pour into 200 mL of aqueous NH₄Cl solution (10%). The crude product was extracted with CH₂Cl₂. The resulting organic layer was washed with a saturated solution of NaCl and water, and the organic layer was dried over magnesium sulfate. After removing the solvent by rotavapor, the resulting solid was purified by column chromatography using dichloromethane as an eluant to yield a colorless solid (1.1 g, 92%). ¹H NMR (ppm, CDCl₃), δ: 0.41 (t, *J* = 7.2 Hz, 6H), 0.88 (t, *J* = 6.9 Hz, 3H), 1.31-1.82 (m, 20H), 1.94 (s, 3H), 2.12 (m, 4H), 3.98(m, 2H), 4.15 (m, 4H), 5.54 (s, 1H), 6.09 (s, 1H), 6.98 (m, 4H), 7.55-7.79 (m, 18H). Elemental analysis for C₅₉H₆₆O₄: Calc. C, 84.45; H, 7.93; Found C, 84.12; H, 7.74. LRMS (EI) *m/z*: Calc. 838.4; Found 838.4.

M2. The synthetic route has been reported in our previous study.⁷⁴ Yield: 83%. ¹H NMR (ppm, CDCl₃), δ: 0.36 (t, *J* = 6.9 Hz, 6H), 1.45 -1.56 (m, 4H), 1.67-1.83 (m, 4H), 1.94 (s, 3H), 2.06 (m, 4H), 4.01 (t, *J* = 6.3 Hz, 2H), 4.16 (t, *J* = 6.6 Hz, 2H), 5.54 (s, 1H), 6.09 (s, 1H), 6.98 (d, *J* = 8.7 Hz, 2H), 7.32-7.36 (m, 3H), 7.55-7.77 (m, 10H). Elemental analysis for C₃₉H₄₂O₃: Calc. C, 83.83; H, 7.58; Found C, 83.52; H, 7.54. HRMS (EI) *m/z*: Calc. 558.3134; Found 558.3126.

Polymerization of macroinitiator SMi. In a Schlenk flask, *N,N,N',N',N''*-pentamethyldiethylenetriamine (PMDETA, 3.46 mg, 0.5 mmol), CuBr (14.3 mg, 0.25 mmol), and styrene (6.8 g, 65 mmol) were added and stirred for 30 min. Ethyl 2-bromo-2-methylpropanoate (195 mg, 1 mmol) was added, and the mixture was immediately frozen in liquid nitrogen under vacuum. After several

freeze-thaw cycles, the flask was sealed under vacuum and put in an oil bath at 100 °C for 20 h. After the reaction, the content was dissolved in chloroform. After being concentrated, the chloroform solution was precipitated into methanol and the precipitation was repeated for three times. The final product was dried at 50 °C under vacuum. Yield: 75%. The number-average molecular weight measured by GPC is $M_n = 6196 \text{ gmol}^{-1}$ with PDI (M_w/M_n) = 1.11.

General synthetic procedures of all polymers

According to analogous procedures as shown in scheme 5.2, **P1 -P4** were synthesized by utilization of different initiators.

An example of polymerization for polymer P2

4 mg (0.04 mmol) of CuCl, 63 mg (0.01 mmol) of **SMi**, and 251 mg (0.3 mmol) of **M1** were mixed under nitrogen. 27 μL (22.9 mg, 0.1 mmol) of 1,1,4,7,10,10-hexamethyltriethylenetetramine (HMTETA) in 3 mL of anisole was added through a syringe. The mixture was degassed three times using the freeze-pump-thaw procedure and sealed under vacuum. After stirring for 30 min at room temperature, the mixture was reacted at 100 °C in a preheated oil bath for 12 h. The solution was passed through a neutral Al₂O₃ column with THF as an eluant to remove the catalyst. The white filtrate was concentrated under reduced pressure and reprecipitated twice into methanol. The white product of polymer was collected by filtration and dried under vacuum. Yield: 125 mg (40%). ¹H NMR (ppm, CDCl₃), δ : 0.35 (broad), 0.88 (broad), 1.28-1.78 (broad), 2.01 (broad), 3.94 (broad), 6.56 (broad), 6.98 (broad), 7.55(broad). The number-average molecular weight measured by GPC is $M_n = 14852 \text{ gmol}^{-1}$ with PDI (M_w/M_n) = 1.15.

PI: Yield: 85 mg (34%). ¹H NMR (ppm, CDCl₃), δ : 0.36 (broad), 0.88 (broad), 1.28-1.94 (broad), 2.03 (broad), 3.97 (broad), 6.94 (broad), 7.57 (broad). The

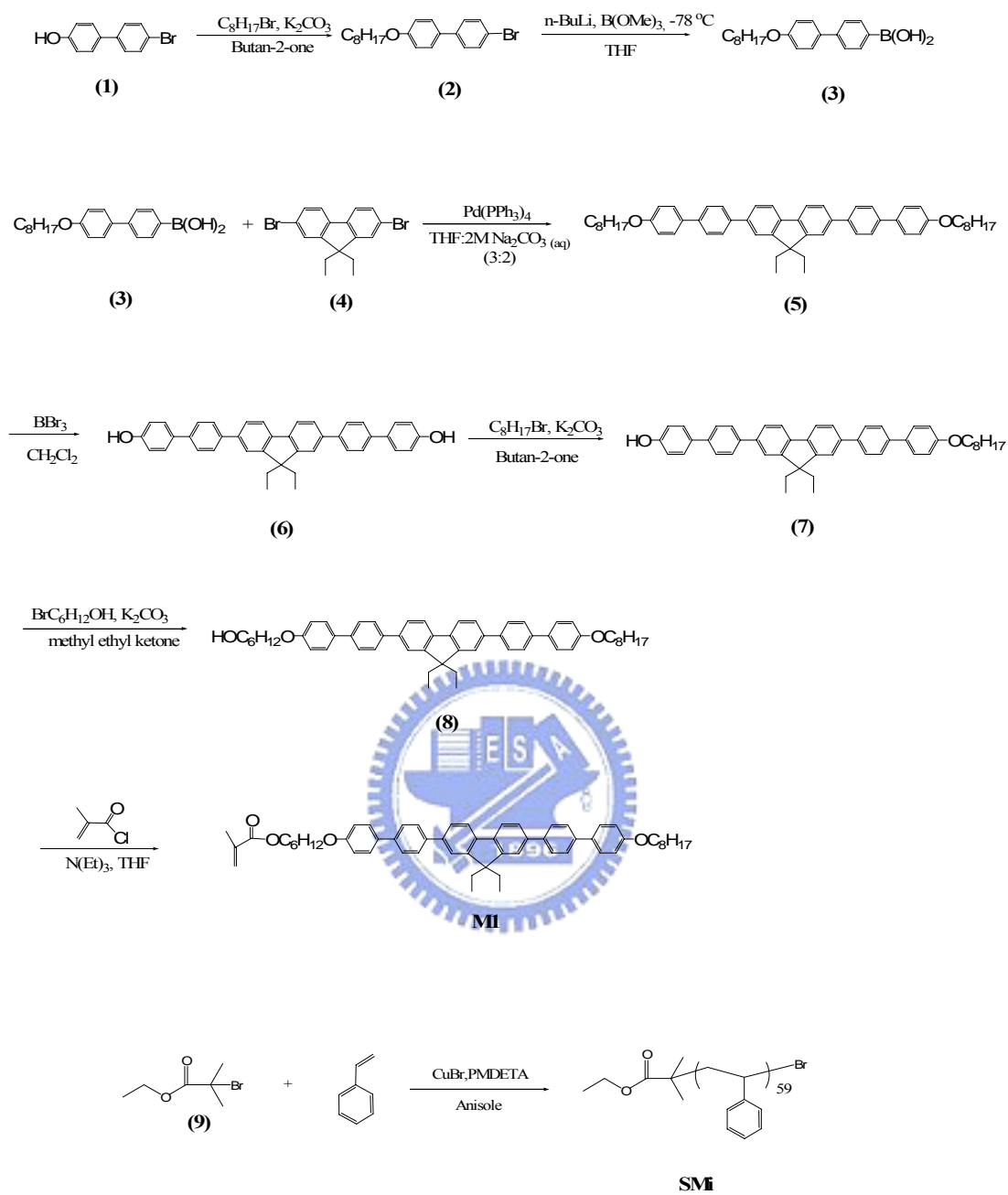
number-average molecular weight measured by GPC is $M_n = 10007 \text{ gmol}^{-1}$ with PDI (M_w/M_n) = 1.21.

P3: (M1/M2/initiator =15/15/1). Yield: 75 mg (30%). ^1H NMR (ppm, CDCl_3), δ : 0.36 (broad), 0.86 (broad), 1.24-1.94 (broad), 2.04 (broad), 3.99 (broad), 6.96 (broad), 7.30 (broad), 7.62 (broad). The number-average molecular weight measured by GPC is $M_n = 6275 \text{ gmol}^{-1}$ with PDI (M_w/M_n) = 1.31.

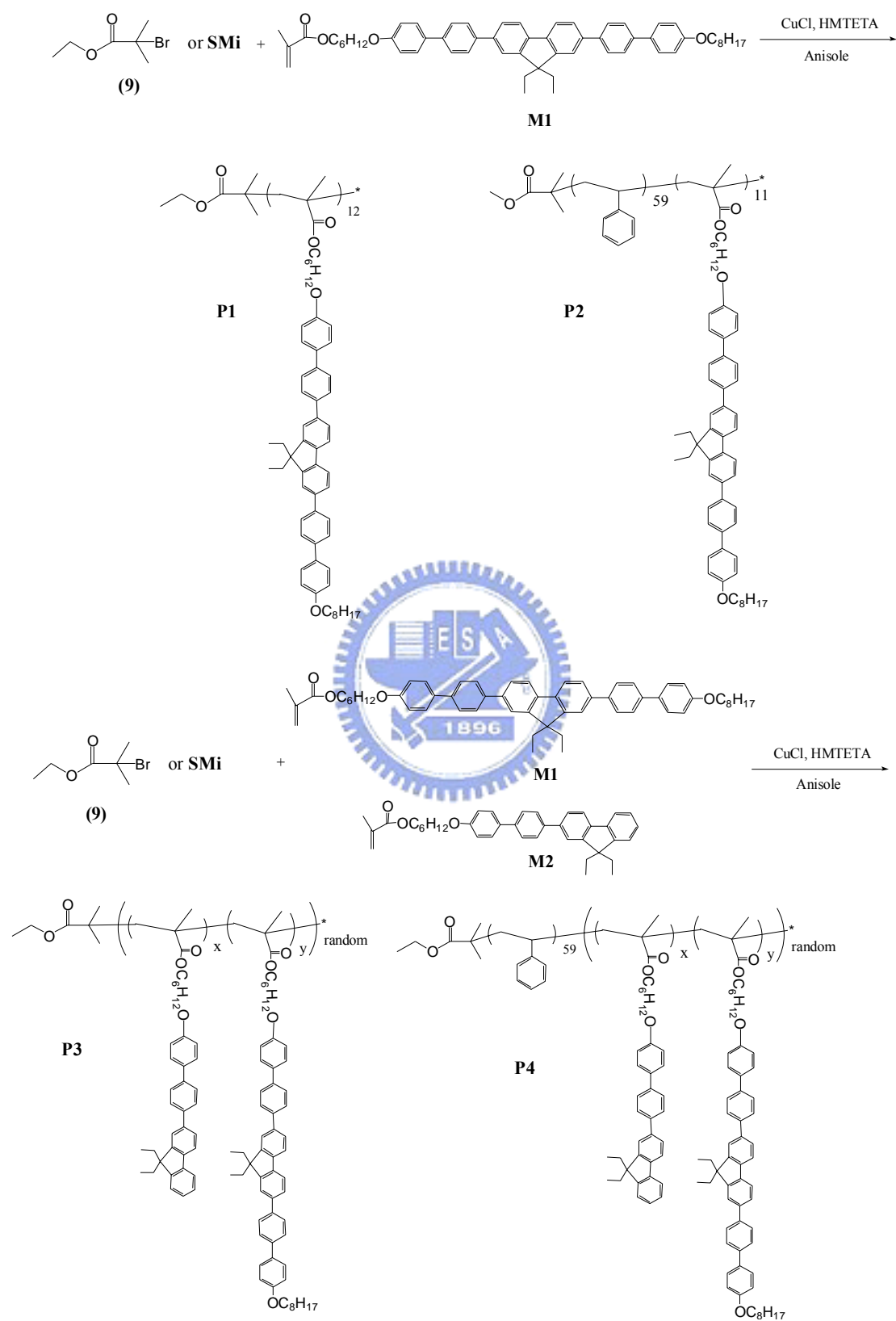
P4: (M1/M2/initiator =15/15/1). Yield: 121 mg (39%). ^1H NMR (ppm, CDCl_3), δ : 0.35 (broad), 0.87 (broad), 1.28-1.79 (broad), 2.03(broad), 3.96 (broad), 6.55 (broad), 6.94(broad), 7.29 (broad), 7.55 (broad). The number-average molecular weight measured by GPC is $M_n = 10643 \text{ gmol}^{-1}$ with PDI (M_w/M_n) = 1.22.



Scheme 5.1 Synthetic routes of the monomer (**M1**) and the macroinitiator (**SMi**).



Scheme 5.2 Synthetic routes of polymers (**P1-P4**).



5.3 RESULTS AND DISCUSSION

5.3.1 Synthesis and Characterization

In this study, the styrene-macroinitiator (**SMi**),⁶⁵ was used to copolymerize with methacrylate monomers containing luminescent 4,4'-bis (biphenyl)fluorene units (**M1**) to produce diblock copolymer **P2** by ATRP. In addition, random copolymer **P3** and block copolymer **P4** containing pendent 4,4'-bis(biphenyl)fluorene units (**M1**) and biphenyl-4-ylfluorene units (**M2**) were synthesized by similar (ATRP) procedures. The number-average molecular weights (M_n) and PDI values of all polymers (**P1-P4**) containing mesogenic 4,4'-bis(biphenyl)- fluorene units and biphenyl-4-ylfluorene units are shown in Table 5.1. The number-average molecular weight (M_n) of macroinitiators (**SMi**) is 6196 gmol^{-1} with a PDI value of 1.11. Comparing NMR spectra of random copolymer **P3** and block copolymer **P4**, a broad peak of **P4** at 6.56 ppm belonged to the chemical shift of polystyrene block and a broad peak at 6.98 ppm incorporated chemical shifts of **M1** and **M2** with that of polystyrene block, so **P4** could be recognized as a diblock copolymer. However, due to the overlapped proton peaks around phenyl and alkyl groups of **M1** and **M2** in NMR spectra of polymers **P3** and **P4**, the molar ratio of **M1** and **M2** in random copolymer **P3** and block copolymer **P4** could not be distinguished, so the values of x and y in the chemical structures of random copolymer **P3** and block copolymer **P4** in Scheme 6.2 are undetermined.

Table 5.1 Molecular weights and polydispersity indexes of polymers **P1-P4**

Polymer	M_n (gmol^{-1})	M_w (gmol^{-1})	PDI (M_w/M_n)
P1	10007	12108	1.21
P2	14852	17137	1.15
P3	6275	8220	1.31
P4	10463	12984	1.22

5.3.2 Thermal and Mesogenic Properties

The thermal stability of polymers (**P1-P4**) under an atmosphere of nitrogen was evaluated by thermogravimetric analysis (TGA), which indicates that T_d (the degradation temperature of 5% weight loss in nitrogen) ≥ 350 °C for all polymers (shown in Table 5.2). The mesogenic properties were characterized by polarizing optical microscopy (POM) and differential scanning calorimetry (DSC). The phase transition temperatures and enthalpies of all polymers are summarized in Table 5.2. Regarding their mesomorphism, all polymers exhibit the nematic phase with mesophasic ranges wider than 200 °C. In our previous studies^{63,74}, block copolymers containing conjugated main-chain fluorene, thiophene, and biphenyl blocks as well as block copolymers containing side-chain biphenyl-4-ylthiophene or cyanoterphenyl blocks possess the smectic A and columnar (Col_h and Col_r) phases, but block copolymers consisting of side-chain biphenyl-4-ylfluorene blocks possess the nematic phase. Compared with the smectic A phase of the polymers in our previous studies, the side-chains of the rigid cores in polymers **P1-P4** composed of pendent 4, 4'-bis(biphenyl)fluorene and biphenyl-4-ylfluorene units were separated by the diethyl groups on 9 position of fluorene units which cause the reduction of lateral interaction among rigid rods and thus to favor the nematic phase. To avoid thermal decomposition, these polymers were only heated up to about 320 °C (with a heating rate of 5 °C/min) and all polymers (**P1-P4**) revealed isotropization temperatures (T_i) around 299 ~ 316 °C. Figure 5.1 showed that a schlieren texture of the corresponding nematic phase of **P1** observed by POM at 280 °C (cooling).

Table 5.2 Thermal properties of polymers **P1-P4**^{a,b,c}

<i>Polymer</i>	Transition Temp. (°C) ^{b,c}	Td (°C) ^a	Tg (°C)
P1	N 299.5 (1.78) I	392.0	60.1
P2	N 316.1 (0.76) I	367.3	88.2
P3	N 308.4 (4.54) I	351.0	56.4
P4	N 298.2 (4.34) I	362.3	89.7

^aTemperature of 5% weight loss measured by TGA under nitrogen.

^bTransition temperatures (°C) and enthalpies (in parentheses, kJ/g) were determined by DSC (with heating rates of 5 °C /min).

^cN = nematic phase; I = isotropization temperature.

Transition temperatures (measured by DSC) of **M1** and **M2**:

M1 : **K** 104.4 °C (31.5 kJ/g) **N** 266.0 °C (1.86 kJ/g) **Ti**

M2 : **K** 60.4 °C (3.4 kJ/g) **N** 98.0 °C **Ti** (Ti was characterized by POM)

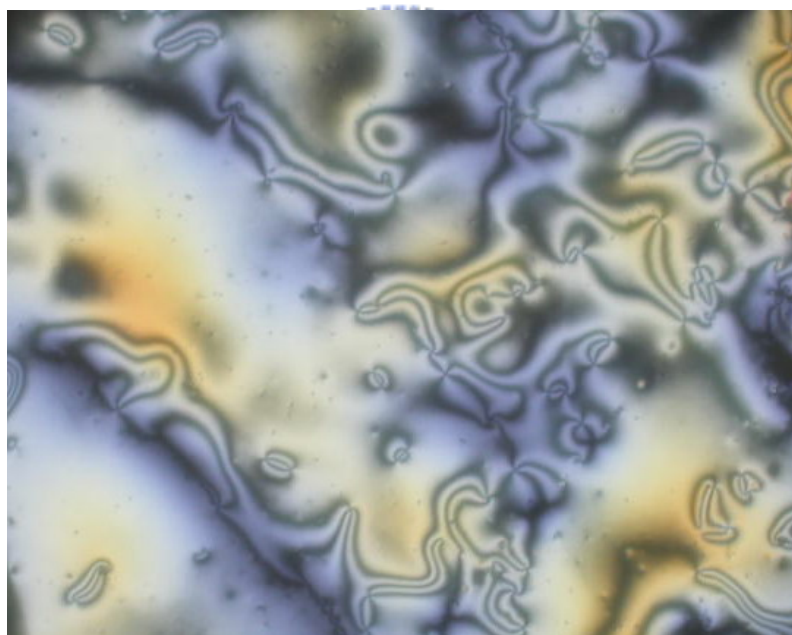


Figure 5.1 The schlieren texture (the nematic phase) of **P1** observed by POM at 280°C (cooling).

Because of the unclear glass transition temperatures (Tg) of these block copolymers, Tg values were detectable in the first heating scans of DSC measurements (with a heating rate of 5°C/min) by quenching of polymers (from 200 °C) in liquid nitrogen.

By this quenching process, the DSC results can reveal Tg values of all polymers more clearly (in the range of 56 to 90 °C as shown in Table 5.2). In Table 5.2, polymers **P1** and **P3** exhibit the glass transition temperatures (Tgs) at 60 and 56 °C, respectively. Tgs of **P2** and **P4** (around 90 °C) were mostly contributed from the polystyrene block.^{51, 52}

In order to elucidate the structures of the mesophases, X-ray diffraction (XRD) measurements were carried out at the temperature ranges of mesophases, which were determined by DSC and POM, for polymers **P1–P4**. The nematic phase of all polymers characterized by the schlieren texture of POM is further confirmed by the results of no refraction peaks observed in the XRD patterns.

5.3.3 Photophysical Properties

The photophysical properties of polymers **P1–P4** including UV-visible absorption spectra and photoluminescence (PL) spectra in THF solutions are summarized in Table 5.3. Due to identical rigid cores of luminescent 4,4'-bis(biphenyl)fluorene pendants (**M1**), the synthesized polymers **P1** and **P2** have almost the same maximum absorption wavelength around 343 nm in solutions and solid films. In addition, the maximum photoluminescence wavelengths ($\lambda_{\text{max,PL}}$) were around 396 nm in solutions and 425 nm in films, respectively. Polymers **P3** and **P4** both possess the biphenyl-4-ylfluorene pendants (**M2**), therefore, they had the same maximum absorption wavelength around 336 nm in solutions and films. Figure 5.2 shows an example of PL spectra of the monomers (**M1** and **M2**) and polymers (**P1** and **P3**) in solutions. Compared with **M2** (which was reported in our previous study)⁵⁸, **M1** consisting of an additional biphenyl unit results in the longer conjugation lengths than **M1**. Hence, the maximum absorption wavelengths and PL wavelengths of **M1** are

more red-shifted than **M2**. In Figure 5.3, due to the biphenyl-4-ylfluorene pendants of **P3**, the maximum absorption wavelength of **P3** was more blue-shifted than that of **P1** (around 343nm) in films and solutions. However, the $\lambda_{\max,PL}$ values of **P1** and **P3** were almost the same (396 nm in solutions and 423 nm in films). This phenomenon may be originated from the energy transfer of biphenyl-4-ylfluorene pendants to 4,4'-bis(biphenyl)fluorene pendants which can be confirmed by the overlapped UV-visible spectra of **M2** and PL spectra of **M1**. However, Intermolecular aggregation of luminescent pendants could cause shoulders of P1 and P3 around 440 nm in Figure 3. In addition, the quantum yields of all polymers consist of 4,4'-bis(biphenyl)fluorene groups (70%) were better than other analogous polymers (around 20%) in our previous studies.^{63,74}

Table 5.3 UV-visible Absorption and Photoluminescence Spectral Data of Monomers **M1-M2** and Polymers **P1-P4**

Sample	$\lambda_{\max,Abs}$ (nm)		$\lambda_{\max,PL}$ (nm)		Φ (%) ^b
	solution ^a	film	solution ^a	film	
M1	344	-	392	-	74
M2 ^c	322	-	385	-	23
P1	344	343	396	425	73
P2	344	340	397	424	70
P3	338	336	395	422	70
P4	337	336	394	423	72

^a Absorption and PL emission spectra were recorded in dilute THF solutions at room temperature.

^b 9,10-Diphenylanthracene in THF is used as the reference of the quantum yield.

^c UV-visible absorption and PL data of **M2** in solutions was reported in our previous study.²²

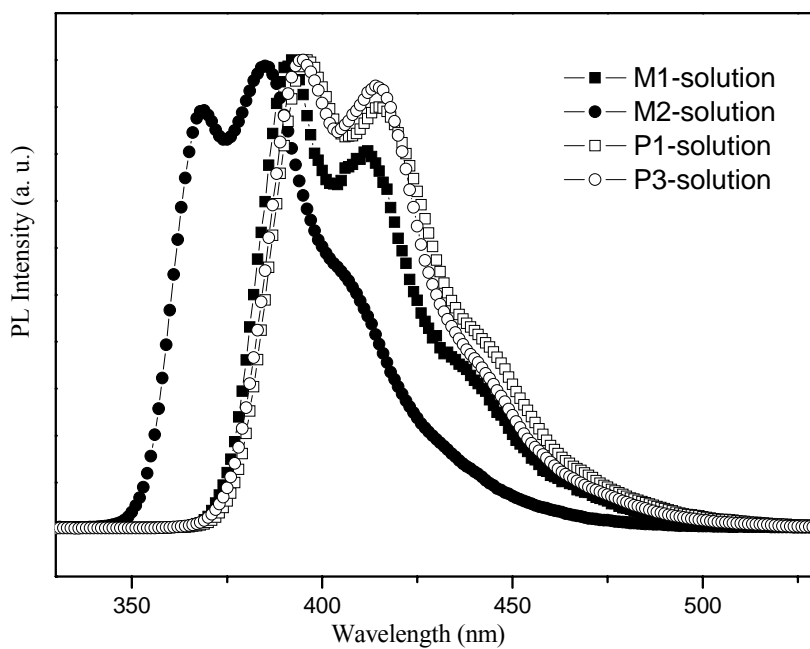


Figure 5.2 PL spectra of monomers (**M1** and **M2**) and polymers (**P1** and **P3**) in solutions.

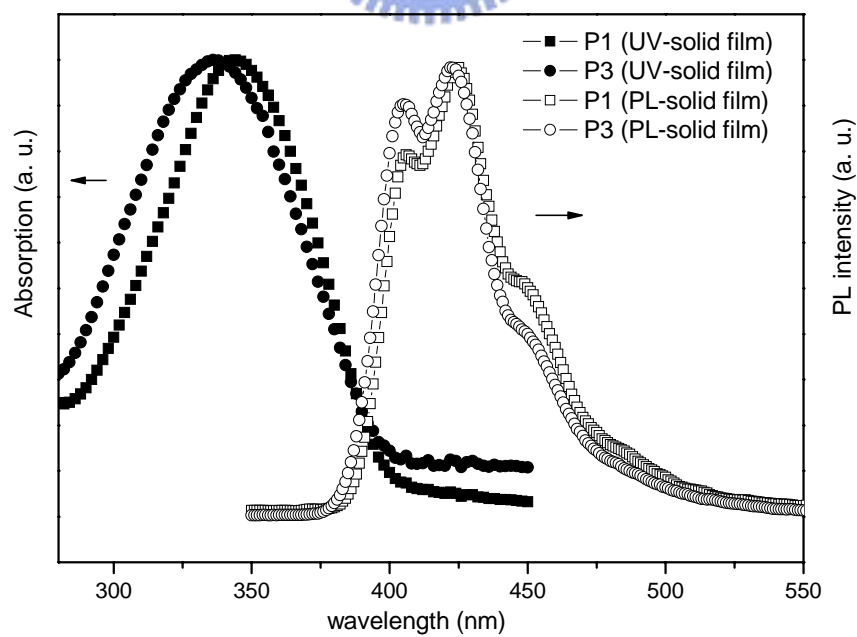
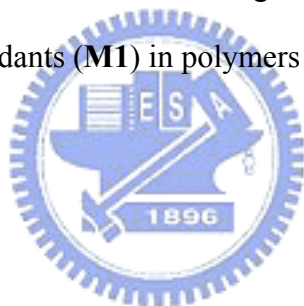


Figure 5.3 UV-visible absorption and PL spectra of **P1** and **P3** in solid films.

5.4 CONCLUSION

Polymers (**P1** and **P2**) containing 4,4'-bis(biphenyl)fluorene pendants (**M1**) and random copolymers (**P3** and **P4**) composed of 4,4'-bis(biphenyl)fluorene pendants (**M1**) and biphenyl-4-ylfluorene pendants (**M2**) are polymerized by atom transfer radical polymerization (ATRP). Thermal and XRD investigations indicate that polymers exhibit the nematic phases which have little relationship with respect to the flexible polystyrene block, but the glass transition temperatures (T_{gs}) of block copolymers **P2** and **P4** containing polystyrene blocks are higher than those of polymers **P1** and **P3** without the polystyrene block. In terms of PL and absorption wavelengths of all polymers in dilute solutions, **P1** and **P2** are a little red-shifted than **P3** and **P4**, which might be due to longer conjugation lengths of the 4,4'-bis(biphenyl)fluorene pendants (**M1**) in polymers **P1** and **P2**.



Chapter 6

Conclusion

A novel conjugated aromatic core containing direct-coupled fluorene, thiophene, and biphenyl groups via Suzuki coupling reaction was synthesized in this study. The rigid hydrophobic core was combined with two different lengths of poly(ethylene oxide)s as hydrophilic flexible chains to form rod-coil diblock polymers. The asymmetrical molecules contain two kinds of poly(ethylene oxide)s (PEO, $M_n = 750$ and 2000 , $n = 17$ and 44) on one side of the rigid cores. It is interesting that the increasing flexible chains lead to different mesophases (and molecular arrangements) and decrease the phase transition temperatures of T_m and T_i . Asymmetrical **FOC₈PEO₁₇** and **FOC₁₆PEO₁₇** contain flexible PEO chains ($n = 17$) display the smectic phases. However, **FOC₈PEO₄₄** and **FOC₁₆PEO₄₄** consisting of flexible PEO chains ($n = 44$) exhibit two kinds of columnar phases, Col_h and Col_r . In addition, alkoxy groups with different lengths ($-OC_8H_{17}$ and $-OC_{16}H_{33}$) on both sides of the rigid cores were used as another flexible chains to form symmetrical molecules. Symmetrical **FOC₈** and **FOC₁₆** exhibit the nematic and smectic mesophases. The XRD patterns and optical textures by POM have proved their mesophasic structures and molecular arrangements. The melting points of the commercial poly(ethylene oxide)s with $M_n = 750$ and 2000 are $30\text{ }^\circ\text{C}$ and $52\text{ }^\circ\text{C}$, respectively. Hence, LC segregation might be influenced with poly(ethylene oxide)s at low temperature. Besides mesophasic properties, the PL and EL properties of all rod-coil polymers and analogous derivatives are also investigated.

Atom transfer radical polymerization (ATRP) was employed to fabricate side-chain LC block copolymers composed of different macroinitiators, including poly(ethylene oxide) (**I1**), polystyrene (**I2** and **I3**), and poly(ethylene oxide)-b-polystyrene (**I4**), and

liquid crystalline cyanoterphenyl-based polymethacrylate blocks. Thermal and XRD investigations indicate that all polymers exhibit the interdigitated packing smectic A phase which have little relationship with respect to the flexible PS and PEO blocks.

Besides, block copolymers consisting of PS (**SMi**) macroinitiators and liquid crystalline polymethacrylate blocks containing biphenyl-4-ylthiophene and biphenyl-4-ylfluorene units were also polymerized by ATRP. Thermal and XRD investigations indicate that polymers containing biphenyl-4-ylthiophene units exhibited the interdigitated smectic A phase which has little relationship with respect to their flexible PS blocks. In terms of PL wavelengths of all block copolymers in dilute solutions, the polymers composed of biphenyl-4-ylfluorene units are more red-shifted than that composed of biphenyl-4-ylthiophene.

Finally, polymers containing 4, 4'-bis(biphenyl)fluorene pendants and random copolymers composed of 4,4'-bis(biphenyl)fluorene pendants and biphenyl-4-ylfluorene pendants are polymerized by atom transfer radical polymerization (ATRP). Thermal and XRD investigations indicate that polymers exhibit the nematic phases which have little relationship with respect to the flexible polystyrene block, but the glass transition temperatures (T_g s) of block copolymers containing polystyrene blocks are higher than those of polymers without the polystyrene block. The quantum yields of all polymers consist of 4,4'-bis(biphenyl)fluorene groups (70%) were better than other analogous polymers (around 20%) in our previous studies

References

- (1) Collings, P. J.; Hird, M.; "Introduction to liquid crystals" (Taylor & Francis).
- (2) Zubarev, E. R.; Pralle, M. U.; Li, L.; Stupp, S. I. *Science* **1999**, *283*, 523.
- (3) Lee, M.; Cho, B. K.; Kim, H.; Zin, W.C. *Angew. Chem., Int. Ed.* **1998**, *37*, 638.
- (4) Tian, Y.; Watanabe, K.; Kong, X.; Abe, J.; Iyoda, T. *Macromolecules* **2002**, *35*, 3739.
- (5) Oriol, L.; Pinol, M.; Serrano, J. L.; Martinez, C.; Alcala, R.; Cases, R.; Sanchez, C. *Polymer* **2001**, *42*, 2737.
- (6) Klock, H. A.; Lecommandoux, S. *Adv. Mater.* **2001**, *13*, 1217.
- (7) Lee, M.; Cho, B.K.; Zin, W. C. *Chem. Rev.* **2001**, *101*, 3869.
- (8) Halperin, A. *Macromolecules* **1990**, *23*, 2724.
- (9) Semenov, A. N.; *Mol. Cryst. Liq. Cryst.* **1991**, *209*, 191.
- (10) Williams D. R. M.; Fredrikcson G. H. *Macromolecules* **1992**, *25*, 3561.
- (11) (a) Radzilowski, L. H.; Wu, J. L.; Stupp, S. I. *Macromolecules* **1993**, *26*, 879. (b) Radzilowski, L. H.; Stupp, S. I. *Macromolecules* **1994**, *27*, 7747. (c) Radzilowski, L. H.; Carragher, B.O.; Stupp, S. I. *Macromolecules* **1997**, *30*, 2110.
- (12) (a) Stupp, S. I.; Lebonheur, V.; Walker, K.; Li, L. S.; Huggins, K.E.; Keser, M.; Amstutz, A. *Science* **1997**, *276*, 384. (b) Tew, G. N.; Pralle, M. U.; Stupp, S. I. *J. Am. Chem. Soc.* **1999**, *121*, 9852. (c) Pralle, M. U.; Whitaker, C.M.; Braun, P. V.; Stupp, S. I. *Macromolecules* **2000**, *33*, 3550.
- (13) (a) Lee, M.; Oh, N. K. *J. Mater. Chem.* **1996**, *6*, 1076. (b) Lee, M.; Oh, N. K.; Lee, H. K.; Zin, W. C. *Macromolecules* **1996**, *29*, 5567
- (14) (a) Lee, M.; Cho, B. K.; Kim, H.; Yoon, J. Y.; Zin, W. C. *J. Am. Chem. Soc.* **1998**, *120*, 9168. (b) Lee, M.; Cho, B. K. *J. Am. Chem. Soc.* **2001**, *123*, 9677.
- (15) Hulvat, J. F.; Sofos, M.; Tajima, K.; Stupp, S. I. *J. Am. Chem. Soc.* **2005**, *127*,

366.

- (16) (a) Lee, M.; Kim, J. W.; Hwang, I. W.; Kim, Y. R.; Oh, N. K.; Zin, W. C. *Adv. Mater.* **2001**, *13*, 1363. (b) Lee, M.; Jeong, Y. S.; Cho, B. K.; Oh, N. K.; Zin, W. C. *Chem. Eur. j.* **2002**, *8*, 876.
- (17) (a) Lee, M.; Park, M. H.; Oh, N. K.; Zin, W. C.; Jung, H. T.; Yoon, D. K. *Angew. Chem. Int. Ed.* **2004**, *43*, 6466. (b) Lee, M.; Jang, C. J.; Ryu, J. H. *J. Am. Chem. Soc.* **2004**, *126*, 8082.
- (18) Miyaura, M.; Suzuki, A. *Chem. Rev.* **1995**, *95*, 2457
- (19) Dingemans, T. J.; Murthy, N. S.; Samulski, E. T. *J. Phys. Chem. B* **2001**, *105*, 8845.
- (20) Kiryanov, A. A.; Sampson, K. S.; Seed, A. J. *J. Mater. Chem.* **2001**, *11*, 3068.
- (21) Percec, V.; Lee, M. *Macromolecules* **1991**, *24*, 1017.
- (22) Collings, P. J.; Hird, M. *Introduction to Liquid Crystals Chemistry and Physics* **1997**, Taylor & Francis.
- (23) Lai, C. K.; Tsai, C. H.; Pang, Y. S. *J. Mater. Chem.* **1998**, *8*, 1355
- (24) Ohta, K.; Azumane, S.; Kawahara, W.; Kobayashi, N.; Yamamoto, I. *J. Mater. Chem.* **1999**, *9*, 2313.
- (25) Wen, C. R.; Wang, Y. J.; Wang, H. C.; Sheu, H. S.; Lee, G. H.; Lai, C. K. *Chem. Mater.* **2005**, *17*, 1646.
- (26) Contoret, A-E. A.; Farrar, S. R.; O'Neill, M.; Nicholls, J. E.; Richards, G. J.; Kelly, S. M.; Hall, A. W. *Chem. Mater.* **2002**, *14*, 1477.
- (27) Sung, H. H.; Lin, H. C. *Macromolecules* **2004**, *37*, 7945.
- (28) Guilbault, G. G., Ed. *Practical Fluorescence*; Marcel Dekker, Inc.: New York, **1990**; Chapter 1.
- (29) Hao, X.; Heuts, J. P. A.; Barner-Kowollik, C.; Davis, T. P.; Evans, E. *J. Polym. Sci. Part A: Polym. Chem.* **2003**, *41*, 2949.

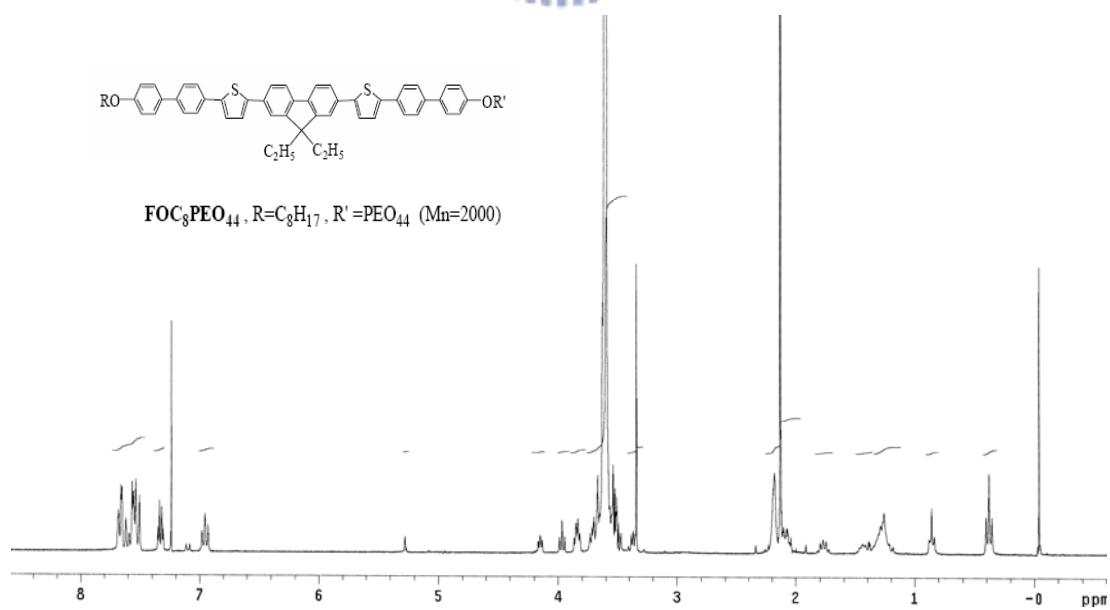
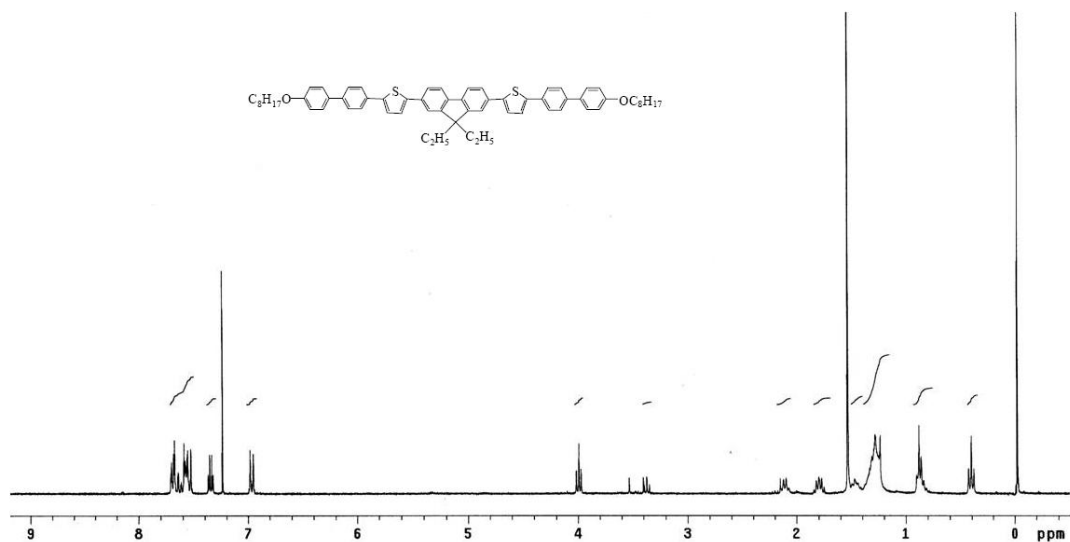
- (30) Lee, K. M.; Han, C. D. *Macromolecules* **2002**, 35, 3145.
- (31) Poser, S.; Fischer, H.; Arnold, M. *J. Polym. Sci. Part A: Polym. Chem.* **1996**, 34, 1733.
- (32) Moriya, K.; Seki, T.; Nakagawa, M.; Mao, G.; Ober, C. K. M. *Macromol. Rapid Commun.* **2000**, 21, 1309.
- (33) Yu, H.; Shishido, A.; Ikeda, T.; Iyoda, T. *Macromol. Rapid Commun.* **2005**, 26, 1594.
- (34) Cui, L.; Zhao, Y.; Yavrian, A.; Galstian, T. *Macromolecules* **2003**, 36, 8246.
- (35) Gopalan, P.; Li, X.; Li, M.; Ober, C. K.; Gonzales, C. P.; Hawker, C. J. *J. Polym. Sci. Part A: Polym. Chem.* **2003**, 41, 3640.
- (36) Hawker, C.J.; Wooley, K.L. *Science* **2005**, 309, 1200.
- (37) Shunmugam, R.; Tew, G. N. *J. Polym. Sci. Part A: Polym. Chem.* **2005**, 43, 5831.
- (38) Denizli, B. K.; Lutz, J. F.; Okrasa, L.; Pakula, T.; Guner, A.; Matyjaszewski, K. *J. Polym. Sci. Part A: Polym. Chem.* **2005**, 43, 3440.
- (39) Schneider, A.; Zanna, J. J.; Yamada, M.; Finkelmann, H.; Thomann, R. *Macromolecules* **2000**, 33, 649.
- (40) He, X.; Zhang, H.; Yan, D.; Wang, X. *J. Polym. Sci. Part A: Polym. Chem.* **2003**, 41, 2854.
- (41) Figueiredo, P.; Gronski, W.; Bach, M. *Macromol. Rapid Commun.* **2002**, 23, 38.
- (42) Özbek, H.; Yıldız, S.; Pekcan, Ö.; Hepuzer, Y.; Yagci, Y.; Galli, G. *Mater. Chem. Phys.* **2002**, 78, 318.
- (43) Hepuzer, Y.; Serhatli, I. E.; Yagci, Y.; Galli, G.; Chiellini, E. *Macromol. Rapid Commun.* **2002**, 202, 2247.
- (44) Anthamatten, M.; Wu, J. S.; Hammond, P. T. *Macromolecules* **2001**, 34, 8574.
- (45) Sanger, J.; Gronski, W.; Maas, S.; Stuhn, B.; Heck, B. *Macromolecules* **1997**, 30, 6783.

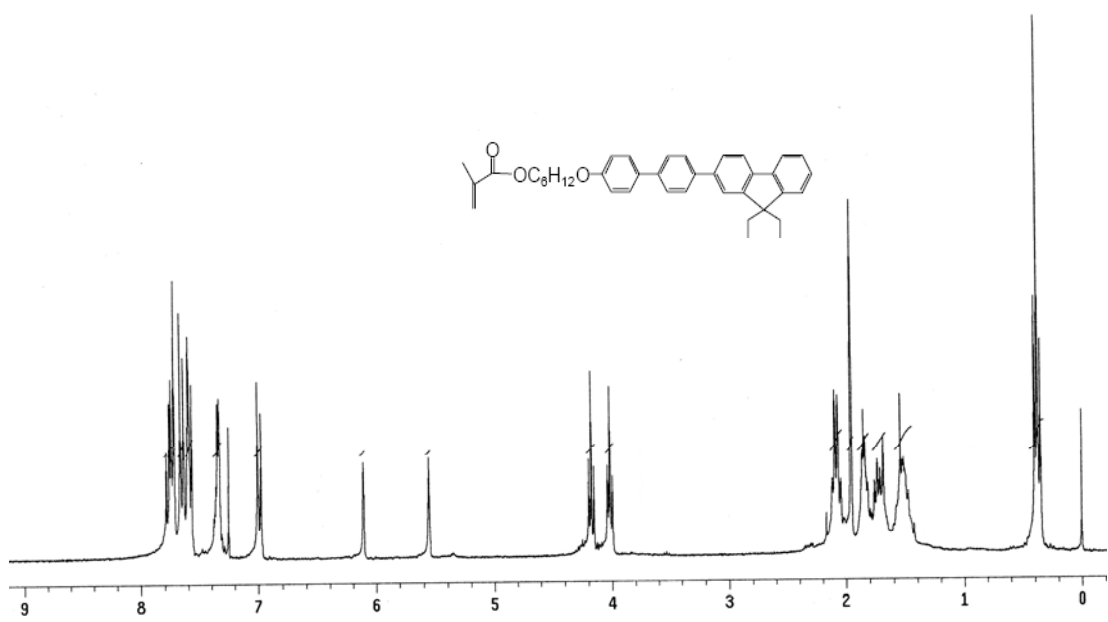
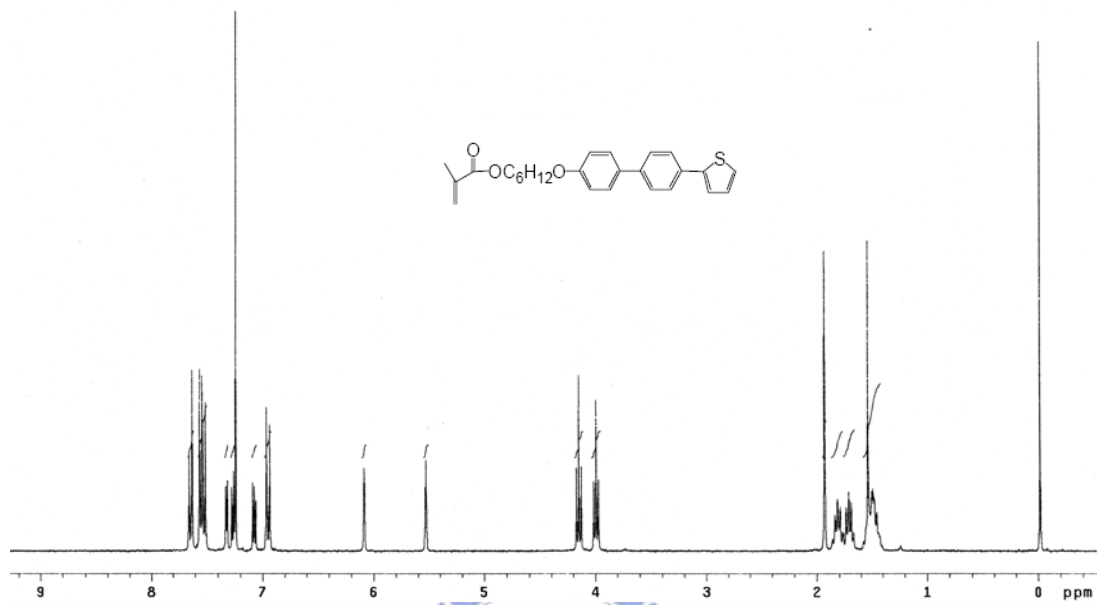
- (46) Anthamatten, M.; Zheng, W. Y.; Hammond, P. T. *Macromolecules* **1999**, *32*, 4838.
- (47) Gray, G. W.; Harrison, K. J.; Nash, J. A. *J. Chem. Soc. Commun.* **1974**, 431.
- (48) Kiryanov, A. A.; Sampson, K. S.; Seed, A. J. *J. Mater. Chem.* **2001**, *11*, 3068.
- (49) Matyjaszewski, K.; Xia, J. *Chem. Rev.* **2001**, *101*, 2921.
- (50) Kamigaito, M.; Ando, T.; Sawamoto, M. *Chem. Rev.* **2001**, *101*, 3689.
- (51) Wang, J.; Mao, G.; Ober, C. K.; Kramer, E. J. *Macromolecules* **1997**, *30*, 1906.
- (52) Schmalz, H.; Bolker, A.; Lange, R.; Krausch, G.; Abetz, V. *Macromolecules* **2001**, *34*, 8720.
- (53) Otmakhova, O. A.; Kuptsov, S. A.; Talroze, R. V.; Patten, T. E. *Macromolecules* **2003**, *36*, 3432.
- (54) Osuji, C. O.; Chen, J. T.; Ober, C. K.; Thomas, E. L. *Polymer* **2000**, *41*, 8897.
- (55) Park, C.; Yoon, J.; Thomas, E. L. *Polymer* **2003**, *44*, 6725.
- (56) Kihara, H.; Kishi, R.; Miura, T.; Kato, T.; Ichijo, H. *Polymer* **2001**, *42*, 1177.
- (57) Minich, E.A.; Nowak, A. P.; Deming, T. J.; Pochan, D. J. *Polymer* **2004**, *45*, 1951.
- (58) Lin, H. C.; Lee, K. W.; Tsai, C. M.; Wei, K. H. *Macromolecules* **2006**, *39*, 3808.
- (59) Tew, G. N.; Aamer, K. A.; Shunmugam, R. *Polymer* **2005**, *46*, 8440.
- Commun.* **2002**, *202*, 2247.
- (60) Li XG, Huang MR, Guan GH, Sun T. *J. Appl. Polym. Sci.* **1997**, *66*, 2129.
- (61) Li XG. *J. Appl. Polym. Sci.* **1999**, *73*, 2921.
- (62) Tang W, Li XG, Yan D. *J. Appl. Polym. Sci.* **2004**, *91*, 445.
- (63) Lee, K. W.; Wei, K. H.; Lin, H. C. *J. Polym. Sci. Part A: Polym. Chem.* **2006**, *44*, 4593.
- (64) Goodman, C. C.; Amanda, C. R.; Tillman, E. S.; Ludwig, B.; Chon, D.; Weigley, M. I. *J. Polym. Sci. Part A: Polym. Chem.* **2005**, *43*, 2657.

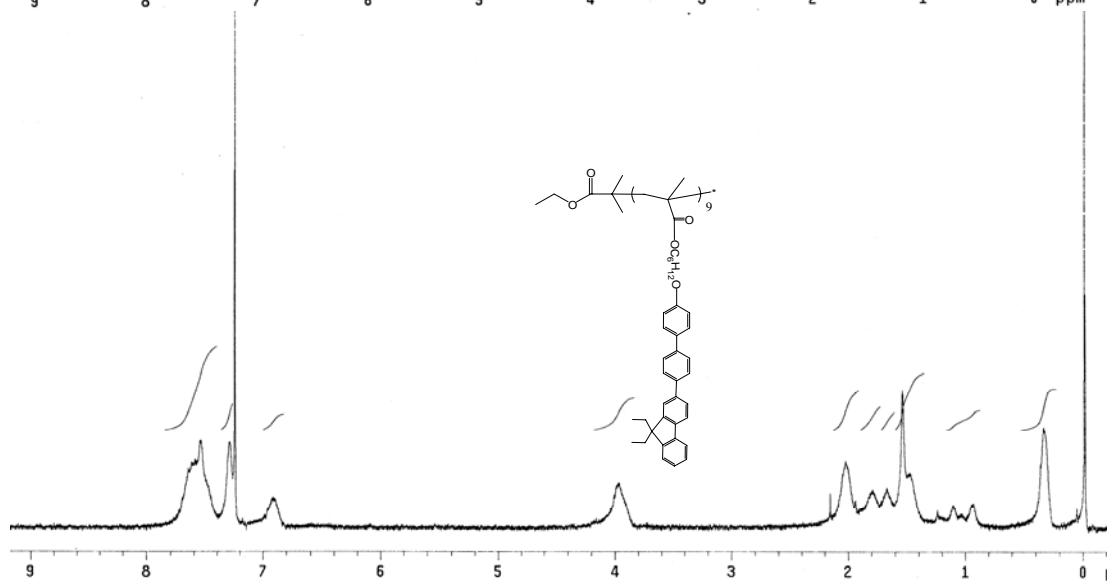
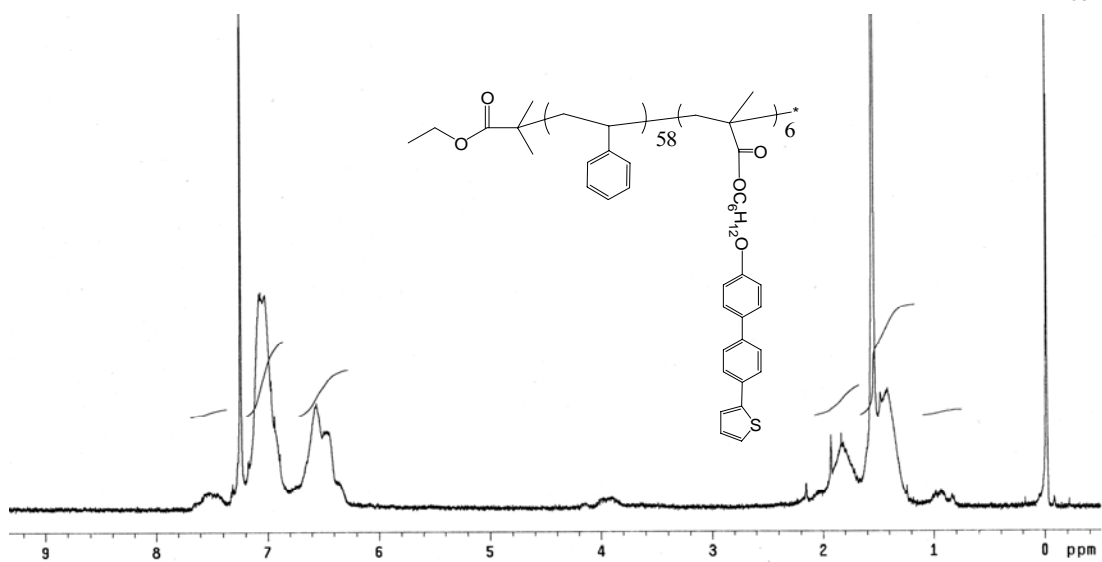
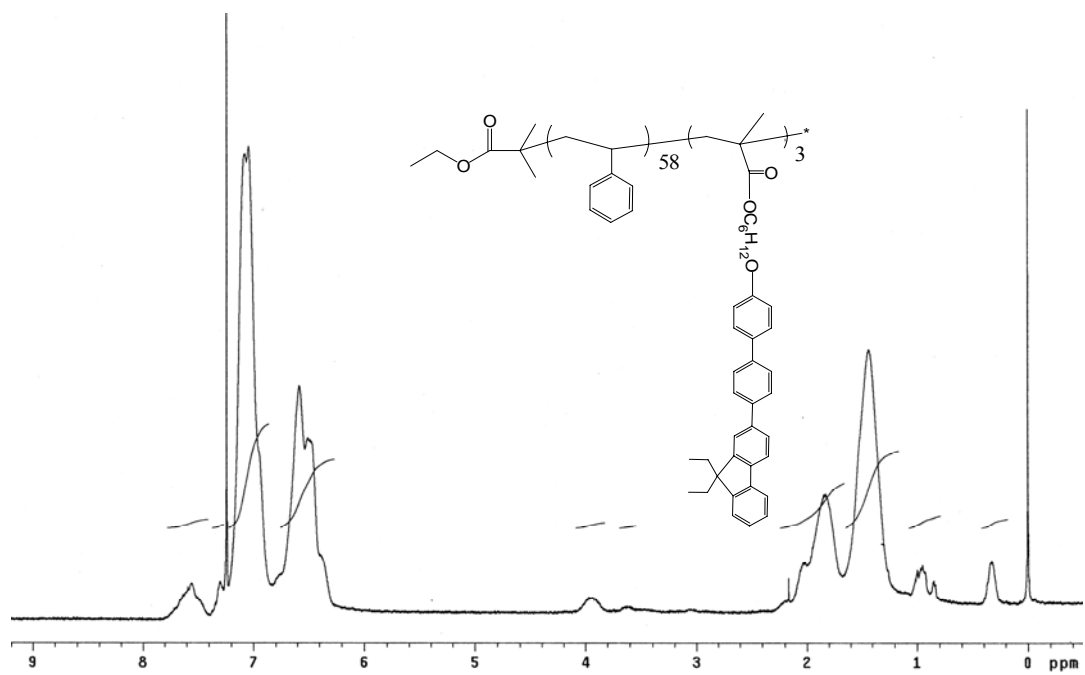
- (65) Wang, J. S.; Matyjaszewski, K. *J. Am. Chem. Soc.* **1995**, 117, 5614.
- (66) Sawamoto, M.; Kamigaito, M. *Trends. Polym. Sci.* **1996**, 4, 371.
- (67) Tsolakis, P. K.; Koulouri, E. G.; Kallitsisi, J. K. *Macromolecules* **1999**, 32, 9054.
- (68) Tsolakis, P. K.; Kallitsisi, J. K.; Tsitsilianis, C. J. *Macromol. Sci. Pure. Appl. Chem.* **2002**, 39, 155.
- (69) Tsolakis, P. K.; Kallitsisi, J. K.; Godt, A. *Macromolecules* **2002**, 35, 5758.
- (70) Yi, Y.; Wan, X.; Fan, X.; Dong, R.; Zhou, Q. *J. Polym. Sci. Part A: Polym. Chem.* **2003**, 41, 2854.
- (71) Lu, X.; He, C.; Liu, P.; Griffin, A. C. *J. Polym. Sci. Part A: Polym. Chem.* **2005**, 43, 3394.
- (72) Yang, S. H.; Li, H. C.; Chen, C. K.; Hsu, C. S. *J. Polym. Sci. Part A: Polym. Chem.* **2006**, 44, 6738.
- (73) Lin, H. C.; Tsai, C. M.; Huang, G. H.; Lin, J. M. *J. Polym. Sci. Part A: Polym. Chem.* **2006**, 44, 783.
- (74) Lee, K. W.; Lin, H. C. *Polymer* **2007**, in press.

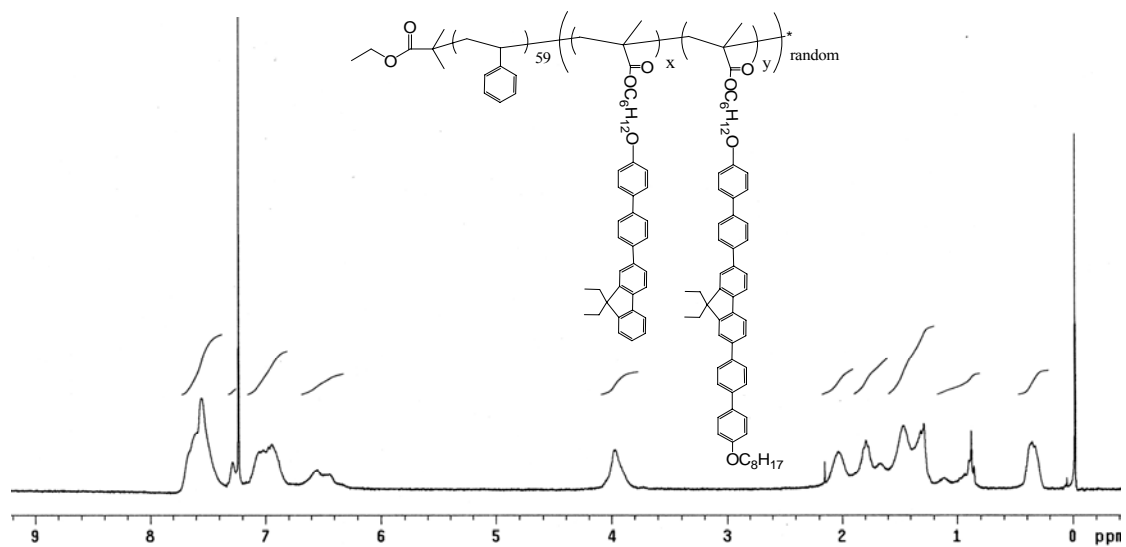
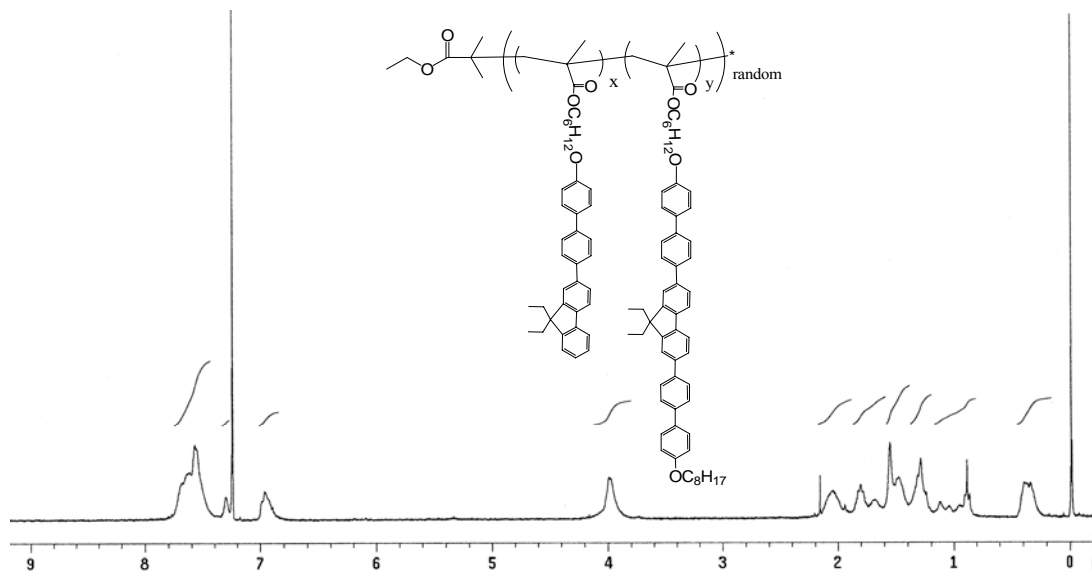
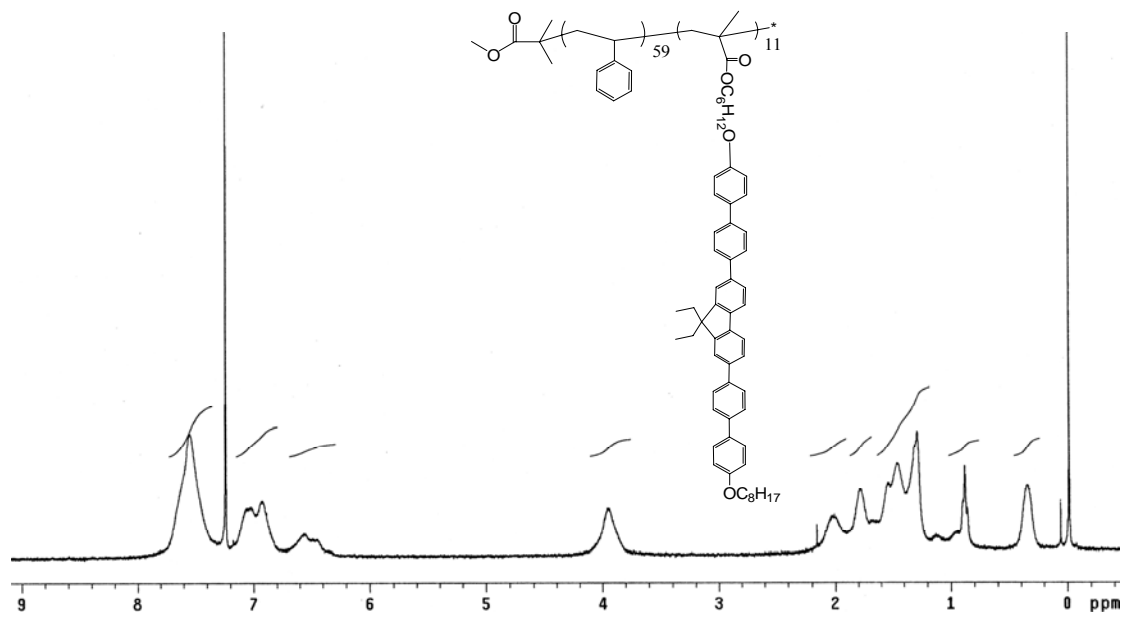


Appendix : NMR spectra



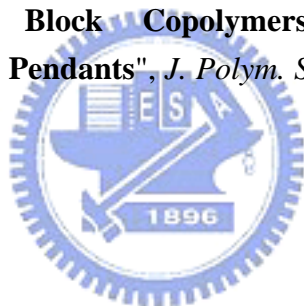






Publication

1. H. C. Lin*, K. W. Lee, C. M. Tsai, K. H. Wei, "**Synthesis and Characterization of Rod-Coil Polymers Based on Poly(ethylene oxide)s and Novel Luminescent Aromatic Cores**", *Macromolecules* **2006**, 39, 3808
2. K. W. Lee, K. H. Wei, H. C. Lin*, "**Synthesis and Characterization of Liquid Crystalline Block Copolymers with Cyanoterphenyl Moieties by ATRP**", *J. Polym. Sci. Part A: Polym. Chem.* **2006**, 44, 4593.
3. K. W. Lee and H. C. Lin*, "**Synthesis and characterization of side-chain liquid crystalline homopolymers and block copolymers containing biphenyl-4-ylthiophene and biphenyl-4-ylfluorene pendants**", *polymer* **2007**, in press.
4. K. W. Lee and H. C. Lin*, "**Synthesis and Characterization of Liquid Crystalline Side-Chain Block Copolymers Containing Luminescent 4,4'-Bis(biphenyl)fluorene Pendants**", *J. Polym. Sci. Part A: Polym. Chem.* **2007**, in press.



學經歷資料表

姓 名	李冠緯
性別	男
出生日期	1979 年 1 月 30 日
婚姻狀況	已婚
E-mail 信箱	wei.mse92g@nctu.edu.tw
聯絡電話	0986005272
通訊地址	新竹縣竹北市縣政七街九號七樓之七
永久地址	高雄市前鎮區崗山西街 2-11 號
學經歷	1997 年 9 月- 2001 年 6 月 國立中正大學化學系 2001 年 9 月- 2003 年 6 月 國立交通大學材料所碩士班 2003 年 9 月- 2007 年 4 月 國立交通大學材料所博士班
專 長	液晶與有機發光材料開發、合成與物性鑑定
學術著作	<p>1. H. C. Lin*, K. W. Lee, C. M. Tsai, K. H. Wei, "Synthesis and Characterization of Rod-Coil Polymers Based on Poly(ethylene oxide)s and Novel Luminescent Aromatic Cores", <i>Macromolecules</i> 2006, 39, 3808</p> <p>2. K. W. Lee, K. H. Wei, H. C. Lin*, "Synthesis and Characterization of Liquid Crystalline Block Copolymers with Cyanoterphenyl Moieties by ATRP", <i>J. Polym. Sci. Part A: Polym. Chem.</i> 2006, 44, 4593.</p> <p>3. K. W. Lee and H. C. Lin*, "Synthesis and characterization of side-chain liquid crystalline homopolymers and block copolymers containing biphenyl-4-ylthiophene and biphenyl-4-ylfluorene pendants", <i>polymer</i>, in press.</p> <p>4. K. W. Lee and H. C. Lin*, "Synthesis and Characterization of Liquid Crystalline Side-Chain Block Copolymers Containing Luminescent 4,4'-Bis(biphenyl)fluorene Pendants", <i>J. Polym. Sci. Part A: Polym. Chem.</i> 2007, in press.</p>